THE FUNCTIONAL ROLES OF RHO-KINASE AND MATRIX METALLOPROTEINASES IN REGULATING CORNEAL STROMAL CELL MECHANICS IN 3-D COLLAGEN MATRICES.

APPROVED BY SUPERVISORY COMMITTEE

W. Matthew Petroll, Ph.D. (Supervising Professor)

Frederick Grinnell, Ph.D. (Chair)

Katherine Luby-Phelps, Ph.D.

Li-ping Tang, Ph.D.

Georgis Alexandrakis, Ph.D.

DEDICATION

I would like to thank my distinguished doctoral supervisor Prof. Matthew Petroll, every faculty member on my Dissertation Committee and other academic colleagues, and my dear family and friends.

THE FUNCTIONAL ROLES OF RHO-KINASE AND MATRIX METALLOPROTEINASES IN REGULATING CORNEAL STROMAL CELL MECHANICS IN 3-D COLLAGEN MATRICES.

by

CHENGXIN ZHOU

DISSERTATION

Presented to the Faculty of the Graduate School of Biomedical Sciences

The University of Texas Southwestern Medical Center

In Partial Fulfillment of the Requirements

For the Degree of

DOCTOR OF PHILOSOPHY

The University of Texas Southwestern Medical Center

Dallas, Texas

December, 2013

THE FUNCTIONAL ROLES OF RHO-KINASE AND MATRIX METALLOPROTEINASES IN REGULATING CORNEAL STROMAL CELL MECHANICS IN 3-D COLLAGEN MATRICES.

Publication No._____

Chengxin Zhou, Ph.D.

The University of Texas Southwestern Medical Center at Dallas, 2013

Supervising Professor: W. Matthew Petroll, Ph.D.

The main focus of my research has been on understanding the biomechanical and biochemical mechanisms of cell-extracellular matrix (ECM) interactions during corneal wound healing, which may allow the development of new therapeutic strategies to promote corneal regeneration.

Previous studies have established that the Rho GTPases play a central role in regulating the cytoskeletal changes associated with cell mechanical activity. A novel force monitoring system was successfully developed to investigate the role of Rho in corneal cell force generation in 3-D collagen matrices. Maximum tractional force generated by 9 million corneal fibroblasts in serum culture was around 265 Dynes. Inhibition of Rho kinase by Y-27632 induced a 69% force

reduction. These results demonstrated that Rho/Rho kinase play a key role in mediating contractile force generation of corneal stromal fibroblasts in serum culture.

I also investigated the functions of Rho GTPase signaling in corneal stromal fibroblast migration and cell-ECM interactions using a 3-D nested matrix construct. The experimental results showed that both the amount and the speed of corneal fibroblast migration and local collagen matrix reorganization were significantly inhibited by Y-27632. Following the inhibition, cells extended thinner dendritic processes into the outer matrix, and generated tractional forces at their leading edge. However, cells were unable to generate contractile forces needed to retract their tail and pull the cell body forward through the collagen matrix.

I also studied the role of Matrix metalloproteinases (MMPs) in corneal cell mechanics, since these have been recognized as an influential component in extracellular matrix turnover and corneal repair. I first assessed the expression and collagenolytic activities of MMPs by primary corneal keratocyte in response to different signaling factors. I then studied the functions of MMPs in regulating keratocyte migration, cell-induced matrix contraction, and cell protrusive activity in 3-D collagen matrices. This study suggested that, in serum free PDGF culture, although collagenolysis was limited to a pericellular scale, primary corneal keratocytes utilized MMPs to facilitate cell migration, ECM contraction, cell spreading in 3-D collagen matrices. Thus MMPs may play a key role in facilitating cell-collagen matrix interactions by corneal keratocytes, without producing widespread disruption of corneal ECM structure.

TABLE OF CONTENTS

PRIOR PUBLICATIONS

1. **Zhou C**, Petroll WM. Rho kinase regulation of corneal fibroblast migratory mechanics in fibrillar collagen matrices. *Cell Mol Bioengng* 3:76-83, 2010.
2. Kim A, **Zhou C**, Lakshman N, Petroll WM. Corneal Stromal Cells use both High- and Low-Contractility Migration Mechanisms in 3-D Collagen Matrices. *Exp Cell Res* 318:741-7523, 2012.
3. Miron-Mendoza M, Koppaka V, **Zhou C**, Petroll WM. Techniques for Assessing 3-D Cell-Matrix Mechanical Interactions *In Vitro* and *In Vivo*. *Exp Cell Res* 319:2470-2480, 2013.
4. **Zhou C**, Petroll WM. MMP Regulation of Corneal Keratocyte Motility and Mechanics in 3-D Collagen Matrices. *Exp Eye Res* (Submitted).

LIST OF FIGURES

LIST OF TABLES

LIST OF APPENDICES

CHAPTER ONE
Introduction

1.1 SPECIFIC AIMS

Migration of corneal keratocytes plays an important role in corneal healing and is required for repopulation of wounded corneal tissue following injury or surgery. In most wounds, quiescent corneal keratocytes transform into an *activated fibroblast phenotype*. Mechanical force generation by *activated corneal fibroblasts* mediates corneal wound contraction and matrix remodeling, and is therefore an important contributor to corneal haze or fibrosis. In many circumstances (e.g. following PRK or LASIK), it is preferable to have corneal fibroblasts repopulate the wound space without remodeling the extracellular matrix or generating large contractile forces, since these activities can reduce corneal clarity and alter its refractive power. **The overall goal of this project is to develop and apply novel 3-D culture models for investigating the migratory mechanics of both activated and quiescent corneal keratocytes.**

Previous studies using 2-D substrates and other cell types have established that the Rho-family of GTPases such as Rho, Rac and Cdc42 play a central role in regulating the cytoskeleton changes associated with cell mechanical activity. Activated Rho stimulates the formation of stress fibers, the development of large focal adhesions, and cellular contraction. Rac and Cdc42 induce the assembly of smaller focal complexes, actin polymerization and cell spreading and

ruffling. Thus, Rho and Rac serve as candidates for regulating the downstream effects of cytokine/growth factors on corneal stromal cells in 3-D collagen matrices. Based on these data we hypothesize that: 1) The generation of corneal stromal fibroblast forces is mediated by Rho/Rho-kinase activation and 2) Activated corneal fibroblast migration in 3-D collagen matrices is regulated, in part, by the Rho-Rho kinase-actomyosin signaling pathway.

In addition to generation of forces on the matrix, remodeling is also mediated by the activity of matrix metalloproteinases (MMPs). Migration of activated (contractile) corneal fibroblasts has been shown to be dependent, in part, on MMP expression by the cells. However, we have recently demonstrated that ***quiescent corneal keratocytes*** cultured in serum-free media can migrate effectively through 3-D collagen matrices when stimulated with platelet-derived growth factor (PDGF), without generating large contractile forces. This low contractility migration may allow cells to repopulate corneal tissue without altering its unique extracellular matrix structure, which is needed to maintain transparency. However, it is not known whether this low-contractility migration mechanism is also dependent on MMPs. We hypothesize that migration of corneal keratocytes stimulated with PDGF can occur in the absence of proteolytic MMP activities.

To test these hypotheses, we propose the following specific aims:

Specific Aim 1

Investigate the role of Rho kinase in regulating cellular force generation and migratory mechanics of activated corneal stromal fibroblasts in 3-D culture. Using a human corneal fibroblast cell line in serum culture, we will: **a)** develop a new tensile culture force monitoring system (t-CFM); **b)** directly assess the role of Rho-kinase in corneal fibroblast generation of tractional force, using the new t-CFM; and, **c)** Assess the role of Rho kinase on corneal fibroblast migration mechanics, using a novel 3-D nested collagen matrix migration model and 3- and 4-D imaging techniques. The established Rho-kinase inhibitors Y-27632 and fasudil will be used to block activation of Rho-kinase.

Specific Aim 2

Investigate the role of matrix metalloproteinases in the migration of *quiescent corneal keratocytes* in 3-D collagen matrices. We will: **a)** establish the effects of synthetic MMP inhibitors on collagen digestion by rabbit corneal keratocytes (NRK cells), using different growth factors present in cornea and tear film during wound healing (e.g. Transforming growth factor β; PDGF); **b)** determine the effects of MMP inhibitors on corneal keratocyte-induced collagen matrix contraction; and, **c)** measure the effects of MMP inhibition on corneal keratocyte migration through 3-D collagen matrices.

1.2. SUMMARY OF RATIONALE AND SIGNIFICANCE

Corneal wounds can be caused by lacerating injury, heat or erosive chemical injury, as well as corneal surgeries such as PRK or LASIK. Consequences of abnormal corneal wound healing include traumatic flap dislocations, opacity of the tissue, scarring, epithelial ingrowth and alterations in corneal shape – all of which can reduce visual acuity. The results of corneal repair are influenced by both biochemical and biomechanical responses of corneal cells during different stages of healing. Previous studies have shown that Rho and Rac can play a central role in regulating fibroblast contractility and cytoskeletal reorganization. However, important gaps in corneal stromal wound healing studies include: 1) there is a lack of suitable 3-D migration models for studying the mechanics of corneal keratocyte migration in response to different growth factor stimulation; 2) the role of Rho-kinase in mediating corneal fibroblast migration has not been established; 3) the role of secreted and membrane-anchored MMPs in regulating quiescent corneal keratocyte migration in 3-D culture has not been investigated previously.

CHAPTER TWO
Review of the Literature

2.1 CORNEAL STROMAL WOUND HEALING AND THE ROLE OF CORNEAL KERATOCYTES

The cornea is the front surface of the eye, and is responsible for 2/3 of the eye's refractive power. The cornea stroma is a highly organized tissue which provides strength while minimizing light scattering. Structurally, the cornea consists of layers of collagen sheets (named lamellae, ~ 0.2 mm in width, 1 -2 μm in thickness, approximate 300 lamellae in human cornea), with small uniform spacing between them (57 nm – 62 nm) [75]. Lamellae consist of tightly packed stromal fibrils which are heterodimeric complexes of type I and type V collagen, and have uniform fibril diameters (31 nm – 34 nm). These elaborate structural features have evolved to provide cornea transparency through destructive interference. Keratocytes have an even and sparse distribution between the lamella. They have a planar dendritic morphology and interconnecting pseudopodia. Corneal stromal collagens usually have slow turnover rates and keratocytes are in a 'quiescent' state with a very slow replication rate [19].

Following corneal injury such as photorefractive keratectomy (PRK) surgery where the corneal epithelium is removed and discarded, a fibrin/fibronectin/collagen type IV provisional matrix is deposited and polymerizes the injury site. Corneal epithelium begins to resurface the wound bed and produces cytokines, such as tumor necrosis factor alpha (TNF-α) and

interleukins. In the stroma, the keratocytes adjacent to the area of damage undergo apoptosis, leaving a zone of devoid of cells [112]. The keratocyte apoptosis response peaks at approximately 4 ~6 hours after injury [41]. This cell death may be the result of cytokines released from the wounded epithelium, or components of the tear film. Next, the keratocytes immediately adjacent to the area of cell death enter the cell cycle and proliferate (~ 24 to 48 hrs after injury for rat and rabbit) [120]. Keratocytes then undergo a phenotype transformation to fibroblasts and migrate into the wound area (this takes up to one week). Corneal fibroblasts have a fusiform shape and express stress fibers. The transformation of fibroblasts into myofibroblasts occurs when cellular repopulation of corneal fibroblasts in the wound area is complete [49]. Myofibroblasts express elevated levels of smooth muscle actin and are involved in contracting the wound, deposing new matrix components, and organizing the matrix fibrils [110]. The extent of myofibroblast formation depends on the type of wound and the extent of the interaction with the epithelium [77]. Large wounds appear to generate a larger number of myofibroblasts than small ones, and the presence of a large number of myofibroblasts is positively associated with cornea haze. Studies have shown that activated corneal fibroblasts and myofibroblasts are not terminally differentiated phenotypes and have the ability to transition into one another [73]. The general pattern of corneal stromal cell responses during corneal wound healing is illustrated in **Figure 2.1**.

Concomitant with these stromal cell responses is the influx of inflammatory cells to the cornea wound [113]. Chemokines released from both epithelial cells and keratocytes/activated

corneal fibroblasts that are up-regulated by cytokines attract different inflammatory cells from the tear film and vessels in the limbal tissue. Inflammatory cells found in wounded cornea include macrophages, monocytes, T cells, and polymorphonuclear cells [44]. These cells are thought to be responsible for cleaning the cellular debris resulting from keratocyte apoptosis.

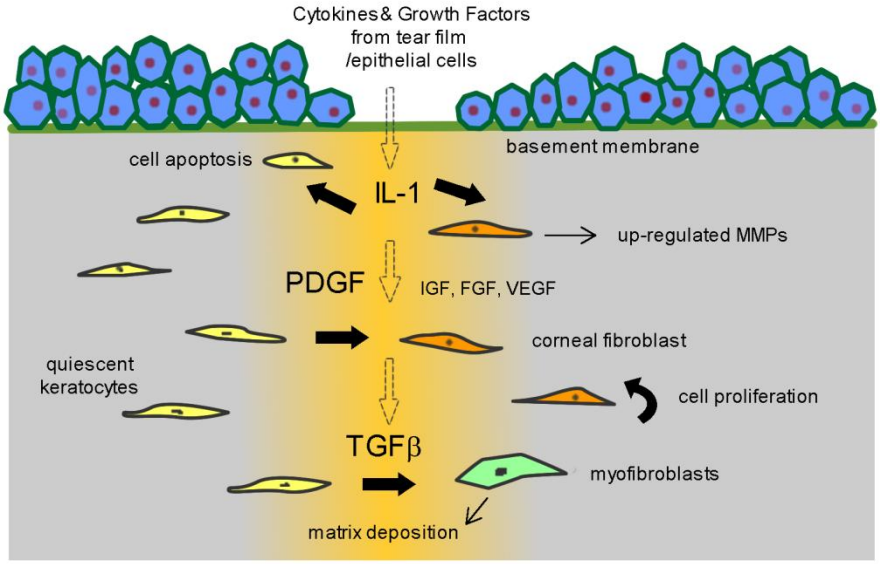

Figure 2.1: Cellular responses and growth factor/cytokine regulation during corneal stromal wound healing.

Wounds that penetrate the corneal stroma stimulate the synthesis of collagens not normally present in the cornea (Type III) and other abnormal extracellular matrix materials, and usually result in corneal scarring, which reduces visual acuity and can persist for years [13, 80].

Recent studies suggest that the periphery of the stroma contains a relatively high number of immature bone marrow-derived cells in addition to the keratocytes [113]. The role of these cells in stromal wound healing has not been established.

As described above, following corneal injury or surgery, activated corneal fibroblasts migrate into the wounded region, generating mechanical force to contract the corneal wound, remodeling the provisional matrix, proliferating and synthesizing new matrix. Due to ECM disorganization and increased light scattering of activated corneal fibroblasts, this process results in corneal haze or fibrosis. In many circumstances, it is preferable to have corneal fibroblasts repopulate the wound space without remodeling the extracellular matrix or generating large contractile forces, since these activities can reduce corneal clarity and alter its refractive power [78]. Our lab has recently demonstrated that quiescent corneal keratocytes cultured in serum-free media can migrate effectively through 3-D collagen matrices when stimulated with PDGF BB, without generating large contractile forces [60]. This low contractility migration may allow cells to repopulate corneal tissue without altering its unique structure, which is needed to maintain transparency.

2.2 BIOMECHANICAL PHENOTYPES OF CORNEAL STROMAL CELLS *IN VITRO*

Normal corneal keratocytes have a quiescent biomechanical phenotype in vivo. Keratocytes have a broad flattened morphology and are interconnected by long cellular

processes. They form an elaborate network between collagen lamellae of the cornea stroma [47, 48] and connexin 43 has been localized to cell-cell junctions [59]. This typical cell morphology is also observed in an *in vitro* culture model consisting of primary keratocytes suspended in reconstituted fibrillar type I collagen matrices, in the presence of defined serum-free medium [59]. Fluorescence and reflection confocal microscopy of this 3-D cell/collagen matrix 3-D culture model demonstrated that collagen fibrils adjacent to cell cortex appeared to be randomly oriented without compaction or alignment, and there were no intracellular stress fibers; i.e. cells maintain a quiescent mechanical phenotype (**Figure 2.2**). Keratocytes had a cortical, membrane associated f-actin organization, with more concentrated labeling near the ends of cell processes. Often these processes had a core of microtubules; however, filopodial extensions were also observed in which tubulin was not detected [59].

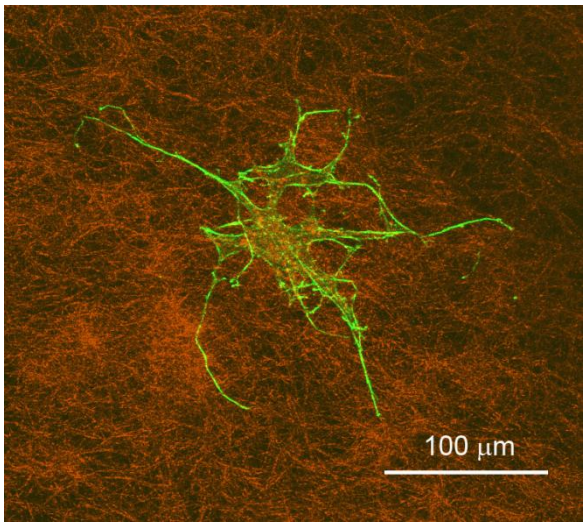

Figure 2.2: Primary rabbit corneal keratocyte. Confocal image is maximum intensity projection of f-actin (green) and collagen fibrils (red) after 4 days of culture in standard 3-D rat tail collagen matrices [65].

In the same 3-D collagen culture model, keratocytes can be transformed into contractile corneal fibroblasts by adding 10% FBS to the media [57]. Activation of Rho by FBS induces retraction of cell processes and cellular contraction in 3-D collagen matrices. Centripetal forces are generated along the cell body, as indicated by collagen fibril realignment and compaction adjacent to cell body [89]. Displacement of focal adhesions in the cell processes correlates significantly with extracellular matrix displacements [106]. This force generation is in part mediated by a Rho/Rho kinase (ROCK)-dependent mechanism [89] and can be largely reduced by using the Rho kinase inhibitor Y-27632. Y-27632 induces relaxation of neighboring collagen fibrils and extension of the cell body, as observed by DIC time lapse live cell imaging [106]. According to a quantitative study of corneal fibroblast biomechanics [95], the maximum force exerted on a collagen matrix by an individual non-migratory rabbit corneal fibroblast was about 9.38 ± 4.16 ($x10^{-8}$) N. And the mean centripetal forces generated during slow partial retraction and extension of pseudopodia by migratory corneal fibroblast were 1.35 ± 1.263 ($x10^{-8}$) N/μm and 0.470 ± 0.32 ($x10^{-8}$) N/μm respectively.

Overall, corneal fibroblasts have a bipolar morphology, produce significant cell-induced collagen compaction and remodeling, and express parallel arrays of stress fibers within the cell body and pseudopodial processes (**Figure 2.3**). Realignment of collagen fibrils is often observed parallel to stress fibers and pseudopodia. In contrast, when Rho or Rho-Kinase is inhibited, such as in corneal fibroblasts expressing dominant negative Rho [64] or after addition of the Rho kinase inhibitor Y-27632 [57, 89], cells become elongated, and have a more cortical f-actin

distribution. Numerous small extensions are also observed along the cell body. Importantly, both local collagen fibril density and alignment are also significantly reduced. When stress fibers were present, their expression was also reduced after the application of Y-27632 [106]. Perfusion of nocodazole to corneal fibroblast culture induces rapid microtubule disruption, increased Rho activation, cellular contraction and matrix compaction. Perfusion of Cytochalasin D in corneal fibroblast 3-D culture induces rapid disassembly of stress fibers and focal adhesions, cell elongation, and ECM relaxation without formation and extension of filopodia [58, 88].

Taken together, these studies suggest that Rho GTPase plays a key role in regulating both the morphology and mechanical behavior of corneal fibroblasts in 3D culture [64]. **However, the role of Rho-kinase in mediating corneal fibroblast migration has not been studied previously.** We hypothesize that: 1) The generation of corneal stromal fibroblast forces is mediated by Rho/Rho-kinase activation. 2) Activated corneal fibroblast migration in 3-D collagen matrices is regulated, in part, by the Rho-Rho kinase-actomyosin signaling pathway. To test this hypothesis, we will: a) develop a new tensile culture force monitoring system (t-CFM); b) directly assess the role of Rho-kinase in corneal fibroblast generation of tractional force, using the new t-CFM; and c) Assess the role of Rho kinase on corneal fibroblast migration mechanics, using a novel 3-D nested collagen matrix migration model and 3- and 4-D imaging techniques. The established Rho-kinase inhibitors Y-27632 and fasudil will be used to block activation of Rho-kinase.

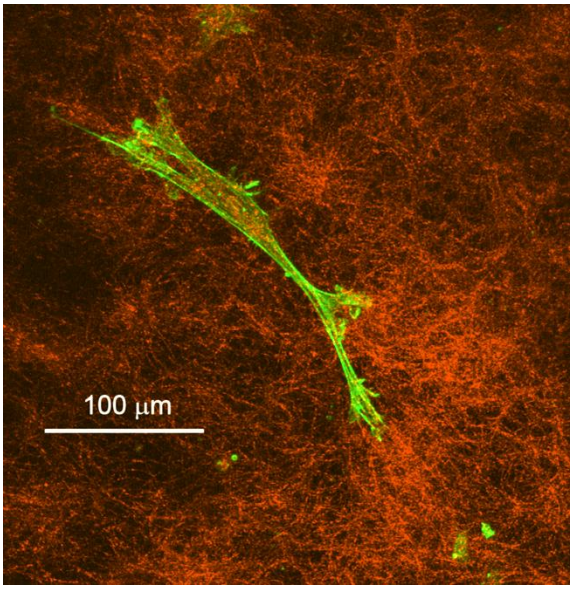

Figure 2.3 : Primary rabbit corneal fibroblast. Confocal image is maximum intensity projection of f-actin (green) and collagen fibrils (red) after 4 days of 10% FBS culture in standard 3-D rat tail collagen matrix.

Transforming growth factor (TGFβ) is secreted by corneal epithelial cells during wound repair. TGFβ1 has been shown to have a weak but significant effect on keratocyte proliferation in 2-D serum-free culture and in ex vivo wounded corneas [10]. TGFβ can also transform keratocytes into myofibroblasts both in vivo and in vitro. Myofibroblasts have up-regulated stress fiber expression, larger focal adhesions, increased fibronectin fibril secretion and assembly, as well as the appearance of α–smooth muscle actin in the cytoskeleton [50]. Studies using CFM on other cell types have clearly demonstrated increased force generation by myofibroblasts [103]. When cultured in 3-D collagen matrices, TGFβ-induced corneal myofibroblasts are much more contractile than the other biomechanical phenotypes induced by

FBS or PDGF. This is exemplified by large amounts of collagen realignment and compaction both locally and globally [66]. Cells in this condition have a spread, stellar morphology (**Figure 2.4**) in the X-Y plane yet fewer cell extensions along the Z-axis [66]. These highly contractile corneal myofibroblasts have an important role in contracting the gap created by incisional corneal wounds, but their presence in vivo has also been correlated with corneal haze [49].

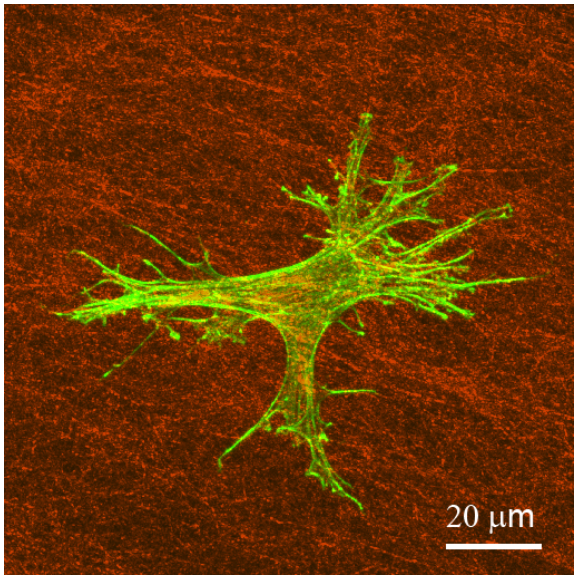

Figure 2.4 : Primary rabbit corneal myofibroblast. Confocal image is maximum intensity projection of f-actin (green) and collagen fibrils (red) after 4 days of TGFβ1 culture in standard 3-D rat tail collagen matrices.

PDGF is endogenously expressed by corneal epithelial cells and also found in the corneal tear film, and keratocytes express the PDGF receptors. Quiescent keratocytes cultured in S- can switch to a more proliferative phenotype when PDGF is added to the media [50]. Studies show that PDGF BB can induce transformation of quiescent keratocytes to a different biomechanical phenotype in vitro. Studies in our lab using restrained 3-D cell/collagen type I matrices

demonstrated that PDGF increases the activation of Rac GTPase and induces cell spreading and extension of numerous dendritic cell processes, which results in an increase in cell length, cell height, cell area and the number of pseudopodial processes (**Figure 2.5**). Extending processes run a tortuous path between and along collagen fibrils and generate small tractional force [90]. No significant stress fiber assembly or strong impact on extracellular collagen remodeling is produced in this model [59]. Quantitative measurement of collagen fibril density and global matrix contraction in the 3-D keratocyte culture model demonstrated that collagen remodeling and compaction induced by primary keratocytes exposed to PDGF is similar to that of the basal media condition, regardless of whether the collagen matrix is made of pepsin-extracted bovine collagen or non-pepsinized rat tail collagen [66]. Direct measurement of tractional force exerted on cell-seeded collagen lattice by chick embryonic fibroblasts (CEF) isolated from 11-day-old chick embryos demonstrated that PDGF and FBS differed in the time course and magnitude of their effects. FBS elicited strong contraction in a rapid phase, while PDGF weakly stimulated a force rise only after a 5-10 min delay [62]. The maximum force reached in the experiment following addition of FBS was 3 times larger than that by addition of PDGF. Moreover, PDGF significantly enhances the migration of corneal fibroblasts at a concentration of 1.0 to 50 ng/mL in vivo and in vitro [46, 59]. PDGF also has a chemotaxis effect on corneal fibroblasts according to studies based on an in vitro transwell assay [61]. We have recently demonstrated that *quiescent corneal keratocytes* cultured in serum-free media can migrate effectively through 3-D collagen matrices when stimulated with platelet-derived growth factor (PDGF), without generating large contractile forces. Thus overall, the PDGF-induced corneal stromal cell

phenotype may facilitate low contractility cell migration during wound repopulation, and may therefore play a critical role in regenerative corneal healing where the clarity of cornea is regained after wound disruption.

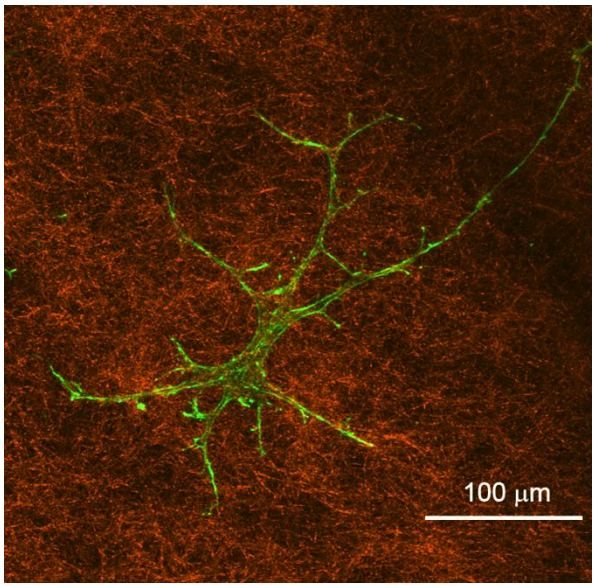

Figure 2.5 : Primary rabbit corneal keratocyte in response to PDGF. Confocal image is maximum intensity projection of f-actin (green) and collagen fibrils (red) after 4 days of PDGF culture in standard 3-D rat tail collagen matrices.

2.3 EXPRESSION OF MMPS IN CORNEA AND THE ROLE OF MMPS IN CORNEAL WOUND HEALING

Members of the large family of Matrix Metalloproteinases (MMPs) have been shown to play essential and highly collaborative roles in various physiological aspects of the corneal wound healing process. In the cornea, MMPs are expressed by corneal epithelial cells, stromal

keratocytes and activated fibroblasts. In the uninjured cornea, proMMP-2 is present in normal corneal epithelium and stroma of rabbits, rats and humans, but is associated with tissue inhibitor of MMP type two (TIMP-2), which blocks its protease activity [8]. MMP-9, collagenases and stromelysin are not normally detected in the cornea [35]. Following injury, however, expression of MMP-2, MMP-9 and other MMP species by activated corneal fibroblasts is elevated [18] and the presence of up-regulated MMP expression has been positively correlated with corneal ulceration, epithelial ingrowth, keratoconus and other complications [7, 15, 29, 30, 72].

In cell culture, primary corneal keratocytes in serum-containing media (corneal fibroblasts) express similar MMP species as those observed during corneal wound healing, such as MMP-2, MMP-9, collagenases and stromelysins [25, 34]. In vitro studies also have shown that MMP expression by corneal fibroblasts is regulated, in part, by growth factors and cytokines found in the tear film, epithelium and stroma during wound healing, such as: interleukine-1 (IL-1), transforming growth factor-β (TGF-β) and platelet-derived growth factor (PDGF). IL-1 (α and β), which is secreted by corneal epithelial cells, can significantly increase MMP production and collagen degradation by corneal epithelial and stromal cells [40, 63, 70, 71, 76]. TGF-β stimulates MMP-2 and MMP-9 secretion by corneal epithelial cells, but has no significant effect on MMP-2 and MMP-9 expression by corneal fibroblasts or myofibroblasts. It also has an inhibitory effect on collagenase and stromelysin secretion [34, 109]. PDGF has not been shown to have a significant effect on MMP expression by either corneal epithelial cells or fibroblasts, with the exception of a slight increase of MMP-2 [68, 86].

While the MMP species described above have been well characterized in corneal studies, a number of less recognized MMP species have been more recently identified in normal and wounded cornea, such as membrane anchored type 1 MMP (MT1-MMP or MMP-14) [11, 14, 84, 101, 116]. MT1-MMP expression is elevated in wounded corneal epithelium and stroma, and studies in an animal model showed that it potentiates basic fibroblast growth factor-induced corneal neovascularization [84]. In vitro, MT1-MMP expression by serum-exposed human corneal keratocytes (fibroblasts) is stimulated by addition of Concanavalin A (Con.A) to the culture system and is significantly correlated with MMP-2 activation [14]. These findings suggest that MT1-MMP may have an important role in regulating the activation of other downstream MMPs. The role of MT1-MMP in corneal wound healing has not been fully elucidated, although MT1-MMP plays an important role in a variety of intracellular and extracellular events of other cell types. In 3-D collagen ECM, MT1-MMP is thought to mediate the matrix degradation and migration process of tumor cells [96].

Following corneal wounding, activated corneal fibroblasts proliferate, migrate into wounded region, generate mechanical force to contract the corneal wound, remodel the provisional matrix, and synthesize new matrix. Due to the resultant ECM being disorganized, these processes are an important cause of corneal haze or fibrosis. These physiological events are accompanied by up-regulated MMP expression/production by corneal fibroblasts [35] and often involve the activities of MMPs [26]. In some cases, the opacity gradually diminishes over time,

due to MMP-dependent remodeling [27]. Meanwhile, endogenous tissue inhibitors of metalloproteinase are also secreted by corneal cells during wound healing [56, 115]. They act in a coordinate manner with MMPs and growth factor/cytokines to form an integrated system to maintain a balance in ECM synthesis and degradation.

In summary, in addition to the forces generated by activated corneal fibroblasts, ECM remodeling is also mediated by the activity of matrix metalloproteinases (MMPs). Migration of activated (contractile) corneal fibroblasts has been shown to be dependent, in part, on MMP expression by the cells. However, we have recently demonstrated that *quiescent corneal keratocytes* cultured in serum-free media can migrate effectively through 3-D collagen matrices when stimulated with platelet-derived growth factor (PDGF), without generating large contractile forces. This low contractility migration may allow cells to repopulate corneal tissue without altering its unique extracellular matrix structure, which is needed to maintain transparency. However, it is not known whether this low-contractility migration mechanism is also dependent on MMPs. We hypothesize that migration of corneal keratocytes stimulated with PDGF can occur in the absence of proteolytic MMP activities. To test this hypothesis, we will **a)** establish the effects of synthetic MMP inhibitors on collagen digestion by rabbit corneal keratocytes (NRK cells), using different growth factors present in cornea and tear film during wound healing (e.g. Transforming growth factor β; PDGF); **b)** determine the effects of MMP inhibitors on corneal keratocyte-induced collagen matrix contraction; and **c)** measure the effects of MMP inhibition on corneal keratocyte migration through 3-D collagen matrices.

2.4 THREE-DIMENSIONAL CELL MIGRATION MODELS

Most previous work on cell motility and MMP regulation have been performed using 2-D substrates. However, cellular interactions with a collagen-coated 2-D substrate are different than what occurs in vivo, because bound, non-fibrillar collagen cannot undergo cell-induced reorganization and alignment. Furthermore, cells reside within 3-D extracellular matrices in vivo, and ECM geometry has been shown to affect cell morphology, adhesion organization and mechanical behavior [3, 4, 16, 17, 21, 32, 37, 92, 102]. An alternative to planar substrates is the fibroblast populated collagen matrix model, in which cells are plated inside a 3-D fibrillar collagen matrix. In this model, matrix contraction occurs predominantly by rearrangement of existing collagen fibrils through the application of mechanical forces. 3-D collagen matrices have been accepted as a standard in vitro model for studying the mechanisms regulating cell mediated matrix reorganization and wound contraction, and measuring overall collagen matrix contraction and/or force generation by fibroblasts. Using this 3-D model has provided valuable insights into the signaling pathways involved in various aspects of cell-matrix mechanical interactions [36]. By extending this model to the study of single cell behaviors and matrix interactions, a more detailed understanding of the pattern of force generation and matrix reorganization at the cellular and subcellular level can be obtained.

A conventional basic migration assay used by many researchers is the transwell migration assay. This model is composed of an upper chamber, a lower chamber and polymer membrane with cell-size pores (often $\leq 10\mu m$) that separates the two chambers. The upper chamber is usually filled with a cell suspension and the lower chamber is filled with culture media containing different growth factors or cytokines. Cells that are attracted by the positive chemotactic growth factors can migrate through the small pores on the membrane from the upper chamber to the opposite side of the membrane. This assay is considered a 2-D migration assay. But it can be upgraded to 3-D cell invasion/migration assay by plating a collagen matrix on top of the membrane. In this model, cells in the upper chamber invade and migrate into the 3-D collagen matrices due to the presence of chemotactic growth factors (such as PDGF) in the lower chamber [96]. The cell migration results can be visualized by staining the cross-sections of the collagen matrices from the experiments. However, this method does not allow direct imaging of the cell migration process and the cell-matrix interactions.

Another commonly used 3-D cell migration assay is a culture construct that consists of a cell-seeded collagen matrix attached on a culture surface, with an additional layer of cell-free collagen covering it [118]. In this model, most cells will migrate on the culture surface, thus the migration is mostly two-dimensional. Another 3-D cell migration model is made of small tissue explants suspended inside 3-D reconstituted collagen gels [31]. In cultivation of this model, malignant tumor explants developed single cell migration, tumor outgrowth, and locomoting cell clusters that migrated within the 3-D collagen matrices [31]. Migrating cells showed a highly

polarized migration front and persistence in the migration direction. In the parallel experiments where malignant tumor explants were cultured on 2-D plastic surfaces without collagen outer matrices, the tumor outgrowth and motility characteristics found in the 3-D collagen culture were not observed. Meanwhile, non-neoplastic tissue cultured in the same 3-D model resulted in only single cell migration. A limitation of this model is that migration of interstitial cells is often hindered by the dense and interconnected natural collagen matrices in the tissue explants. Furthermore, the corneal stroma is maintained in a highly dehydrated state in vivo, and swells dramatically when explanted; thus this technique is problematic when using corneal explants and is highly dependent upon the source of the tissue [55].

Another 3-D cell migration model has been developed which consists of a fibroblast seeded, contracted collagen matrix (also called tissue equivalent) nested inside an acellular collagen matrix [38, 39, 96]. This model simulates the organization of the wound site and is a ture three-dimensional cell migration assay. However, fabricating this model requires pre-incubation of the cell-seeded matrix in serum media to stimulate cell-induced global matrix contraction before encasing the tissue equivalent, and thus it cannot be used for serum-free primary corneal keratocyte studies. Thus for our research, it is important to develop a new 3-D migration model that can mimic the biomechanical environment of corneal wounds while maintaining the keratocyte phenotype. More importantly, the model should be suitable to observing and imaging cell-ECM interactions during cell migration. Our lab has developed a model for directly assessing cell–matrix mechanical interactions during migration in which cell-

seeded compressed collagen matrices (also called the inner matrix, or button) are nested within 3-D acellular uncompressed collagen matrices (outer matrix) [55]. The compressed matrices can be generated rapidly without pre-incubation, and have some similar structural and mechanical properties to native corneal tissue [1, 9]. In the studies described in this dissertation, I modified this nested collagen matrix model to facilitate time-lapse live cell imaging, thereby allowing direct visualization of the pattern of cell–matrix interactions during migration.

2.5 THE TENSIONING CULTURE FORCE MONITOR

The original tensioning culture force monitoring system (t-CFM) was first reported by Eastwood, Brown *et al* in 1994 [23]. A t-CFM system was built in our lab by a previous postdoctoral researcher, Dr.Karamichos, who learned the technique during his PhD research in Dr. Robert Brown's lab. The CFM system was based on a strain measuring beam (denoted as **f** in **Figure 2.6**). The beam (100mm × 10mm) was manufactured from 0.15mm thick Copper-Beryllium sheet. The strip had a transducer class strain gauge in a full bridge network attached to it to measure force-induced bending of the beam. The electrical current from the strain gauge was amplified, analog to digital converted, imported via a data acquisition card in a PC and plotted using a custom program in LabView (**Figure 2.6-2**).

While this system has been successfully used for dermal fibroblasts, which are largely contractile and produce a large signal to noise ratio, it did not work well for corneal fibroblasts.

After extensive tests of the original force transducer constructed by Dr. Karamichos, it was determined that the characteristics of this strain measuring beam had limitations for our experimental application. Problems associated with this apparatus include: thermal drifting of baseline signal, large signal oscillation, significant noise sensitivity in its transduction pathway, nonlinearity of signal when under large beam strain, sensitivity to force perturbations in the environment, sensitivity to transient temperature changes and to small fluctuations in the electrical supply. Furthermore, the physical bonding between the bar and collagen lattice was mediated by a hydrophilic microporous Vyon polymer strip (70mm x 5mm x 5mm). The justification for this was that 'the hydrophilic nature of the Vyon and the hydrophobic nature of the cell channel encourages cell and substrate attachment to the Vyon bar'. However, the bonding force between the Vyon substrate and collagen matrix is largely dependent on the polymerization outcome of collagen monomers, which results in variability in the bonding force from sample to sample. Also, the bonding was often not robust enough to ensure a constant attachment over an extended culture period (>48 hrs). To overcome this limit, Dr.Karamichos replaced the Vyon polymer film with Velcro loop strips. Velcro can better interweave with the collagen matrix and therefore establish a stronger attachment between the bar and the collagen lattice. However, this modification also came with a drawback: The design of the original force transmission bar consisted of a large piece of Velcro that was wrapped around a heavy metal hook. This bar was not buoyant and became so heavy after soaking in media that it created frictional force along the force transmission axis. Overall, the system needed more delicate engineering considerations, such as: a more spacious culture chamber to avoid friction between

the wall and the collagen construct, an adjustable alignment gear for the force transducer, and a less invasive way to injecting drugs to the media than direct syringe injection. Therefore I re-designed the CFM system for the proposed research.

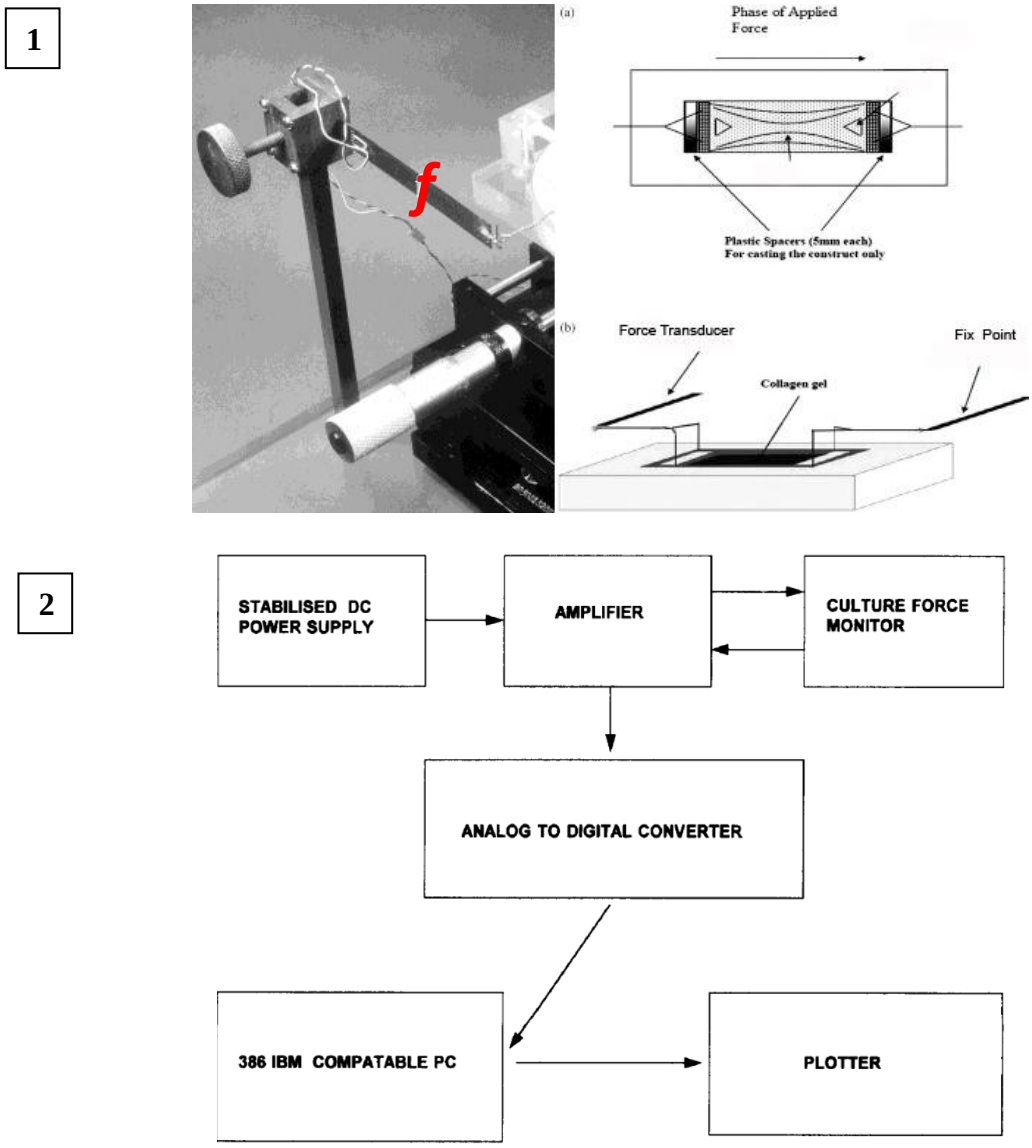

Figure 2.6: (1) The tensioning-Culture Force Monitor [24, 54]. (2) Configuration and work flow of the t-CFM system [23].

CHAPTER THREE
Methodology

3.1 THE ROLE OF RHO GTPASES IN REGULATING THE MECHANICAL BEHAVIOR OF ACTIVATED CORNEAL FIBROBLASTS IN SERUM-CONTAINING MEDIA.

3.1.1 Cell Culture.

A telomerase-infected, extended life-span human corneal fibroblast cell line (HTK) from our lab was used [51]. Cells were maintained in "complete media" (or **S+**) consisting of Dulbecco's modified Eagle's minimum essential medium (DMEM, Invitrogen, CA) with 1% penicillin/streptomycin amphotericin B (Fungizone, Bio-Whittaker Inc., MD) and 10% fetal bovine serum (Sigma-Aldrich, MO).

3.1.2 Development of a New Tensile Culture Force Monitor (CFM) System.

The core module of a force monitor system is a force transducer that has sufficient sensitivity to measure small cellular force. For my application, the measurement scale of a competent cell force transducer needed to cover the range of 0 to ~1g (≈ 1000 Dyne). After a survey of different transducers used in related publications, I selected an isometric tensile force transducer from Harvard Apparatus (MA1 72-4480). This transducer operates on the principle of converting picofarad capacitance changes into an amplified DC output voltage by means of a

patented circuit. The transducer consists of a stiff beam suspended between two capacitor plates. This forms a differential capacitor. Using this principal, the beam can be exceptionally stiff, approaching the ideal of measuring force without motion. The linearity is within ±1% with a high DC voltage output and has minimal drift. The transducer is capable of measuring force from 0g to 0.5g, which produces a voltage output $0 \leq$ and ≤ 5 VDC. The transducer also has an OFFSET control, which can adjust the voltage output to 0 when there is no force applied on transducer. Output voltage signal is transmitted to an analog to digital signal converter (iWorx System Inc., NH) via BNC connection. The digitalized voltage signal is imported into a data acquisition and processing software iWorx LabScribe2 (iWorx Systems Inc., NH) running on a PC platform via USB port. A force versus time curve is plotted by the software in real-time.

The cell force generation core should consist of a cell-seeded polymerized collagen lattice, collagen-attaching bars, force transmitting axis and live cell-supporting milieu. To implement this idea, I engineered a constrained, uniaxial cell force reactor, as illustrated in **Figure 3.1** (#1~#6) below. A pair of vertical bars was placed in the left and right longitudinal ends of the mould. Each bar consisted of a stainless steel handle with a wire loop and a strip of Velcro nylon network adhered to the loop. The cell/collagen lattice was polymerized to the two Velcro strips by soaking the Velcro strip with cold neutralized monomer collagen solution in the mould and then heat-polymerizing the whole construct in a 37 °C, humid incubator for 1 hour. The resultant physical bonding between the collagen lattice and Velcro was strong enough to endure the cellular tensile stress developed near the constrained area, and capable of transmitting

this force to the force transducer. A porous light-weight polymer membrane (Polytetrafluoroethylene, pre-washed, sterilized, cell toxicity checked) was also attached to the bar, which provided sufficient buoyancy to suspend the entire bar structure when culture media was added to the mould (as a culture chamber). This feature helped to minimize the friction that may occur along the force transmission axis. Moreover, a suitable cell culture environment was needed in addition to the mechanical module. A nontoxic autoclavable macropolymer mould was thus custom made to give adequate room for culture media and collagen lattice. To reduce media evaporation and contamination, a custom transparent hood was also made to cover the cell force generation module.

Calibration of the force transducer: To calibrate this force measurement system, a set of small identical weights in the measurement range were made. Each weight has the same 50 Dyne gravity force. The weights were vertically loaded to the sensing head of the force transducer one by one in an ascending manner. The corresponding digital voltage output was recorded at each loading point to give a calibration tensor (x= digital voltage output, y = corresponding actual gravity of weights). The serial data set for (X= digital voltage outputs, Y = actual gravities of weights) was mapped in a plane coordinate system in Office Excel. A linear regression function **'y = a·x+b'** of actual gravity of weights (y) *vs.* the digital voltage output (x) was achieved and coded into the data acquisition and processing software iWorx LabScribe2 to convert the imported voltage data to an accurate force value.

Initial testing of the complete system: Validation tests of this t-CFM were performed. Briefly, $9x10^6$ HTK cells were added into cold, neutralized, monomer rat-tail type I collagen solution (collagen concentration = 2.5mg/mL, BD Bioscience, MA). The solution was then poured into a 75mm (L) x 25 mm (W) x 30 mm (H) rectangular mould and polymerized in a 37 °C incubator for 1 hour. 20 mL of serum-free basal media was added to the mould. The cell seeded collagen lattice was cultured in the S- media for 5 hours so that cells were starving in serum free basal media at the beginning of the experiment. 2 mL of warm pure fetal bovine serum was injected to the basal media to stimulate cell contraction. When the force plateaued for a period of ~16 hours after adding FBS, a small volume (4mL) of warm 100% ethanol was injected into the media chamber, to induce cell death. Monitoring of force generation was paused during the administration procedure to avoid false interference, and resumed 5 minutes after finishing the procedure. The entire experiment was run for ≥60 hrs.

3.1.3 Assessment of the Role of Rho-kinase in Regulating Corneal Fibroblast Force Generation by the t-CFM System.

Tension developed in corneal fibroblast-populated reconstituted collagen lattices by cell tractional force was measured with or without the Rho kinase inhibitor Y-27632 (InSolution, Calbiochem, MA). 9×10^6 HTK cells were added to 9 mL cool, neutralized rat-tail type I collagen solution, to yield final collagen concentration of 2.5 mg/mL. Then the solution was poured into a rectangular 75mm (L) x 25 mm (W) x 30 mm (H) mould. Two vertical stainless steel bars attached with Velcro pads (loop side) and foam pads were inserted in the left and right

ends of the rectangular slot to form physical attachment between the collagen lattice and the force transduction bars. Collagen together with the mould was polymerized in a 37 °C incubator with 5% CO_2 for 1 hr. 20mL 10% FBS media was added to the mould chamber. The entire collagen lattice was carefully detached from the cast surfaces and was free floating in the culture media. One vertical bar was connected to a tensile force transducer. The other bar was attached to a static fixture. The force generation module was completely suspended in media, which helped to minimize friction force in the axis of force transduction. The experimental setup is illustrated in **Figure 3.1** below. The CFM system was built inside a 37 °C 5% CO_2 humidified incubator to provide suitable conditions for cell growth and force generation over an extended time course. 70 Dyne pre-stress was applied to the collagen lattice using a micro-stepping motor (Parker Automation, USA), in order to stabilize the construct and to reduce noise. Cell force monitoring was started right after the application of pre-stress. 40 μL of Y-27632 stock solution was added to the media when the force profile plateaued, which resulted in 10 μM final concentration of Y-27632 in serum media. The after the administration of Y-27632, cell force monitoring continued. The monitoring was ended when a new continuous force plateau was shown on the t-CFM profile.

The force signal sent by the transducer was sampled by a signal acquisition and analysis software iWorx LabScribe2 in a PC system. Sample rate was set to 1 sample/second. Upon finishing of the experiment, the force measurements were exported to MS Office Excel or MatLab for further numerical analysis. Force vs. time profiles were generated.

Positive control for the experiment was the measurement of HTK cell force generation using the same experimental setup and culture conditions described above, except 4mL of pure ethanol was administrated into the culture media when the force generation reached its maximum plateau. Negative control was force measurement of acellular collagen lattice in the same experimental setting and culture condition over the same time course. Experiments were repeated at least 3 times for each condition. Quantitative parameters such as force/hour/million cells in different cell contraction phases were calculated using the t-CFM data record.

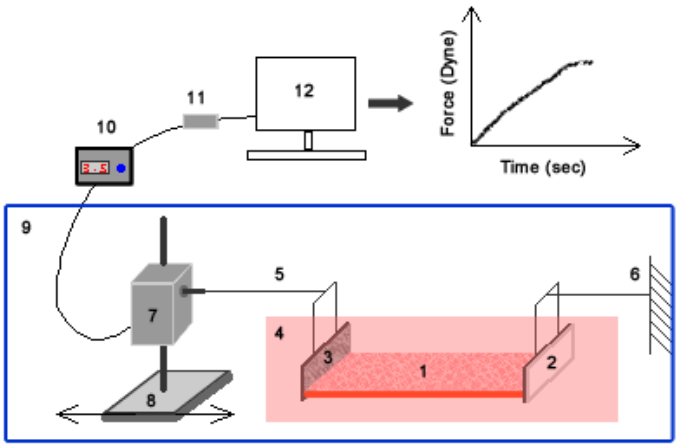

Figure 3.1 : Schematic for cell force measurement system: 1. Cell-populated collagen lattice; 2. Attaching Pad (foam side); 3. Attaching pad (Velcro loop side); 4. Culture media in the mould (covered); 5. Stainless steel bar (free floating side); 6. Stainless steel bar (static side) and height-adjustable fixture; 7. Isometric force transducer, fixed to pole via a height-adjustable vernier; 8. Micro-stepping motor stage; 9. 37 ˚C humidified 5%CO_2 incubator; 10. Output voltage indicator/ amplifier/ power supply. 11. Analog to digital signal converter; 12. Data acquisition software and PC;

3.1.4 Optimization of Live Cell Imaging System and Time Lapse Live Cell Imaging of HTK Migration in the 3-D Nested Collagen Matrix Model.

3.1.4.1 Optimization of the In Vivo® Microincubation System for Live Cell Imaging Application.

Live-cell microscopy and associated techniques have been an integral component of our lab's research in corneal biomechanics. Much of our research has been accomplished using the Biopetch Delta T perfusion system (Bioptechs Inc, PA). This live-cell imaging system is comprised of a media perfusion pump/tubing, objective heater and electronic controller, culture dish heater and electronic controller, and CO_2 ventilation. This perfusion/incubation system allows us to image cell mechanical behaviors in response to changes in growth factor conditions, without any interruption of the imaging process. Although it is innovative, the system is complicated in design and can only sustain proper imaging environments for cells (pH of media, temperature of culture dish) for approximately 12 hours. For instance, a problem associated with the heating system is that the circuit-regulated heater for Delta T culture dish cannot make the temperature converge to 37 ºC smoothly. 20% of the time the temperature is higher than the target temperature. Furthermore, the heat transfer from the heating circuit to the media in the dish is not efficient (due to the thermal conductivity difference in the assembly) and the resultant temperature gradient can exacerbate the temperature fluctuation. Also, because the dish heater only has a small effective heating area (9.5 cm^2), thermal drift in the dish can occur as a result of temperature fluctuations in the room in which the microscope is located. Moreover, the

Bioptechs system requires the use of an exclusively made, disposable culture dish, which significantly increased the cost for live cell imaging experiments.

To overcome these limitations, we switched to another live-cell imaging supporting system: an In Vivo® Scientific microincubation system (In Vivo® Scientific, MO). The in Vivo live-cell incubation system is comprised of a plexiglass microscope incubator, air heater with temperature controller and ventilation tubing, and CO_2 system (electronic CO_2 concentration and flow regulator, an air humidifier, and stage cover with tubing), as shown in **Figure 3.2** below. The most advantageous feature of this incubation system is the stability and uniformity of ambient temperature in the microscope incubator, due to a unique air diffusion grid design in combination with both a directional air input and an air return, according to the manufacture's empirical report, as illustrated in **Figure 3.3**. Moreover, the CO_2 system from In Vivo Scientific is much more sophisticated than the direct CO_2 air ventilation, which greatly extends the applicability of this system to different live-cell microscopies.

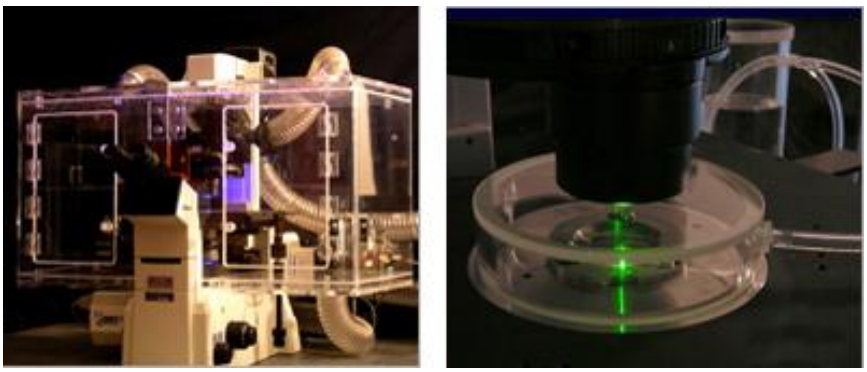

Figure 3.2 : Pictures of *In Vivo* live-cell imaging support system (Left : microscope incubator, heated air tubing. Right: stage cover with tubing, air humidifier. Images are adopted from *In Vivo Scientific* website).

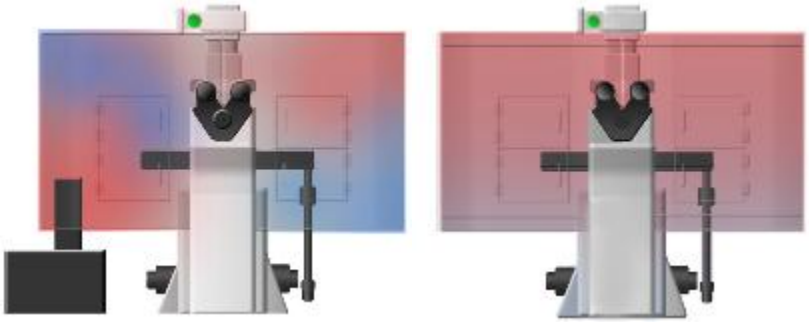

Figure 3.3 : Temperature uniformity of other incubators (left) vs. In Vivo Scientific incubators [51]. Warmer temperature is indicated by red and cooler temperature is by blue (adopted from *In Vivo Scientific* website).

I have performed numerous live-cell experiments with this new system, which has provided an in-depth understanding and allowed optimization for my experiments. To better observe the migration process of corneal cells in our matrix migration model, my goal was to run the live-cell time-lapse imaging for 48 ~ 72 hours in each experiment. This application set a challenge to the environmental stability of the live-cell imaging system. In my initial experiments, I found that after about 24 hours, the culture environment inside the In Vivo system deteriorated rapidly, which had an adverse impact on cell behaviors, and disrupted our

observation of cell migration. I identified three major problems in these pilot long-term live-cell imaging experiments: PH elevation, over-heating and over-evaporation. I speculated that PH elevation in the culture media was due to a large loss in water after 24 hrs culture (approximately 50%), weak buffering of culture media, and insufficient CO_2 concentration. Therefore, I added 0.02M HEPES (Sigma,MO) into the culture media, placed several water dishes inside the stage cover, and increased CO_2 concentration (from 5% to 8%) in the air flow to the stage cover, via the electronic CO_2 regulator. Furthermore, I also measured the spatial temperature distribution in the plexiglass microscope incubator. It was observed that, when the temperature controller was set to 37ºC, although the temperature in microscope stage area had little fluctuation, the temperature was detectably higher than preset (~38ºC). Also the air temperature in the lower level of the incubator was also significantly higher than 37 ºC (~40 ºC), which may also contribute to excessive water evaporation. Thus, I lowered the temperature setting to 35ºC on the temperature controller. The temperature in the microscope stage area was found to decrease to 37ºC, and maintained at this temperature constantly, and the air temperature in lower level of the incubator cooled down to 38 ºC. To provide a less dynamic air atmosphere and in order to minimize water evaporation, I reduced the flow speed of CO_2 air flow perfused into the stage cover to14 mL/min from the default 50mL/min on the CO_2 regulator, and also reduced the fan speed of the temperature controller from 100% to 40%. Following these optimizations to our In Vivo live-cell imaging support system, our time-lapse imaging experiment was able to run for over 3 days without any apparent changes in cell activity or viability.

3.1.4.2 20× DIC Time Lapse Live-Cell Imaging of HTK Migration in the 3-D Nested Collagen Matrix Model

Compressed collagen matrices were made using the procedure developed by Brown and coworkers [9]. Briefly, approximately 1mL of acetic acid-resolved rat-tail type I collagen was diluted in 4mL 0.02 N acetic acid, followed by adding 0.6 mL of 10x MEM (Invitrogen, MD). After drop-wise neutralization of the collagen mixture with 1N sodium hydroxide, a suspension of ~ 7 x 10^6 HTK cells in S+ media was added to the collagen mixture. Final concentration of the collagen solution was ~ 2.5mg/mL. The neutralized solution was then poured into a 3 x 2 x 1cm rectangular mould, and incubated in humidified incubator at 37°C for polymerization. The polymerized gel was then compacted by compression and blotting, as illustrated in **Figure 3.4**. In detail, a layer of nylon mesh (~50μm mesh size) was placed on top of filter paper. The collagen gel was placed on this nylon mesh, covered by another layer of nylon mesh and a pane of glass, and loaded with a stainless steel weight for 5 minutes at room temperature. This leads to the formation of one flat collagen sheet approximately 250 microns thick. 15-20 buttons (6 mm diameter) were cut from the compressed collagen sheet using a 6mm diameter corneal trephine, and washed in media. Each button was embedded in a drop of cold neutralized bovine Type I collagen solution (final concentration ~2.5 mg/mL; PureCol, Advanced BioMatrix, Inc., CA) spread on a glass bottom culture dish (MatTek, MA). The construct was then incubated in humidified in 5% CO_2 atmosphere at 37 ºC for 1 hour. Each of the nested matrix constructs was then overlaid with 2 mL of media containing either 10% FBS, 1% FBS, 1%FBS + 10μM Y-27632, 1%FBS + 50μM Y-27632, or 1%FBS + fasudil (HA-1077, 20 μM, Sigma).

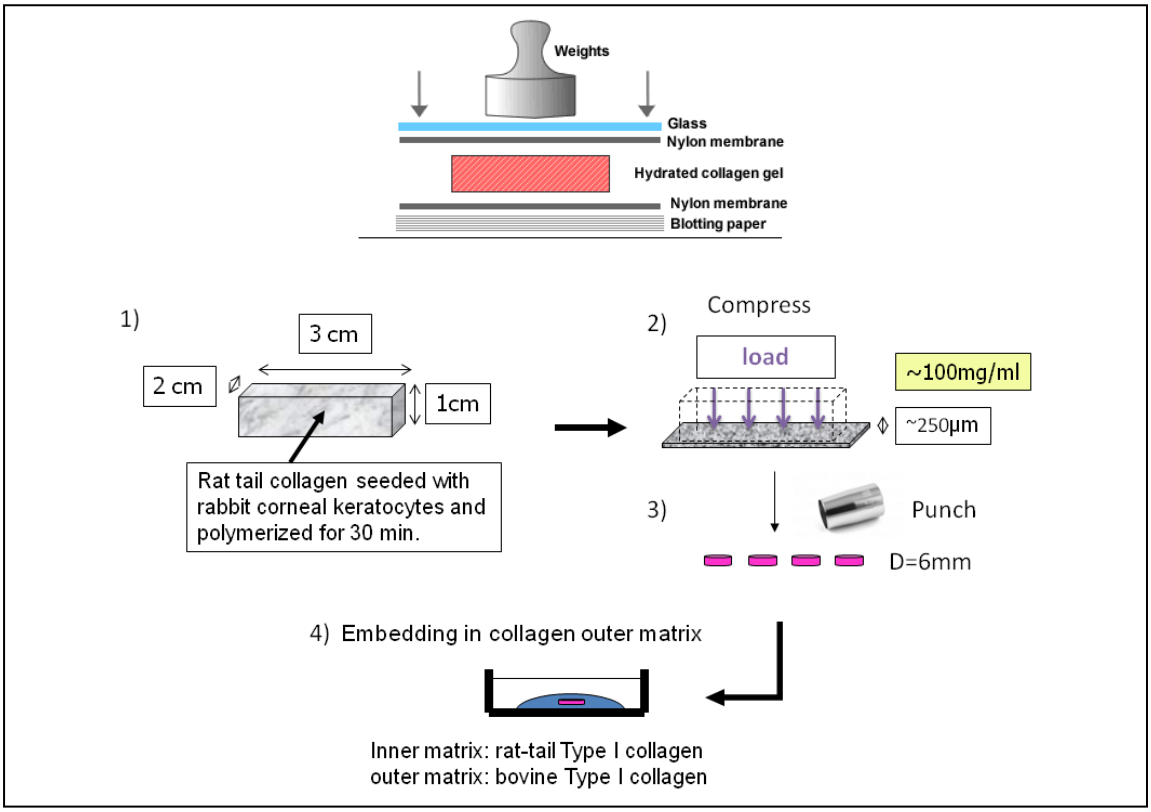

Figure 3.4: Experiment setup for mechanical compression of cell-seeded collagen gel.

In some experiments, to better assess the contractility of migratory cells, an aliquot of carboxylate-modified red fluorescent latex bead stock solution (2.0 µm diameter, Molecular Probes, OR) was mixed with the hydrated non-cellular collagen solution for the outer matrix at a 1:10 (v/v) ratio prior to polymerization.

After one hour of incubation, 20× live-cell imaging of the samples was performed using a Nikon TE300 inverted microscope equipped for time-lapse differential interference contrast

(DIC) imaging. The optimized In Vivo® live-cell imaging support system was used to control temperature, humidity and CO_2 concentration of the atmosphere for the culture samples during time-lapse imaging (see **section 3.1.4.1**). All media used for the time lapse experiments were supplemented with 0.02M HEPES. At each 15 minute time interval, a 3-D DIC image stack of optical sections was collected from the top to the bottom of the construct, at the interface of the inner and outer matrices, using Nikon Elements image acquisition software (Nikon Instruments, NY). Imaging was run for 48 hours and produced a 4-D dataset which captured the cell migration process from the inner matrix to the outer matrix. Triplicate experiments were performed for each condition.

3.1.5 Cell Migration Speed and Bead Movement Analysis using 4-D DIC Image Stacks of HTK Cell Migration in the 3-D Nested Matrix Model.

Time-lapse sequences for one particular z-plane were extracted from the 4-D DIC image stacks of HTK cell migration. In some experiments, there was a shift in the position of the edge of the inner matrix over the course of the experiment. The "Align Stack" tool in MetaMorph software (version 7.7, Molecular Devices, CA) was used to correct for this shift prior to quantitative analysis. Beads in outer matrices were manually tracked using the "track points" module of MetaMorph, and the X-Y coordinates were logged into an Excel file. A custom written "C" program then generated tracks of bead movement over time [87]. To measure cell migration paths, movement of the cell nuclei were tracked using the same procedure. Noise can accumulate when tracking every frame over a long time-lapse experiment, which could reduce

the reliability of those results. Thus we used net bead and cell displacements for quantitative analysis (measured from first and last frames in a sequence) to avoid this issue. Analysis was also limited to beads that were beyond the leading edge of the migration front.

3.1.6 Confocal Imaging of Migratory Corneal Fibroblasts in the 3-D Nested Matrix Model with and without Rho-kinase Inhibition, Followed by Quantitative Analysis.

After 3 days of culture, samples from the migration experiments were fixed in cold 3% paraformaldehyde and conjugated with Alexa Flour 488 Phalloidin (1:50, Molecular Probes, OR) for f-actin labeling, and propidium iodide (PI, 1:100, Molecular Probes, OR) for cell nuclei labeling. Laser confocal fluorescence and reflection microscopy (Leica SP2, Heidelberg, Germany) of the samples was performed at 3 excitation wavelengths: 488 nm (Argon laser) for f-actin, 543 nm (GreNe laser) for PI, and 633 nm (HeNe laser) for confocal reflection imaging of the fibrillar collagen. Each migration sample was scanned following the regime of scanning as shown in **Figure 3.5**. 4 regions across the interface of the inner matrix and outer matrix were randomly selected for each sample. A 3-D confocal image stack of optical sections was acquired for each region, imaged by changing the position of the focal plane in 10μm steps using a 20× objective (non-immersion) or 1 μm steps using a 63x objective (water immersion). When the sample was imaged using the 20× objective, multiple overlapping image stacks were taken for each region until the leading edge of migratory front was reached. Maximum intensity projection images of f-actin and PI were generated for each Z-series stack in MetaMorph and overlaid with reflection images. Photoshop (version CS3, Adobe, CA) was then used to stitch

together these overlapped images, resulting in a 750 μm wide montage image for each quadrant. As an index of cell migration, the average number of cells per 750 μm wide region that had migrated out of inner matrix was counted (n=3). The distance that cells had traveled was also calculated, by drawing a straight line between the interface and the leading edge cells – an average of 10 cells was used for each image of each experiment.

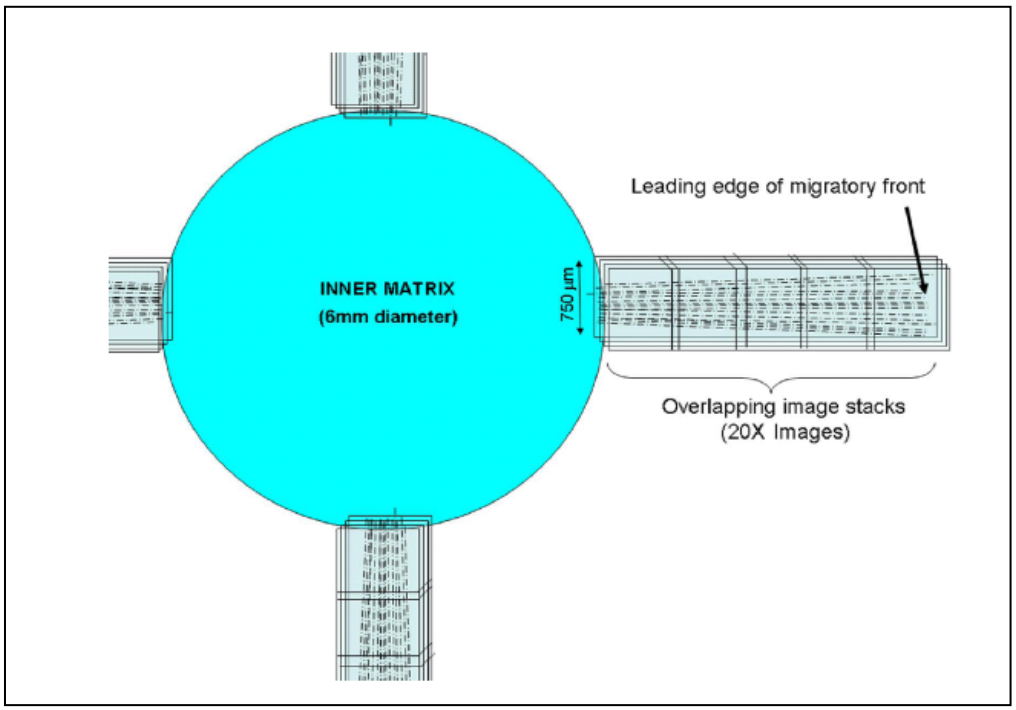

Figure 3.5 : Schematic showing the montage of 3-D image stacks collected in each sample using laser scanning confocal imaging.

3.2. THE ROLE OF MATRIX METALLOPROTEINASES IN QUIESCENT KERATOCYTE MIGRATION INSIDE 3-D COLLAGEN MATRICES.

3.2.1 Materials

Dulbecco's modified Eagle medium (DMEM), MEM non-essential amino acids and 0.25% trypsin/EDTA solution were purchased from Invitrogen (Gaithersburg, MD). Platelet-derived growth factor BB isotype (PDGF), GM6001 (also known as galardin or ilomastat) were obtained from Millipore (Billerica, MA). BB-94 (also known as batimastat) was purchased from Tocris (Bristol, UK). Fetal bovine serum (FBS), fatty acid-free and fraction V bovine serum albumin (BSA), RPMI vitamin mix, HEPES, DMSO, thymidine and Sodium bicarbonate were obtained from Sigma-Aldrich (St. Louis, MO). Penicillin, streptomycin, and amphotericin B were obtained from Lonza inc. (Walkersville, MD). Type I rat tail collagen was purchased from BD Biosciences (Bedford, MA). PureCol® Type I bovine collagen was purchased from Advanced BioMatrix, Inc. (San Diego, CA). Alexa Fluor 488 and Propidium Iodine (PI) were obtained from Molecular Probes, Inc. (Eugene, OR). Collagenase D from Clostridium histolyticum and RNase (DNase free) were purchased from Roche (Indianapolis, IN). Rabbit eyes were purchased from Pel Freez (Rogers, AR). Human glu-plasminogen was purchased from Haematologic Tech (Essex Junction, VT). Glass bottom dishes were purchased from MatTek (Ashland, MA). MT1-MMP mouse-anti-human monoclonal antibody was purchased from Santa Cruz (C9, Santa Cruz, CA).

3.2.2 NRK Cell Culture and NRK Cell Proliferation Assay in 3-D Collagen Matrices in the Presence or Absence of MMP Inhibitors.

3.2.2.1 Cell Culture

Corneas were harvested from rabbit eyes (Pel Freez, Rogers, AR) as previously described [66]. Briefly, to isolate the stromal keratocytes (NRK), corneas stripped of both endothelium and epithelium were placed in a solution of collagenase (KGMP) overnight at 37 ºC. The keratocytes were dispersed in the solution, centrifuged and re-suspended in serum-free basal media [111] consisting of DMEM containing pyruvate (Invitrogen, CA), supplemented with HEPES (Sigma-Aldrich, MO), 1% RPMI media (Sigma-Aldrich, MO), 1% 100x MEM non-essential amino acids (Invitrogen, CA), 100μg/mL ascorbic acid, and 1% penicillin, streptomycin, amphotericin B (BioWhittaker, MD) to maintain the keratocyte phenotype [106]. Keratocyte suspensions were seeded into tissue culture flasks in a 37 ºC, 5% CO_2 humidified incubator and cultured for up to 7 days before use.

3.2.2.2 Cell Proliferation Assay

Hydrated collagen matrices were prepared by mixing acid-resolved, monomeric rat tail Type I collagen with 10× DMEM to achieve a final collagen concentration of 2.5 mg/mL. After adjusting the pH to 7.2 by addition of NaOH, a suspension of cells was immediately mixed with the above collagen solution to achieve a final cell density of 125 cells/μL. A 40 μL aliquot of the cell/collagen mixture was evenly spread over a circular central region on glass bottom dishes. The specimens were then incubated for 30 min at 37 ºC to allow polymerization of the collagen,

followed by overnight pre-culture in S- media. The dishes were randomly assigned to different experimental conditions (3 samples/condition) and media was changed to S- supplemented with PDGF-BB [50 ng/ml] and either GM6001 [25μM], BB-94 [8μM] or DMSO (vehicle control, same dilution ratio). Dishes were then cultured for an additional 4 days. In some experiments, 2mM thymidine was also added to the media to evaluate its anti-proliferation effect.

Following overnight pre-culture and after 4 days of culture, cells were fixed using 3% paraformaldehyde in phosphate buffer for 10 min and permeabilized with 0.5% Triton X-100 in phosphate buffer for 3 minutes. Propidium iodine (1:100) and RNase were then added to each construct to stain the cell nuclei. Cells were then incubated for 15 minutes and washed with PBS (3 times for 5 minutes). After labeling, fluorescent images were acquired using laser confocal microscopy (Leica SP2, Heidelberg, Germany). 3-D image stacks of cell nuclei were acquired by optically scanning throughout the entire thickness of the matrix, in 3-4 randomly chosen 10X fields for each dish. Maximum-intensity projections were used to combine all of the cell nuclei in a 3-D stack into one image. The overall cell density of each culture condition was calculated by counting the number of cells in each projected image.

3.2.3. Effect of Growth Factors and MMP Inhibitors on Type I Collagen Degradation by NRK cells

3.2.3.1 Collagen Matrix Dissolution Assay

A collagen matrix dissolution assay [5] was used to test the ability of NRK cells to degrade polymerized rat tail collagen extracellular matrices in response to different growth factors in vitro, and to evaluate the inhibitory function of BB-94 and GM6001 on MMP activities. An aliquot of cell suspension containing 5×10^4 cells was dropped onto the center of a dry, polymerized, fibrillar rat tail Type I collagen film that had been pre-coated on every culture surface of a multiple well plate. The droplet of cell suspension was incubated at 37 ºC for 5 hours to ensure cells attached to the collagen substrate. Cells were overlaid with S- media and cultured overnight to allow cell spreading. On the second day, media were switched to S- supplemented with selected growth factors (1mL/well) and either GM6001, BB-94 or DMSO. In some experiments, 20μg/mL human glu-plasminogen was added to the media to activate latent soluble MMPs (Pro-MMPs). The plates were cultured for 7 days, followed by trypsin digestion to remove all of the cells from the collagen films. Coomassie blue staining was then used to visualize the dissolution pattern cells produced on the collagen film. Photos of the stained wells were taken using a digital camera.

3.2.3.2 Fluorimetric DQ-Collagen Degradation Assay and Live Cell Confocal Imaging

For quantitative assessment of collagen degradation by NRK cells in different culture conditions**,** a fluorimetric assay based on FITC-conjugated dye-quenched collagen Type I (DQ-collagen) was developed [114]. Cold, neutralized, acid-resolved rat tail Type I collagen solution was mixed with DQ-collagen Type I (20:1 v/v) and an NRK cell suspension. 80μL of the cell-collagen mixture was immediately spread over each well (5×10^4 cells/well) of a 12-well plate in an ice bath. The plates were incubated at 37 ºC for 50 min for polymerization, followed by overnight culture with 1mL/well of S- media. On the next day, all culture wells were supplemented with or without PDGF-BB [50 ng/ml], and with either DMSO vehicle, BB-94 [8μM], or GM6001 [25μM]. All media were phenol-red free. The positive control for the experiment group was a set of wells with the same DQ-copolymerized collagen substrate, incubated with 1mg/mL purified collagenase from Clostridium histolyticum. The negative/background control was no-cell DQ-copolymerized collagen incubated with S- media. Culture supernatant was sampled at 1 and 4 days. FITC fluorescence intensity of the supernatant was measured in a fluorescence microplate reader equipped with standard FITC fluorescent filters (Synergy2, BioTek). Background fluorescence measured from the negative control was subtracted from each measurement. For each condition, the relative fluorescence intensity was the average of 4 experiments.

For 63× laser scanning confocal imaging of the DQ-collagen degradation pattern in the live cell culture, the samples were prepared in the same manner as described above except that

cells were cultured on MatTek glass bottom dishes. Following the overnight S- culture, media were supplemented with either: 1) Interleukine-1α w. Human plasminogen; 2) PDGF-BB; 3) 10% FBS; or 4) left unchanged (S- basal control). In some experiments, the cell culture samples were further supplemented with BB-94 [8μM]. Cells were cultured for an additional 4 days. Live cell confocal imaging of the DQ-collagen/cell culture samples was performed on the 4th day of culture, using a Life Imaging Services (Basel, Switzerland) temperature + CO_2 control system.

In order to give comparable image data between samples, we used the same excitation laser intensity and offset, the same Z-axis scanning step size, and the same image acquisition parameters. For each culture condition, at least two cell culture samples were scanned to get multiple 63× confocal image Z-stacks. FITC fluorescence images, confocal reflection images, and DIC images were simultaneously acquired through areas of interest in the 3-D matrices. Z-axis image stacks were maximum-intensity projected to visualize the overall morphologies of cells.

3.2.3.3 Membrane Type 1-MMP (MMP-14) staining

S- cultured primary NRK cells were seeded on collagen-coated MatTek dishes and pre-cultured in S- media overnight for cell attachment and spreading. Following the overnight S- culture, media were changed to either Interleukine-1α w. Human plasminogen or PDGF-BB. Cells were then cultured for an additional 4 days. At the end of culture, cells were fixed in 3% paraformaldehyde for 10 min, blocked by 1% BSA for 1 hour, labeled with MT1-MMP mouse-anti-human monoclonal antibody (1:50) overnight at 4°C, then washed in phosphate buffered

saline (PBS; 3 times for 5 minutes) and conjugated with secondary FITC goat-anti-mouse antibody (1:1000) for 1 hour at room temperature. After immunochemical labeling, the samples were imaged using laser scanning confocal microscopy (Leica SP2, Heidelberg, Germany). Fluorescent confocal (for MT1-MMP) and DIC images were obtained simultaneously with a water-immersion 63× objective (1.2 NA, 220 μm free working distance). Z-axis image stacks were maximum-intensity projected to 2D images to display the overall morphologies of cells.

3.2.4 Investigation of the Role of MMPs in Cell-induced Matrix Contraction in 3-D Collagen Matrices.

3.2.4.1 Global Matrix Contraction Assay

Primary NRK cells were seeded within reconstituted rat tail Type I collagen. 30μL of this cell-collagen mixture (containing ~50,000 cells) was spread over a 10 mm diameter circular region on a MatTek dish and then polymerized at 37 ºC. Since the bottom of the matrices remain attached to the dish, cell-induced contraction results in a decrease in matrix height [36]. The height of each matrix was measured by focusing on the top and bottom of the matrix at 5 different locations at day 1 and day 4, using a 20X DIC imaging as previously described [65]. Measurements were performed in triplicate for each culture condition, and repeated 3 times. The percentage decrease in matrix height over time was then calculated.

3.2.4.2 Assessment of Cell Morphology and Local Matrix Reorganization

At the end of each Global Matrix Contraction experiment (4 days), cells were fixed, permeabilized, labeled with Alexa Fluor 488 Phalloidin (1:50) for 1 hour and then washed in phosphate buffer saline (PBS; 3 times for 5 minutes). After labeling, fluorescent (for f-actin) and reflected light (for collagen fibrils) confocal images were acquired simultaneously using a 63X objective. A HeNe laser (633nm) was used for reflection imaging, and an Argon (488 nm) laser was used for fluorescent imaging of f-actin.

Maximum intensity projection images of f-actin were then generated in MetaMorph. The images were then imported into Image J and segmented to produce binary images, from which cell outlines were generated. Quantitative morphometric measurements were made from each cell outline using the 'Analyze Particles' module in Image J. For each experimental condition, measurements were taken on 24 single cells randomly sampled from 4 day culture samples.

3.2.4.3 Assessment of Dynamic Cell Activity

Cell-seeded collagen matrices were prepared as described for *Global Matrix Contraction Assay,* except with a lower cell density (6000 cells/dish). Live-cell imaging was performed using a Nikon TE300 inverted microscope equipped with an environmental chamber (In Vivo Scientific, MO) [119]. 20X differential interference contrast (DIC) images were collected at 20-min intervals for 24 hrs (72 intervals total). To measure the dynamics of cell protrusion and retraction over 24 hrs, a custom circular grid was overlaid on each cell (**Figure 3.6**). The grid

consisted of 5 rings; each 52 μm (80 pixels) wide. Each ring was divided into an inner and outer region. The number of cell process segments within each region was counted at each time point. The change in the numbers of process segments from one time interval to the next was then calculated for each ring. The cumulative and normalized dynamics of cell activity over 24 hrs was then calculated for each cell using following equations:

$$\textbf{\textit{Cumulative Dynamics}} = \sum_{i=1}^{5} \sum_{j=1}^{71} \left| N_{i,j} - N_{i,j+1} \right| \qquad \text{(Equation 1)}$$

$$\textbf{\textit{Averaged Total Number of Segments}} = \left(\sum_{j=1}^{72} \sum_{i=1}^{5} N_{i,j}\right)/72 \qquad \text{(Equation 2)}$$

$$\textbf{\textit{Normalized Dynamics}} = \frac{Cumulative\ Dynamics}{Averaged\ Total\ Number\ of\ Segments} \qquad \text{(Equation 3)}$$

i = ring number, ***j*** = time interval, $\mathbf{N}_{i,j}$ = total number of process segments in ring ***i*** at time interval ***j***. For each culture condition, dynamics were calculated using 10 randomly picked cells.

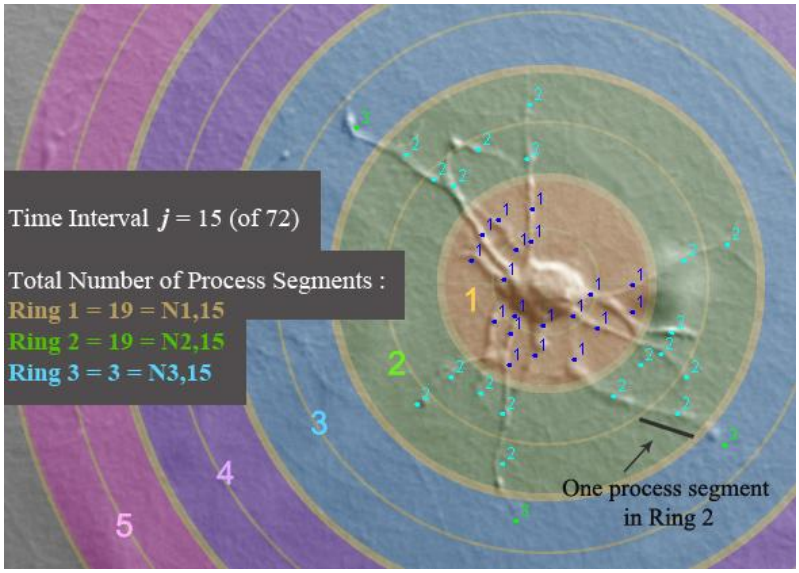

Figure 3.6 : An example of cell dynamics analysis based on a circular grid. Each colored circular ring has a radial width of 52 microns. To evaluate the length of cell protrusion and

retraction more accurately, each colored band was bisected so that a process 26< and ≤ 52 microns in length was counted as 2 segments, and a process segment ≤ 26 microns in length was counted as 1 segment. The number of process segments/ring was counted manually at each time point using Image J and logged. The change in the number of segments from one interval to the next was used as an indicator of the frequency and amount of pseudopodial extension and retraction.

3.2.5 Investigate Dependency of Corneal Keratocyte Migration on MMPs Using the 3-D Nested Collagen Matrix Migration Model Developed in 3.1.4

Nested collagen matrices were prepared as outlined in **Figure 3.7.** Compressed collagen matrices were first prepared as described previously by Brown and coworkers [9]. Type I rat tail collagen was diluted using 0.02N acetic acid and 10× DMEM. After drop-wise neutralization with 1N NaOH, a suspension of 8×10^6 keratocytes basal media was added to the collagen mixture. The solution containing cells and 2.5mg/mL collagen was poured into a 3×2×1cm stainless steel mould and allowed to set for 30 minutes at 37°C. Matrices were then compacted by a combination of compression and blotting. A layer of nylon mesh (~50 μm mesh size) was placed on a double layer of absorbent paper. The polymerized matrices were placed on the nylon mesh, covered with a second nylon mesh, and loaded with a 130 g stainless steel block for 5 min at room temperature. This process squeezes media out of the matrix, leading to the formation of a flat, cell/collagen sheet with high mechanical stiffness. To produce the nested matrix, 6 mm "buttons" were then punched from the compressed matrix and placed within acellular uncompressed Type I collagen matrices [119]. The outer matrices were made from either rat tail collagen or bovine collagen. The constructs were placed in a humidified incubator for 60 minutes to allow polymerization of the outer matrix. Constructs were then overlaid with 1.5ml of S-

media. After overnight pre-incubation, media was replaced with either S- or S- plus PDGF BB, supplemented with either GM6001, BB-94 or DMSO. In some experiments, media was also supplemented with 2mM thymidine in order to inhibit cell proliferation.

After 4 days, constructs were labeled with Alexa Fluor 488 Phalloidin and Propidium Iodide, as described above in '***3.2.4.2 Assessment of Cell Morphology and Local Matrix Reorganization***'. After labeling, fluorescent (for f-actin and nuclei) and reflected light (for collagen fibrils) 3-D confocal image stacks were acquired simultaneously. In order to assess overall cell migration into the outer matrices and the associated subcellular cytoskeletal changes, four regions across the interface of the inner and outer matrix and encasing the migrating front of cells were randomly selected. A 3-D confocal image stack was acquired for each region imaged by changing the position of the focal plane in 5μm steps in the Z-axis using a 10× objective (**Figure 3.8**). Maximum intensity projection images of f-actin and PI were generated for each 3-D confocal image stack, and were overlaid with reflection images of the collagen. The 10× projection images were used to create a 1.5mm wide montage image for each quadrant. As an index of cell migration, the average number of cells that had migrated out of inner matrix was counted in each quadrant. The distance that cells had traveled was calculated by drawing a straight line between the interface and the leading edge cells – an average of 10 cells was used for each montage.

Live cell time-lapse DIC imaging of migration in the construct was also performed, using the Nikon system described above. At each time interval, a 3-D DIC image stack was collected from the top to the bottom of the construct, at the interface of the inner and outer matrices. Images were collected every 15 minutes for 48 hours. This produced a 4-D dataset which captured the cell migration process from the inner matrix into the outer matrix. Triplicate experiments were performed for each condition. Time-lapse sequences for single planes of interest were extracted from the 4D stack.

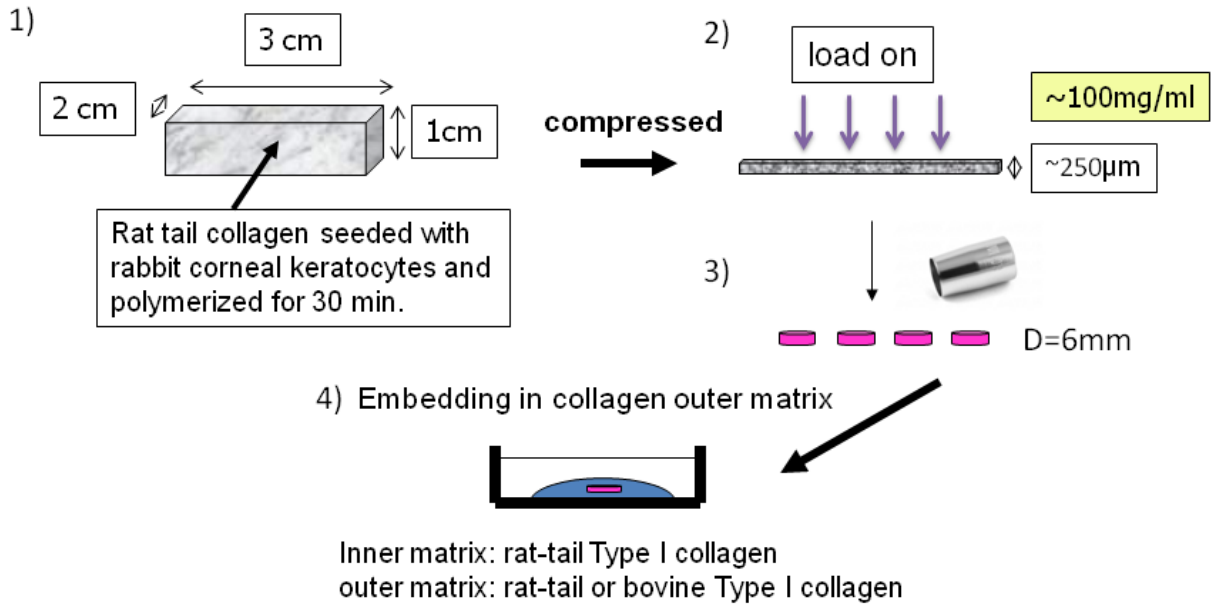

Figure 3.7: Schematic for constructing nested matrix model

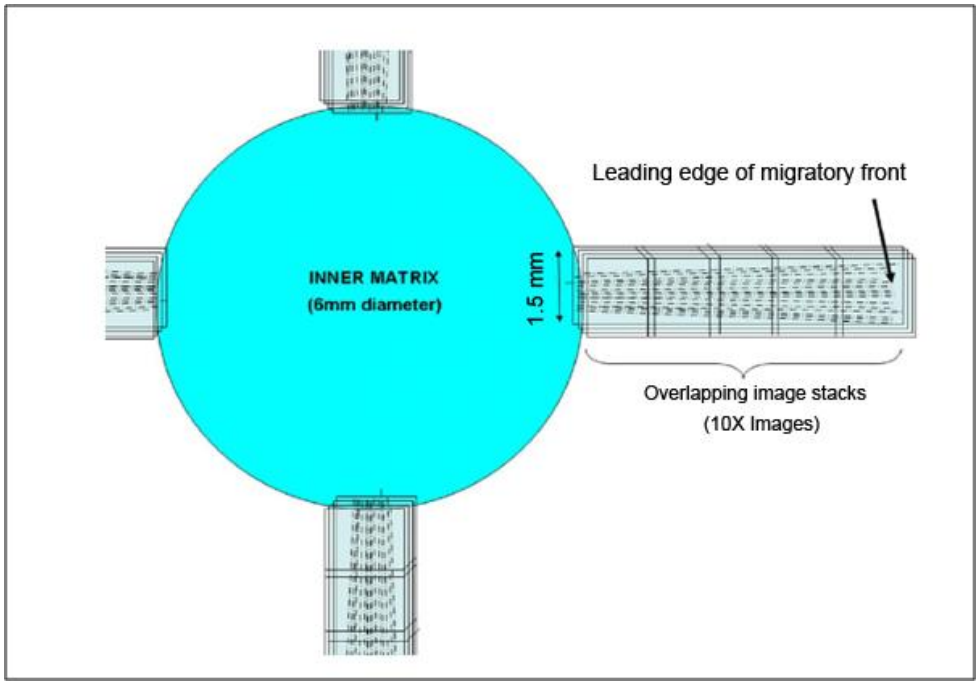

Figure 3.8: Schematic showing the montage of 3-D image stacks collected in each sample using laser scanning confocal imaging.

3.2.6 Statistics

All statistical analyses were performed using SigmaStat version 11.0 (Systat Software Inc., CA). Analysis of variance (ANOVA) was used to compare group means. Post-hoc multiple comparisons between groups were performed using the Holm–Sidak method. Differences were considered significant if $P<0.05$.

CHAPTER FOUR
Results

4.1 RHO KINASE REGULATION OF FIBROBLAST MIGRATORY MECHANICS IN FIBRILLAR COLLAGEN MATRICES

4.1.1 Performance of the Tensile Culture Force Monitoring System

4.1.1.1 Results of Force Transducer Calibration

The voltage output of the force transducer must be converted to a force value in Dynes (=10^{-5} Newton) via a ratio factor (Dyne/Volt). The output signal was calibrated by using a set of small 50 Dyne weights, in the range of expected tensional force applied to the transducer sensing head in our experiments.

As shown in the calibration results (**Figure 4.1**), all of the voltage output of the force transducer is linearly related to the actual gravity force applied (from the standard weights). The converting factor is 99 Dyne/Volt and the function of applied cell-induced tensional force **y** to the voltage output of the force transducer **x** is **$y = 99 \cdot x + 0.4854$**. This function was coded into the data acquisition and processing software to convert all the voltage signals acquired from the transducer into actual forces at the time of measurement. This linearity between force and voltage output provided a reliable, responsive and accurate infrastructure for the force monitoring system.

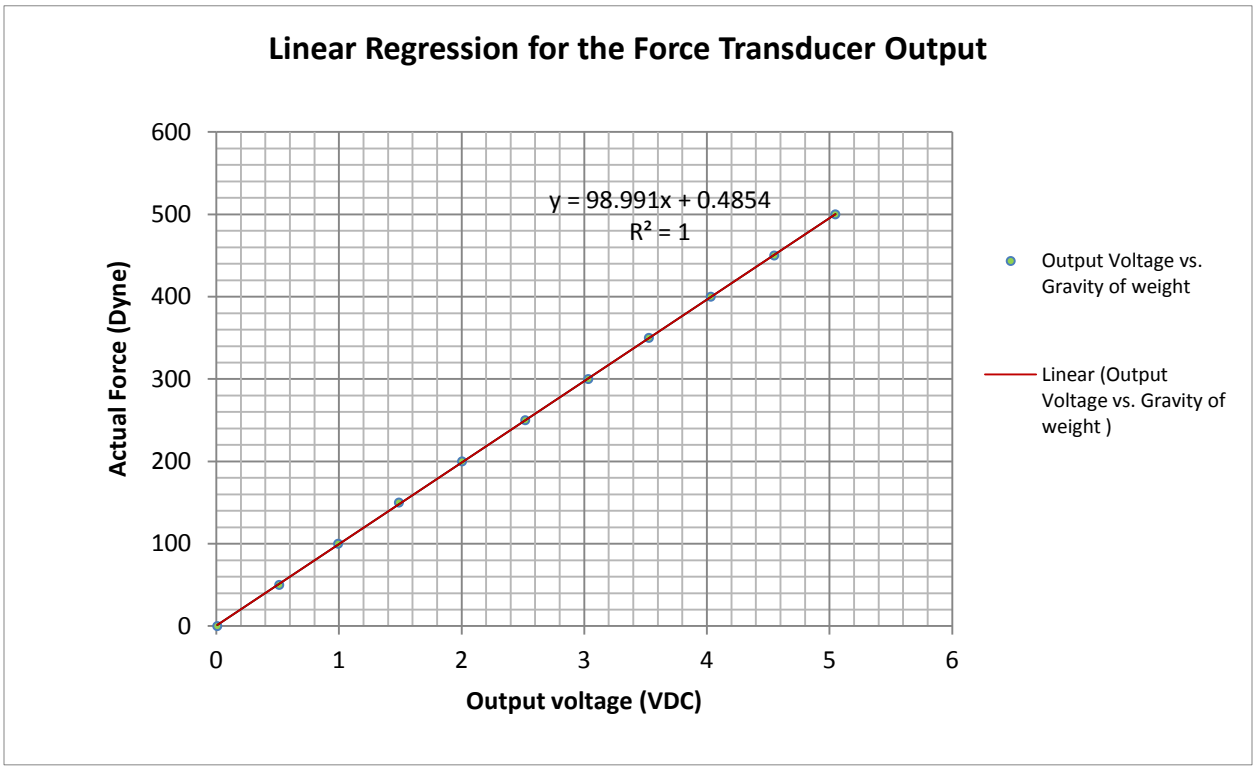

Figure 4.1: Linearity of voltage output by the force transducer. Test was done in accordance with the method described in 3.1.2.

4.1.1.2 Results of Validation Experiments with Ethanol

The t-CFM system was successfully developed and tested for cellular force generation monitoring. A representative t-CFM profile recorded by the system during a validation test is shown in **Figure 4.2**. In the validation test, HTK cells were starved in serum free basal media at the beginning of the experiment, and therefore generated little contractile force. As a response, the t-CFM system did not show significant force generation in the profile during period of the serum free culture (from 0 ~ 19.5 hours). After a small volume of pure fetal bovine serum was

injected into the basal media to activate the Rho GTPase and stimulate cell contraction, cell tension in the force reactor increased. When the force increased to plateau, 4 mL warm 100% ethanol was injected into the media chamber, to induce cell death. Consequently, a substantial force drop in the force profile was observed after adding ethanol, as indicated by the sharp descending curve in the representative t-CFM profile in **Figure 4.2** below. The experiment was repeated 3 times. Evident and consistent cell force decreases after the ethanol poisoning were recorded by this t-CFM system in all of the experiments. The residual force is consistent with previous studies and is likely due to “permanent” remodeling of the collagen.

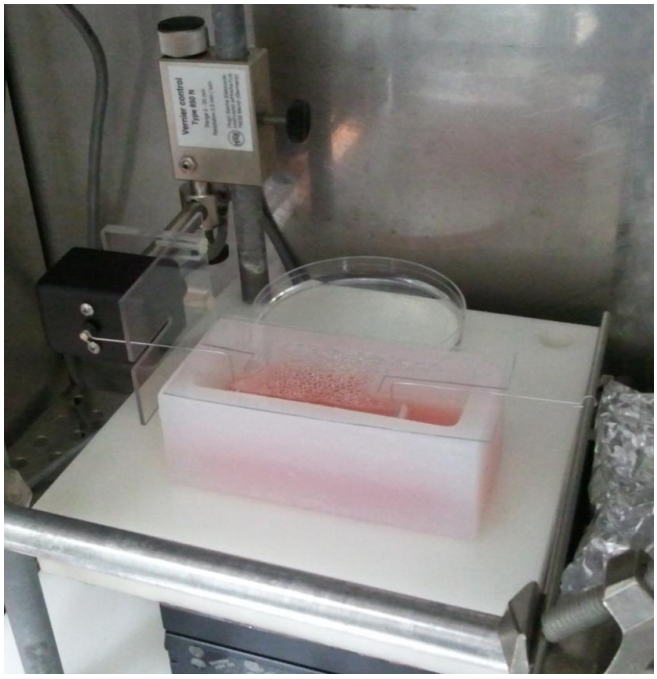

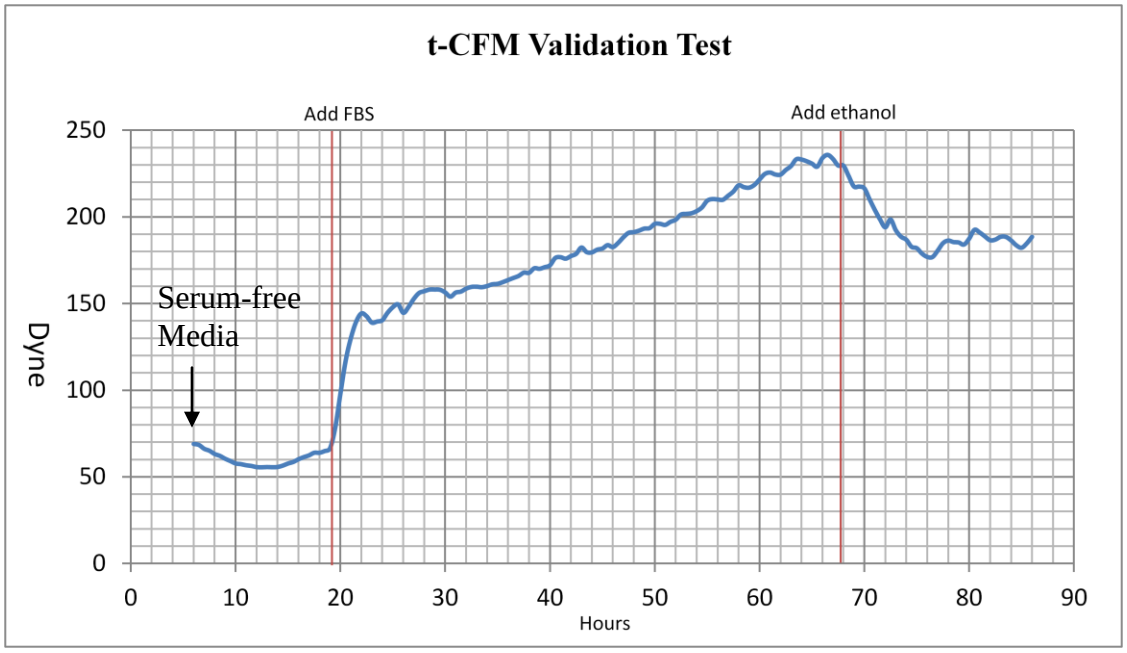

Figure 4.2: (A) The force generation core of the t-CFM system. (B) A representative t-CFM profile from a validation test using HTK cells. There is little cell-induced force generation in the serum free media, only the pre-tension given by applying extension to the collagen lattice is observed. Following addition of serum, the force increased to a maximal tensional force of 240 Dyne in about 49 hours. Force decreased by ~60 Dyne over 8 hours after adding ethanol.

The results of t-CFM validation tests suggest that the new t-CFM system is capable of detecting global changes in the cell-induced tension built up in the collagen lattice. This device can be an effective platform for studying the mechanical response of these cells to different growth factors or inhibitory compounds.

4.1.2 HTK Cellular Force Generation in 3-D Collagen Matrices and the Role of Rho/Rho Kinase in this Process.

The role of Rho-kinase in regulating HTK cellular force generation was assessed using the new t-CFM system. Force was monitored for 13-19 hours in serum containing media, then the Y-27632 was added to block Rho kinase activation. The experiment was repeated 3 times. As shown in **Table 4.1**, the mean maximum force generated by 9 million HTK cells in 10% FBS culture was 265 ± 85 Dynes. The mean rate of cellular force generation was 1.82 Dyne/ hour/ 1 million cells. The mean force decrease resulting from Rho kinase inhibition by 10 μM Y-27632 was 162 ± 14 Dynes (= 61.13% reduction of the maximum force).

Experiment	1st	2nd	3rd	**AVG**
Maximum Cell Force (Dyne)	363	219	212	265
Time Period (Hour)	16	13	19	16
Y-27632 Induced Force Decrease (Dyne)	176	163	148	162
Percentage of Y-27632 Induced Force Decrease	48.48%	74.43%	69.81%	64.2%
Time Period (Hour)	1.5	6	5	4.2

Table 4.1 : Results of t-CFM experiments on HTK cell force generation in 3-D rat tail Type I collagen matrices (2.5mg/mL). Maximum cellular force was the difference between the initial force in equilibrium after the pre-loading and the maximum force in the profile before adding Y-27632. The average force decrease after Y-27632 inhibition of Rho kinase is the difference between the maximum force before addingY-27632 and the minimal force. Time period is the time frame over which initial force generation (top) or Y-27632 induced decrease (bottom) took place.

A representative t-CFM profile recorded by iWorx LabScribe2 in one of the experiments is shown in **Figure 4.3**.

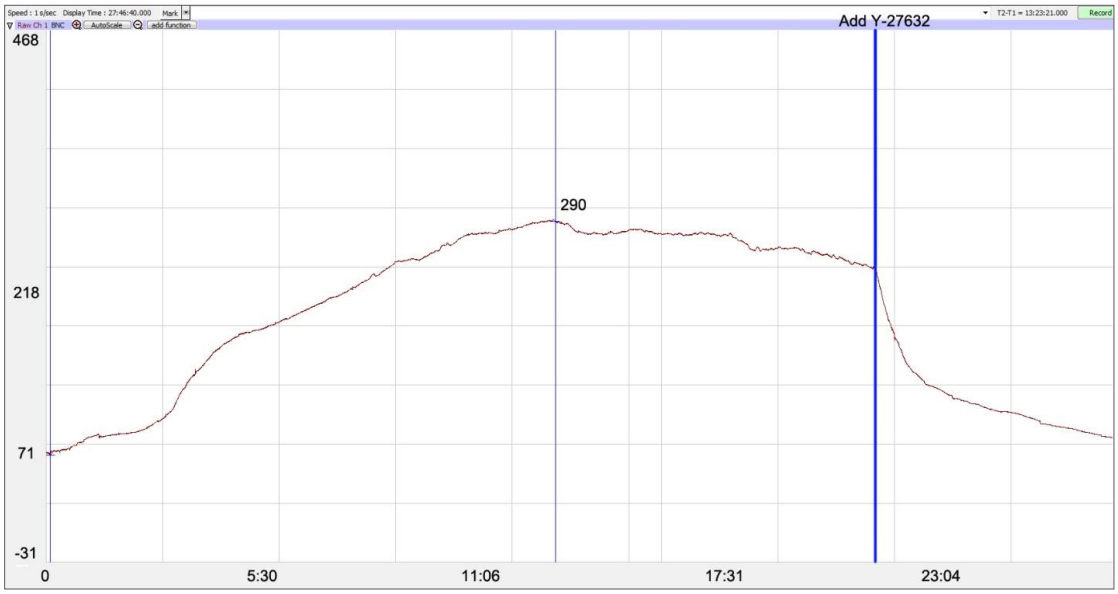

Figure 4.3 : A representing t-CFM profile of HTK cellular force generation in 10% FBS media and the cell force response to Rho kinase inhibitor Y-27632.

In the negative control experiment, where the same experiment was done except that no cells were added to the collagen gel, no significant force generation was observed.
In another control experiment, where the same experiment was done except that Y-27632 was added to the media prior to cell force monitoring, no significant force generation was observed.

These t-CFM results demonstrated that Rho kinase mediates the contractile force generation of HTK cells suspended in 3-D collagen matrices in serum culture. Y-27632 inhibition of Rho kinase induced a significant drop in force in a short time, but the tension in the matrix was not completely dissipated (approximately 39% residual force).

4.1.3 HTK Cell Migration in 3-D Collagen Matrices in Serum-Containing Media

To study the function of Rho/Rho kinase in HTK cell migration in the 3-D collagen matrices, I performed a series of cell migration experiments using the 3-D nested collagen matrix model in serum-containing culture using a variety of cell imaging techniques. I first attempted to visualize the migratory process in the nested matrix constructs cultured in media containing 10% FBS. However, cells contracted the inner compressed matrix in 10% FBS media, which resulted in inward displacement of the inner matrix edge (due to the decrease in diameter) and made long-term time-lapse imaging problematic (**Movie 4.1**). While serum contains several pro-migratory growth factors (including PDGF), it also contains factors such as lysophosphatidic acid (LPA) and sphingosine-1-phosphate (S1P) which stimulate cell contractility through activation of the Rho/Rho Kinase pathway [53]. Thus to reduce the amount of cellular force generation, I tried a lower serum concentration. Inward movement of the matrix edge was significantly reduced when using 1% FBS, thus this concentration was used for all subsequent time-lapse experiments.

In 1% FBS, corneal fibroblasts began to extend pseudopodial processes into the outer matrices 6-10 hours after plating (**Movie 4.2**, **Figure 4.4A**). By 24 hours, many cells had completely escaped the inner matrix (**Figure 4.4B**). Beads in the outer matrix were pulled inward due to cell spreading and migration (**Figure 4.4**, red tracks); control experiments without cells did not show any bead movement. By 48 hours, cells were oriented at random angles with respect to the edge of the inner matrix (**Figure 4.4C**); this pattern was more clearly observed in reconstructions of confocal images collected at 72 hours (**Figure 4.5-1B**). Inspection of time-

lapse movies of individual cells revealed significant tractional force generation during migration, as indicated by deformation of the collagen ECM at the leading edge (**Movie 4.3**). At the rear, apparent rupture of cell-matrix adhesions resulted in elastic recoil of the tail and release of ECM tension, as indicated by collagen movement away from the cell. Fibroblasts generally assumed an elongated spindle-shaped morphology; however, there were often multiple pseudopodial processes at the leading edge. Cells continuously extended and retracted these processes as they moved into the outer matrix, which resulted in more dynamic behavior than is typically observed on planar substrates (**Movie 4.3**).

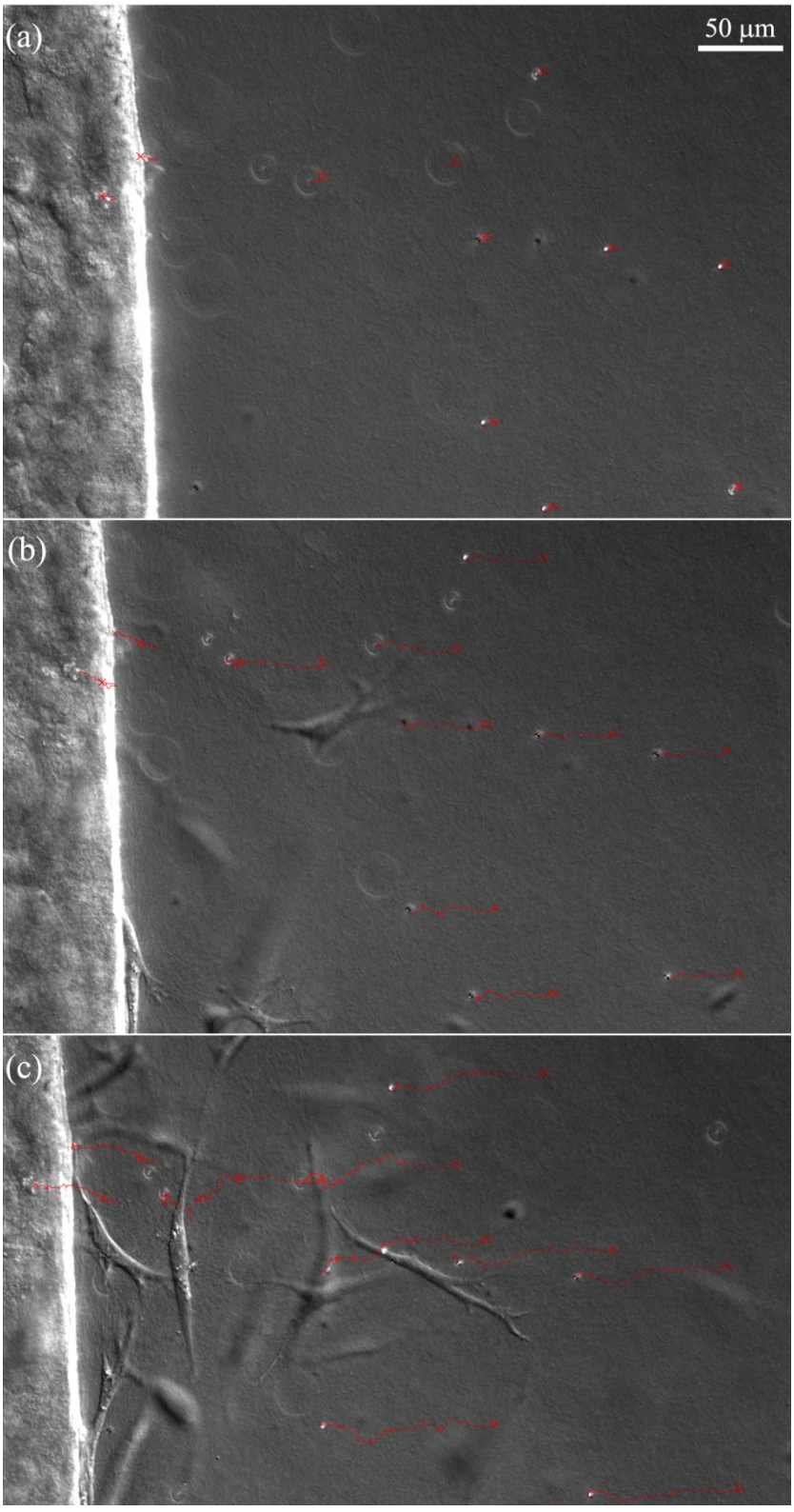
(a)
50 µm
(b)
(c)

Figure 4.4 : Time-lapse DIC images collected at 6 hours (a), 24hours (b) and 48 hours (c) from an experiment in which cells were cultured in 1% FBS. Red tracks show movement of embedded microspheres (crosses mark starting positions). Note that as fibroblasts move out of the inner matrix (left), the beads are pulled inward.

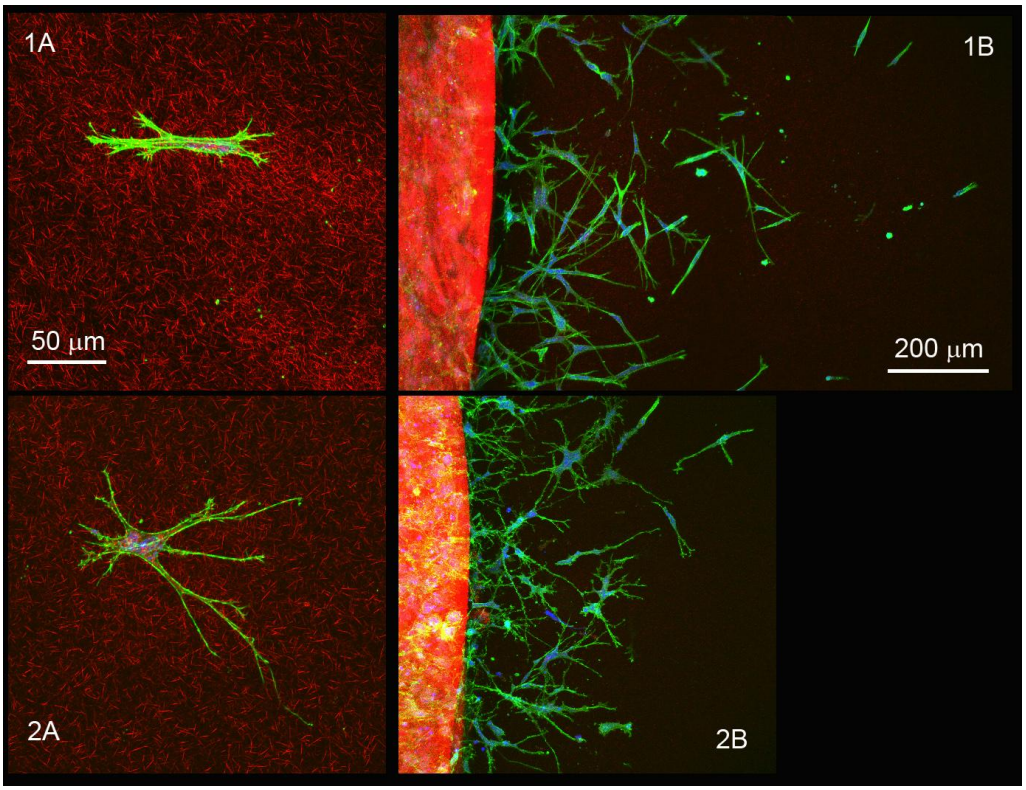

Figure 4.5 : 20× and 63× confocal maximum intensity projection images of f-actin (green), collagen fibrils (red) and PI (blue) following 72 hours of culture in 1 %FBS media (Row 1) or 1%FBS + 10 μM Y-27632 (Row 2). Column A: 63× overlay confocal images. Column B: 20× overlay confocal images.

There was a large degree of variability in the speed and pattern of cell migration observed in 1% FBS. In general, faster moving cells had clear, persistent leading edges with active pseudopodia and a streamline tail (**Figure 4.6A**). Slower migrating cells tended to be less

polarized, with both the front and rear exhibiting active pseudopodial processes and associated collagen displacements (**Figure 4.6B**). This "tail plasticity" has also been observed when using micropatterned 1-D substrates to simulate 3-D cell migration [107].

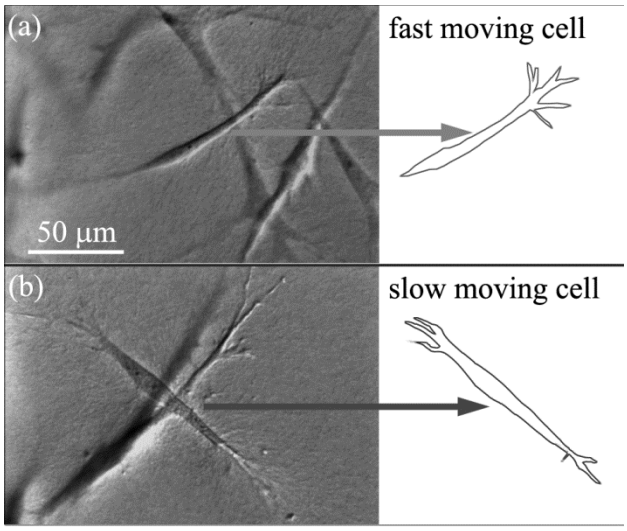

Figure 4.6 : DIC images of typical fast and slow moving cells in 1% FBS. (A) Fast migrating cell has a clear, persistent leading edge with pseudopodia, and a streamline tail. (B) Slow migrating cell has less distinctive leading and rear edges. Both the front and rear have appreciable pseudopodia.

4.1.4 Effect of Rho Kinase Inhibition

The Rho kinase inhibitor Y-27632 has previously been shown to prevent formation of stress fibers, reduce cell contractility, and inhibit cell-induced matrix reorganization in 3-D culture [57, 81]. To assess the impact of Rho kinase on the migratory mechanics of corneal fibroblasts, Y-27632 was added to the culture media at the time of plating. When Rho kinase was inhibited using Y-27632, cells extended thin dendritic processes into the outer matrix (**Figure 4.7A**).

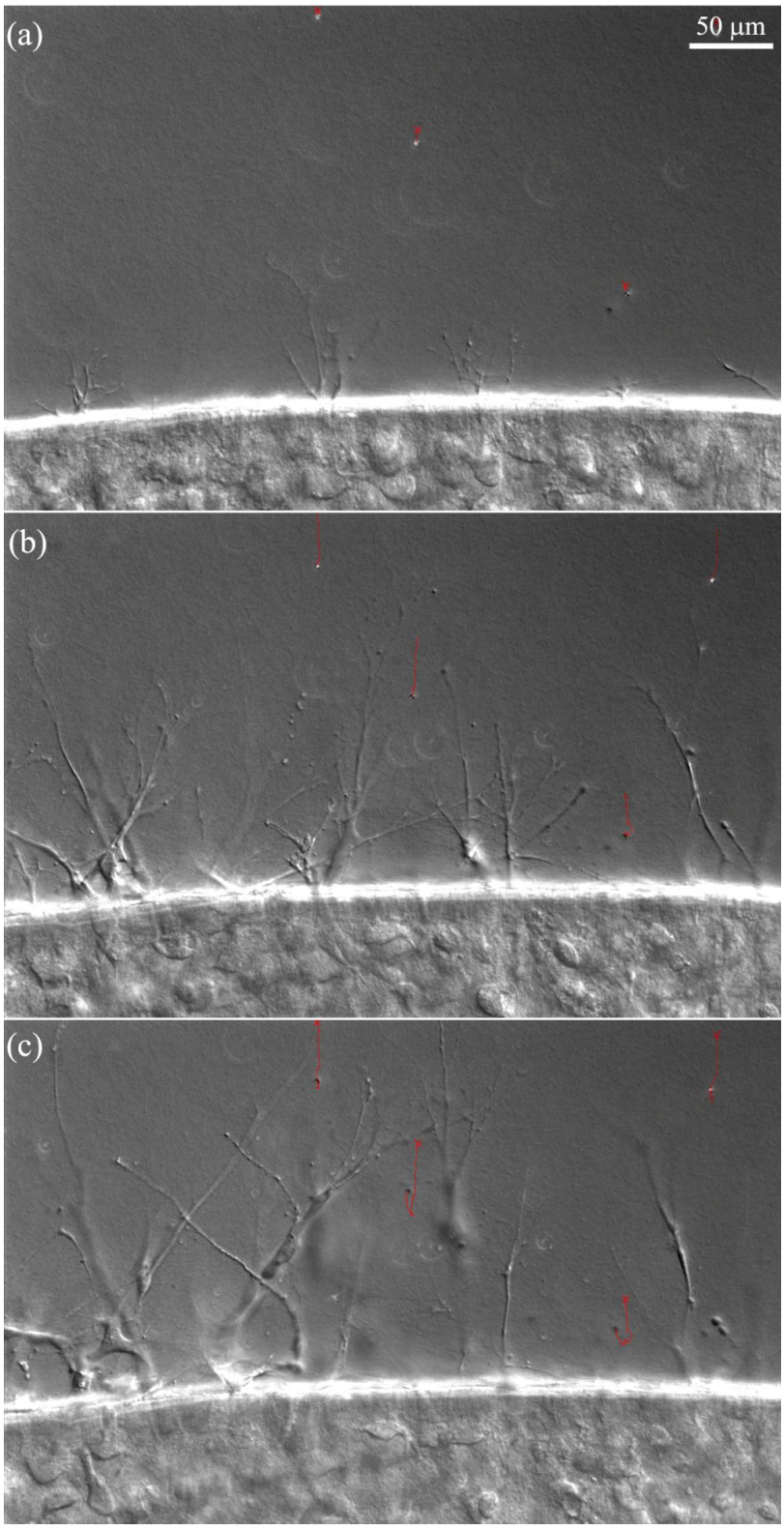
(a)
50 μm
(b)
(c)

Figure 4.7 : Time-lapse DIC images collected at 6 hours (a), 24 hours (b) and 48 hours from an experiment in which cells were cultured in 1% FBS + Y-27632. Red tracks show movement of embedded microspheres (crosses mark starting positions). Note that as fibroblasts move out of the inner matrix (bottom), the beads are pulled inward a substantial distance. However, cells assume a more dendritic morphology following Rho kinase inhibition (compare to Figure 4.4), and take longer to completely escape the inner matrix.

During this process, beads in the outer matrix were pulled inward (**Movie 4.4**). At 24 hours, cells had only partially escaped the inner matrix (**Figure 4.7B**), and few cells had completely left the inner matrix even after 48 hours. Thus despite rapid extension of processes into the outer matrix, translocation of the cell body appeared to be impaired. All cells maintained numerous thin branching processes (**Figure 4.7C**), which were best appreciated from confocal reconstructions (**Figure 4.5-Row2**). While the pseudopodial processes observed in 1% FBS were generally parallel to the bottom of the dish, the dendritic processes observed following Rho kinase inhibition were more randomly oriented and extended along the z-axis, consistent with previous observations [57]. All quantitative data was obtained using 10 μM Y-27632, which is the standard dosage that provides maximum inhibition with minimal loss of specificity. To assess whether the residual traction might be due to residual Y-27632 activity, a few additional experiments were performed using 50μM Y-27632. A similar response was observed qualitatively. We have also performed experiments using another ROCK inhibitor, fasudil, which has a different inhibition profile. Fasudil induced a change in cell morphology and apparent reduction in cell migration similar to Y-27632 (**Figure 4.8**), suggesting the ROCK inhibition is primarily responsible for these effects.

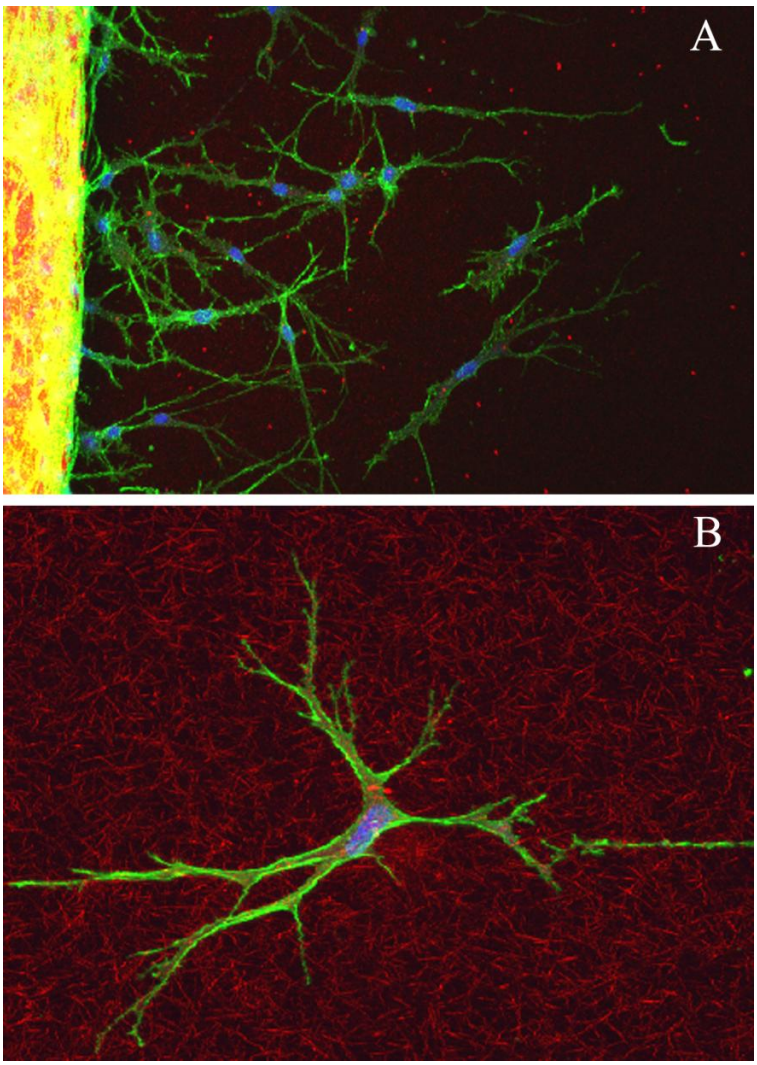

Figure 4.8 : 20× and 63× confocal maximum intensity projection images of f-actin (green), collagen fibrils (red) and PI (blue) following 72 hours of culture in 1%FBS + 20 μM fasudil. A: 20× overlay confocal images. B: 63× overlay confocal images..

Quantitative analysis confirmed that both the number of cells that migrated into the outer matrix and the distance they traveled was significantly reduced when Rho kinase was inhibited (**Figure 4.9A**). Furthermore, the rate of cell migration decreased following Rho kinase inhibition (**Figure 4.9B**). Interestingly, when the net inward displacements of the beads were compared

(i.e. movement perpendicular to the interface), there was no difference between 1% FBS and 1% FBS plus Y-27632 (**Figure 4.9B**). The pattern of bead movement appeared to be more circuitous in 1% FBS, presumably due to the numerous extensions and retractions of pseudopodial processes and the more random pattern of cell alignment. It should be noted that the net inward bead displacements (measured from first and last frames in a sequence being analyzed) were used for quantitative analysis to maximize signal to noise, and this could potentially underestimate total bead movement, particularly in 1% FBS conditions. However, the predominant direction of bead movement was always perpendicular to the interface, thus this error should be low.

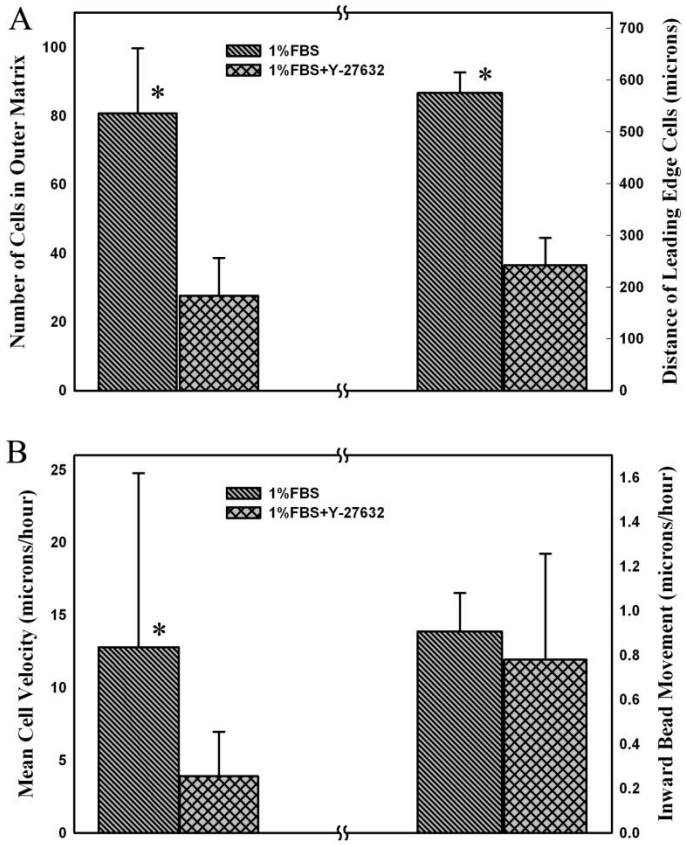

Figure 4.9 : Quantitative analysis of 72 h confocal (A) and time-lapse DIC (B) image data. (A) Comparison of number of cells in outer matrix and the distance cells travelled in 1% FBS and 1%FBS + 10 μM Y-27632. Graphs show mean and standard deviations of three constructs per condition. (B) Speed of cell and bead movement under different culture conditions from time-lapse DIC imaging experiments. Inhibiting Rho kinase with Y-27632 significantly reduced the rate of cell movement, but not the net inward bead movement. (Number of cells analyzed was 29 for 1% FBS and 19 for 1% FBS + 10 μM Y-27632. Number of beads analyzed was 15 for 1% FBS and 13 for 1% FBS + 10 μM Y-27632.) * $p < 0.05$

A decrease in the amount of local cell-induced matrix reorganization (i.e. compaction and alignment of collagen fibrils) was also observed at 72 hours following Rho kinase inhibition (**Figure 4.5, Column A: 63× confocal images**). This could result from reductions in the number of cells in the outer matrix, and/or the amount of contractile force that each cell generates. For

tumor cells invading 3-D matrices, ROCK-dependent collagen alignment at the leading edge provides contact guidance that facilitates local invasion of mammary epithelial cells [91]. ROCK-mediated myosin II contractility has also been shown to inhibit endothelial cell branching, which promotes 3-D ECM invasion by encouraging directional persistence [28]. Studies on corneal fibroblasts have demonstrated that Rho kinase dependent contractile forces are localized to the cell body or at the base of pseudopodial processes [89, 106]. The results of the current study suggest that during fibroblast migration, these contractile forces are responsible for pulling the cell body forward through the collagen matrix following extension of the leading edge. Because of its increased collagen density and stiffness, it is possible that reduced contractility may impair the cells ability to pull themselves free of the inner matrix. However, the rate of migration (as indicated by nuclear translocation) did not change substantially after cells left the inner matrix. Thus the decrease in migration rate is not unique to our model configuration. As mentioned previously, there was a large amount of variation in cell migration speed in 1% FBS. As shown in **Figure 4.10**, this variability was lower following ROCK inhibition.

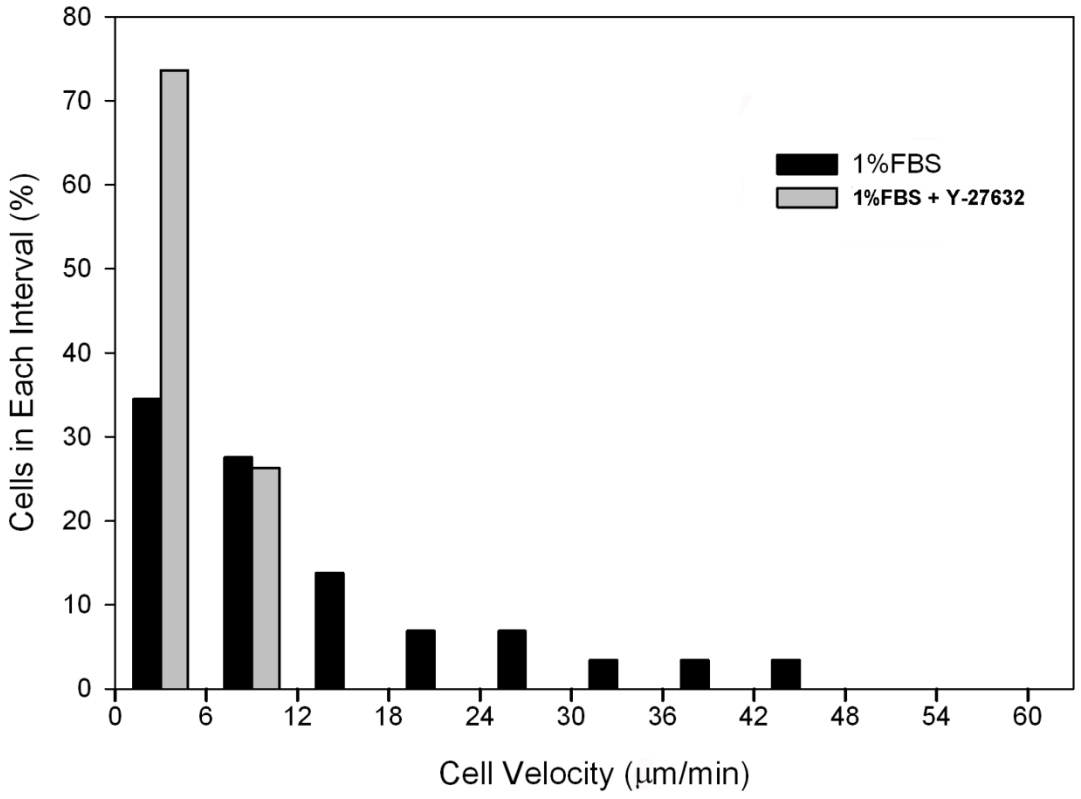

Figure 4.10 : Histograms of cell velocities under different culture conditions, from time-lapse DIC imaging experiments. Inhibiting Rho kinase with 10 μM Y-27632 dramatically reduced the range of cell velocities

4.1.5 Discussion

In the new t-CFM system, design of the force reactor integrated various considerations of mechanical engineering and material mechanics to ensure a precise and practical implementation. The t-CFM relied on the assumption of the force reactor being a 'rigid body', in which the tension at any point along the force transmission axis is balanced and equivalent. However, the mechanical effects of internal forces on a cell-seeded collagen lattice is better

simulated via continuum mechanics. Finite element analysis has revealed that the longitudinal strain in collagen lattice is greatest in the central region of the collagen lattice, and smallest in the area close to the attaching bar [24]. There may also be non-uniform stress distribution in the collagen lattice so that the tension applied on the attaching bar may not be exactly the tension present in the central area of the lattice. Nevertheless, the transducer still has adequate sensitivity to detect changes in cellular force level and can serve as an indirect but effective indicator of cellular force generation in gross. Other factors that could interfere with the measurement are the buffering of the culture media, environmental temperature, and collagen maturation [23]. Also, due to the necessity of applying a pre-strain in the collagen lattice to remove background noise in the early phase of cell contraction, as well as the viscoelastic property of collagen gel, it is important to pre-incubate the lattice until the baseline tension reaches a steady state, prior to data collection.

The results of our t-CFM experiments were consistent with previous work by others. Rho is known to promote increased phosphorylation of myosin light chain via Rho-kinase (ROCK) inhibition of myosin light chain phosphatase (MLCPase), resulting in increased actin-myosin II based cell contractility [2, 85]. In time-lapse studies of corneal fibroblasts plated on top or within restrained 3-D collagen matrices, addition of LPA activates Rho, and induces retraction of cell processes and a corresponding pulling in of the surrounding ECM [89, 94]. In contrast, inhibiting ROCK induces rapid cell body elongation, formation and extension of dendritic cell processes, and a corresponding relaxation of cell-induced tension on the matrix [106] .

Quantitative analysis of static confocal images has directly demonstrated that when Rho kinase is inhibited, cell-induced matrix reorganization (compaction and alignment of fibrils) is also significantly reduced [57, 67]. The t-CFM experiment with Y-27632 provides direct evidence that Rho and its downstream effector Rho kinase mediated, in part, corneal fibroblast force generation in serum-containing culture.

The Rho kinase inhibitor Y-27632 did not completely block the force measured in the matrix, as there was still 39% residual force in the t-CFM profile. Previous studies done in our lab demonstrated that, although global matrix contraction, and compaction and alignment of pseudopodia were significantly reduced when Rho kinase was inhibited, they were still greater than control matrices without cells [57]. In previous studies using time-lapse DIC imaging [106], Dr.Petroll and coworkers investigated the dynamic pattern of force generation by corneal fibroblasts within 3-D collagen matrices. This study demonstrated that in serum culture condition, 5 minutes after cell culture samples were perfused with serum plus Y-27632 media, rapid extension of pseudopodia and formation and extension of new filopodia were observed. After the initial cell extension and relaxation of tension in the matrices, a small, transient inward movement of collagen fibrils was also observed in association with the tips of the cell processes, suggesting generation of small tractional forces on the ECM. Furthermore, Grinnell and coworkers have demonstrated that LPA stimulated dermal fibroblasts can displace the collagen surrounding them when Rho kinase is inhibited (as indicated by movement of embedded microspheres) [32].

The residual force seen in the t-CFM profile after adding Y-27632 may also be caused by permanent collagen matrix remodeling and compaction resulting from HTK cell protrusive activities (extension and retraction of cell processes) during the initial serum culture. The original collagen lattice was cast by a rectangular mould. However, during the t-CFM experiment, a necking phenomenon in the central region of the collagen lattice was observed, as the collagen lattice changed its shape to a bilaterally concave shape (dog-bone shape). This geometry change was induced by HTK cells cultured inside the lattice in serum media. Removal of the constraint in the t-CFM system from the collagen lattice after the experiment did not significantly affect the geometry change, indicating the collagen structure has been permanently reorganized by HTK cells. Due to this permanent remodeling and compaction of collagen fibrils in the lattice, it is reasonable to suspect that tension between the two floating bars was physically elevated from its original level to a slightly higher level. That is, some tension was transferred from the cells to the matrix as time progressed.

Cell migration by corneal fibroblasts in serum containing media generally consisted of several key steps, including protrusion of cell processes (pseudopodia), formation of new adhesions with the substratum, contraction of the cell body and disassembly of the cell/substratum adhesions at the rear (**Figure 4.11**). Rho and Rho kinase are commonly linked to the cell contraction step. Rho acts via Rho kinase to promote myosin light chain phosphorylation, which allows stronger actomyosin contractility and leads to cell contraction and extracellular

matrix remodeling and compaction. The HTK cell migration study presenting here and studies by other researchers with other cell types [83, 100] have shown that Rho and Rho kinase can directly mediate the cell contraction step and therefore potentiate cell migration.

Interestingly, the maximum cell speed was reduced more than the mean cell speed. Thus the inability to achieve a fusiform morphology and/or create and aligned collagen path following ROCK inhibition likely prevents any of the cells from achieving optimal migration conditions. Importantly however, cells were still able to migrate through the collagen ECM when Rho kinase was inhibited, albeit slower (**Movie 4.5**). These cells extended dendritic processes at random orientations with respect to the leading edge, and did not exhibit the coordinated mechanical behavior typical of mesenchymal cell migration (extension, contraction, tail retraction). Cells also produced significant tractional force, as indicated by inward displacement of the ECM in front of cells. Together, our data suggests that ROCK impacts 3-D migration by affecting morphology, polarization, and mechanical coordination between the leading edge, cell body and trailing edge of corneal fibroblasts [33].

HTK cell migration can also be induced by PDGF, and the amount of migration can be even larger than that in FBS [55]. PDGF promotes cell migration primarily via activation of Rac, therefore the contractile force is weaker than the Rho/ROCK-dependent force generated in serum culture. For instance, our previous study showed that primary corneal keratocyte migration in

response to PDGF uses a low contractility migrating machinery, which does not induce strong matrix remodeling and compaction, and is less dependent on Rho kinase [60].

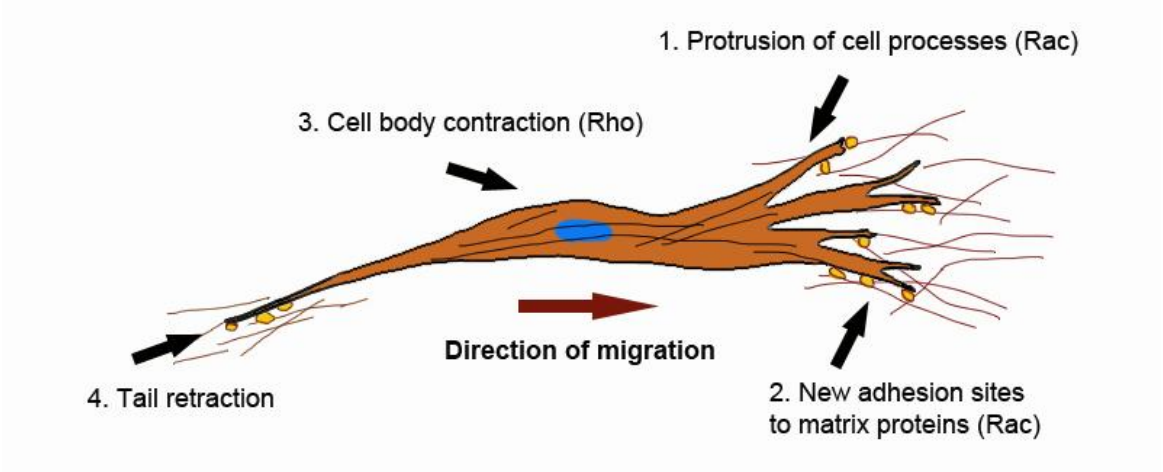

Figure 4.11 : Key steps in cell migration mechanism and the primary roles of Rho family of GTPases in the different steps.

Overwhelming Rho activation can cause a negative effect on cell migration in some cases. For example, a study by Dr.Karamichos showed the amount of HTK cell migration was increased when the FBS concentration in culture media was reduced from 10% to 1% [55]. In the same study, PDGF (in serum-free media) also stimulated a large amount of HTK cell migration, similar to the 1% FBS condition. Global and local matrix remodeling induced by the HTK cell migration were most pronounced in 10% FBS condition, were significantly attenuated when using 1% FBS, and appeared to be least in PDGF. Dr.Grinnell and coworkers investigated human dermal fibroblast migration out of a tissue equivalent into 3-D cell-free collagen matrices,

and assessed the effects of FBS, lysophosphatidic acid (LPA, Rho activator), and PDGF [38]. For the dermal fibroblasts, all the 3 agonists stimulated collagen matrix contraction and remodeling. Neither LPA nor 10% FBS effectively stimulated cell migration into the outer matrices, whereas PDGF appeared to be the most effective agonist for stimulating dermal cell migration in this study. Yet, this PDGF-stimulated cell migration was still Rho kinase, myosin II, and matrix metalloproteinase dependent.

It is worth noting that many of the inhibitors we use are not absolutely specific for one protein. The contribution of particular signaling proteins will vary depending on cell type and culture conditions. Thus, a model for the signaling pathways of the Rho family and the consequent cell responses that are regulating the migration of some cell types may not be applicable to other systems or other cell types.

4.2. THE ROLE OF MATRIX METALLOPROTEINASES IN QUIESCENT KERATOCYTE MECHANICS INSIDE 3-D COLLAGEN MATRICES

4.2.1 MMP Inhibitors do not affect Keratocyte Viability or Proliferation

Consistent with previous studies, NRK cells harvested from corneas and cultured in 3-D collagen matrices in serum free basal media (S-) maintain the quiescent, dendritic keratocyte phenotype observed *in vivo* [48, 65]. The number of cells in 3-D collagen matrices cultured with PDGF media increased by 69.4% after 4 days of culture, and neither GM6001, BB-94 or DMSO (vehicle) affected keratocyte proliferation in response to PDGF (p=0.7583, one-way ANOVA, blue series in **Figure 4.12**). We also examined the anti-proliferation effect of thymidine in our cell culture system. After 4 days of culture, there was no significant change in cell density in any treatment groups. Thus, NRK cell proliferation in response to PDGF was blocked by thymidine, regardless of whether MMP inhibitors were in the media (p=0.9535, one-way ANOVA, red series in **Figure 4.12**). In all experiments, cells maintained a dendritic morphology with no indication of toxicity. Overall, the results suggest that DMSO, GM6001 and BB-94 do not significantly affect NRK cell viability or proliferation in 3-D rat tail type I collagen matrices at the concentrations evaluated.

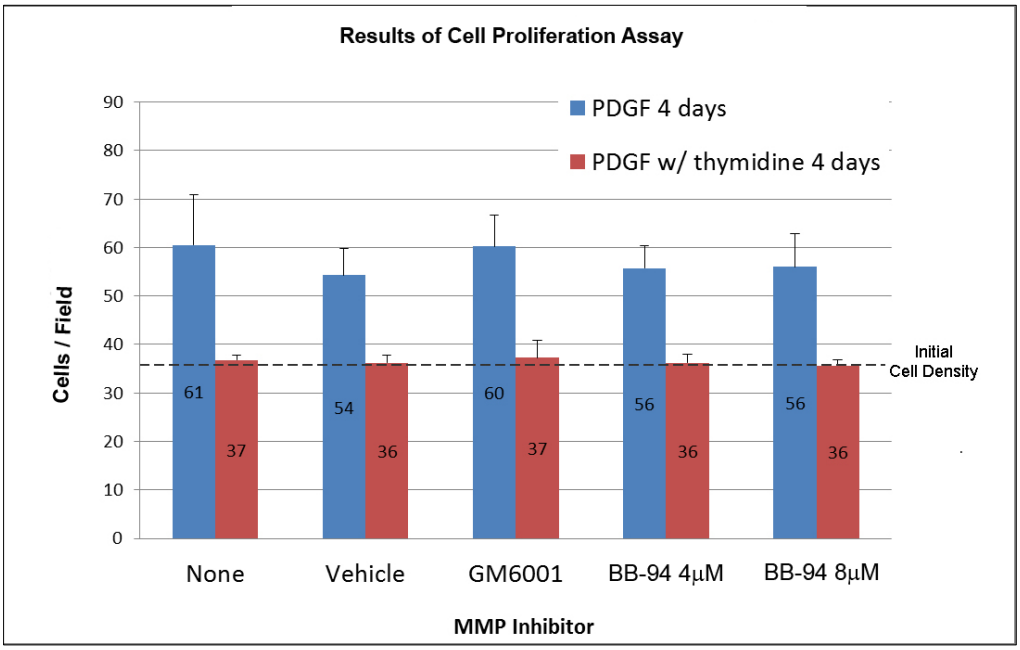

Figure 4.12 : Cell proliferation in 3-D collagen matrices, with or without thymidine blocking. Cell density is the average of 3 experiments. Initial cell density at Time 0 was 36 ± 3.8 cells/unit area.

4.2.2 Keratocytes in PDGF Produce Low Levels of Matrix Degradation

A collagen matrix dissolution assay was used to test the ability of keratocytes to degrade polymerized fibrillar collagen matrices in response to different growth factors, and also to evaluate the inhibitory effects of BB-94 and GM6001. In this assay, two degradation patterns can be identified. 1) Pericellular, where collagen adjacent to cell membranes is degraded by activated MMPs on the cell membrane [42, 97]. In this case collagen degradation is limited to the area where the cell cluster was originally seeded onto the collagen matrix. 2) Distal degradation, which is produced by secretion of soluble collagenolytic MMPs. In this case collagen degradation is observed beyond the edges of the area where the cells have been plated.

Plasminogen was used to activate latent soluble MMPs (e.g. pro-MMP1, pro-MMP-8), presumably via the plasminogen-plasmin-proMMP activation cascade [82, 111].

IL-1α has been shown to stimulate both expression and production of MMPs by corneal stromal cells [63, 70, 71, 76]. In our assay, IL-1α alone stimulated only minor pericellular collagen degradation by keratocytes in the absence of plasminogen (**Figure 4.13**, **column 6**). In contrast, dissolution of fibril collagen matrix in IL-1α culture was dramatically elevated and expanded beyond the area of the cell cluster in the presence of plasminogen (**Figure 4.13**, **column 5**), suggesting that IL-1α stimulates expression of soluble pro-collagenases [108], and these soluble pro-collagenases are subject to plasmin-mediated activation [40]. Diffusion of these water-soluble, activated collagenases results in collagen degradation in distal areas of the well. Keratocytes in 10%FBS, PDGF, TGF β1 and S- basal media appeared to produce only pericellular collagen degradation, even though plasminogen was present in each of these conditions. The synthetic MMP inhibitor GM6001 only partially blocked these collagenolytic activities, whereas BB-94 completely blocked collagen dissolution in all conditions studied (**Figure 4.13, rows 2 and 3**). It should be noted that FBS contains factors that can block soluble MMP activity, thus any effects of FBS on secreted MMPs may be masked in this assay (**Figure 4.13, column 1**). Serum-free media was used for all other conditions (**columns 2 – 6**).

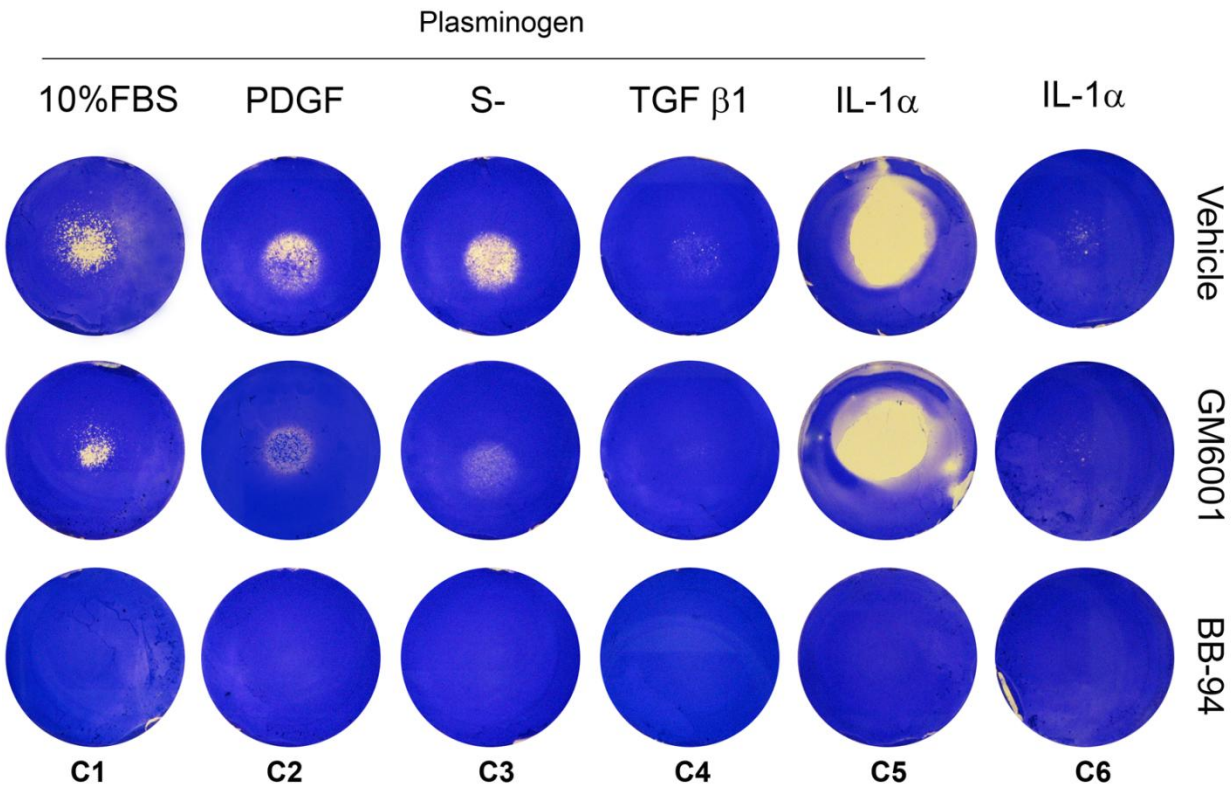

Figure 4.13 : Dissolution patterns produced on fibrillar rat tail collagen matrices by primary NRK cells, following culture with different growth factor/cytokines. **1. Vehicle control** (first row): The areas where cell pellets were seeded had reduced staining, as a result of pericellular collagenolysis. 10% FBS, PDGF, and S- cultures each induced a similar amount of matrix dissolution; whereas TGF β produced less collagen dissolution. IL-1α and plasminogen induced the strongest collagen degradation, and this extended well beyond the area of cell pellet. **2. GM6001** (second row): Dissolution patterns were weaker when GM6001 was present in culture media, except for IL-1α + PLG. **3. BB-94** (third row): No dissolution marks were left on the matrices when 8μM BB-94 was present in culture media, suggesting that both pericellular and secreted collagen degradation was blocked by BB-94. Images were from one experiment, representing the results of 4 independent experiments.

In order to quantify collagen degradation activities and the efficacy of MMP inhibition in 3-D culture, we developed an assay based on dye-quenched (DQ™) collagen. DQ-collagen can be efficiently digested by reactive MMPs, yielding highly fluorescent peptides that can be

visualized by fluorescence microscopy [99], or optically assessed by fluorimetric plate reading devices [45, 105]. Under 63× fluorescence confocal live cell microscopy, small clusters of fluorescent spots were associated with NRK cells within 3-D DQ-collagen matrices in S- PDGF culture, which is indicative of on-going pericellular collagen degradation (**Figure 4.14**). The fluorescence intensity of the culture supernatant in our DQ collagen assay was also monitored, using a fluorescent plate reader. The fluorimetric results showed that, in PDGF culture, FITC fluorescence continuously intensified from day 1 to day 4, demonstrating that collagenolytic MMPs produced by NRK cells were acting on the collagen substrate, and releasing fluorescent positive peptides into the media (**Figure 4.14).** The supernatant of PDGF vehicle condition had an average fluorescence intensity of 4700 RU on the 4^{th} day of culture - only 6% of the positive control. Experiments using only conditioned culture supernatant to react with DQ collagen substrate did not show any fluorescence changes over time, suggesting that the concentration of soluble MMPs in our NRK cell culture system was not sufficient to digest the collagen. Thus the DQ collagen degradation was most likely the result of pericellular collagenolytic activity by membrane-associated MMPs. In the presence of GM6001 or BB-94, the fluorescence intensity was reduced to 72% and 64% of the vehicle, respectively (**Figure 4.14**). Hence, it appears that BB-94 blocked the collagenolytic MMPs more effectively than GM6001.

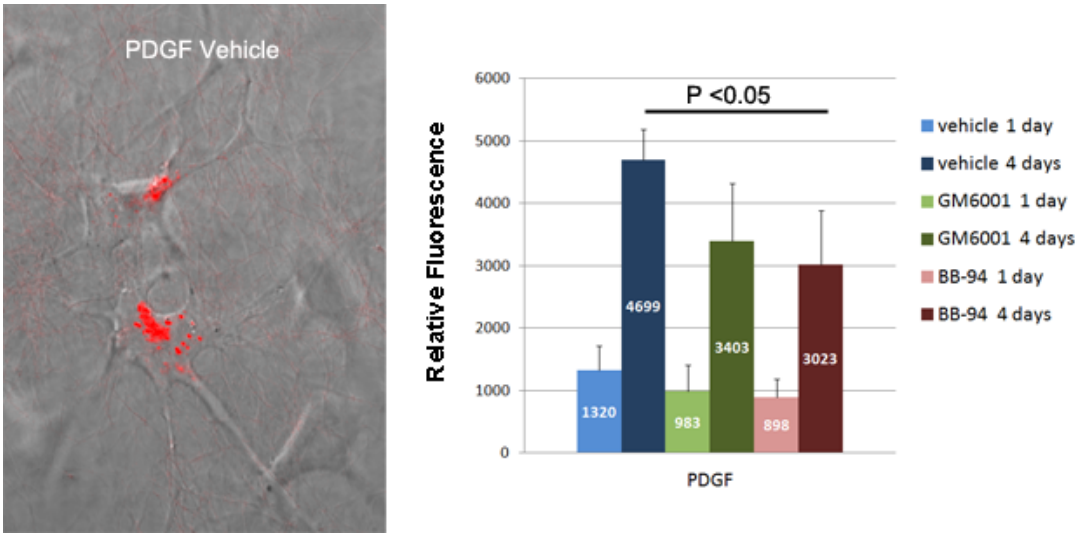

Figure 4.14 : Left. Fluorescent spots adjacent to the cell membranes, due to pericellular DQ-collagen degradation by NRK cells (Red). Image shown is maximum projection of a 63× FITC confocal image series (Z-stack) overlaid with the best of focus DIC image. **Right** : Fluorescence of culture supernatant after 1 and 4 days incubation of keratocytes in DQ-collagen matrices using PDGF containing media (n = 4 independent experiments). All values have been normalized by subtracting the background fluorescence level of no-cell controls measured on the same day, to eliminate the effects of spontaneous DQ collagen degradation. MMP inhibition reduced collagen degradation. Complete digestion of DQ-blended collagen with exogenous collagenase D in no-cell samples raised the fluorescence intensity to ~70,000 units.

While matrix degradation was mild and remained pericellular in PDGF, secreted species of MMPs induced strong and extensive collagen matrix degradation in the IL-1α plus Plasminogen condition, as indicated by disrupted and shortened fibrils in confocal reflection images on the 4th day of culture (**Figure 4.15**). This observation is consistent with the results of the 2-D matrix dissolution assay (**Figure 4.13**).

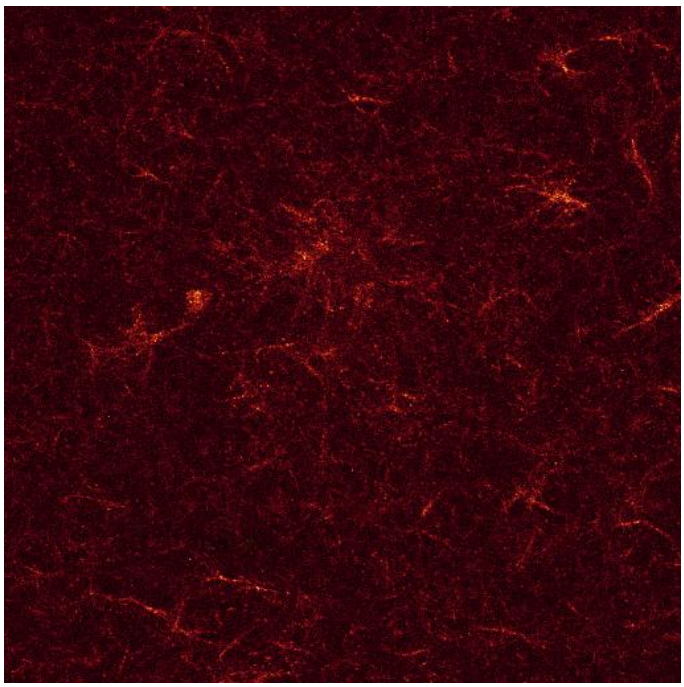

Figure 4.15 : Single plane confocal reflection image of reconstituted rat tail collagen matrix after 4 days of culture in IL-1α with Plasminogen. Owing to collagenolysis of soluble MMPs produced by NRK cells, the matrix had disrupted, shorter collagen fibrils and a lower fibril density, as compared to the parallel PDGF group.

Membrane type-1 MMP is generally the major protease involved in pericellular collagen degradation. To investigate the correlation between the collagen degradation activities of NRK cells and this membrane-associated MMP, MT1-MMP expression was evaluated using by immunochemical staining. **Figure 4.16** shows representative images of the MT1-MMP staining for PDGF and IL-1α conditions. Positive MT1-MMP staining was observed in PDGF, consistent with the pericellular collagen degradation demonstrated in the matrix dissolution assay (**Figure 4.13**). In contrast, the fluorescence signal of MT1-MMP immunochemical staining was barely

detectable in IL-1α culture. This is also consistent with the matrix dissolution results (**Figure 4.13 -C6**).

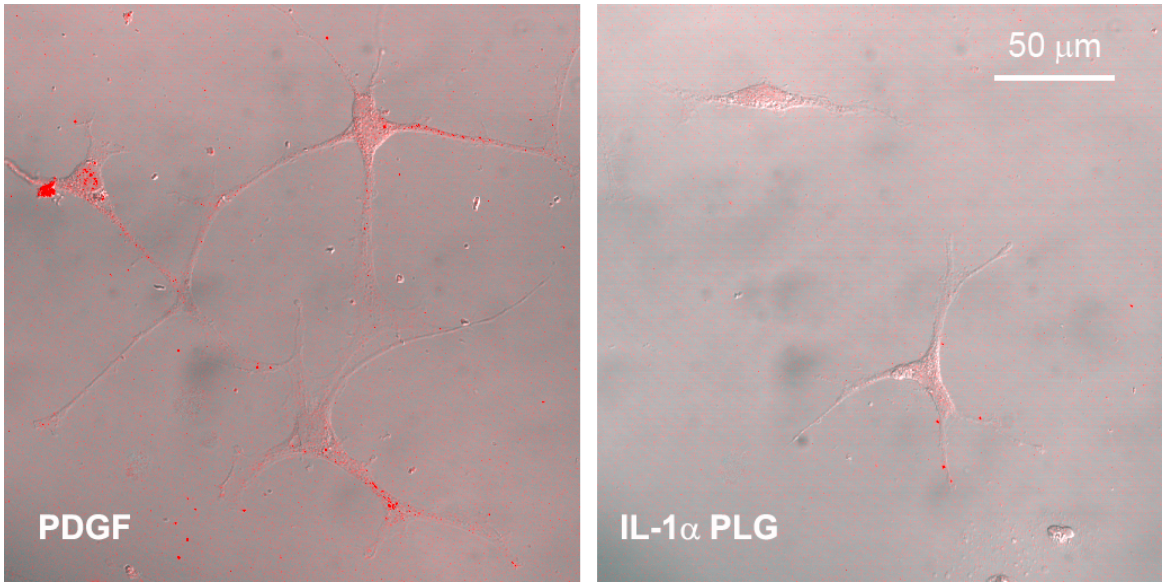

Figure 4.16 : MT1-MMP labeling of NRK cells. In PDGF, MT1-MMP was detectable on the cell membranes (Red fluorescent spots). The fluorescence signal of MT1-MMP immunochemical staining was reduced NRK cells in IL-1α condition. No specific fluorescent signals were observed on cell membranes in the 'no primary antibody' staining control (not shown).

4.2.3 Cell Invasion is Suppressed by MMP Inhibition

To investigate the role of MMPs in NRK cell migration, a nested collagen matrix model was used. PDGF BB was used in all experiments to stimulate cell migration [60]. As shown in **Figure 4.17**, when the enzymatic functions of endogenous MMPs were inhibited by GM6001 or BB-94, the ability of NRK cells to invade and migrate into the rat tail collagen matrices was suppressed, resulting in a smaller migration index. Overall, the inhibitory efficacy of BB-94 on cell migration appeared stronger than GM6001 (P=0.008 for BB-94, P=0.139 for GM6001). A similar inhibition was found when thymidine was added to the media, thus the differences were

not due to changes in cell proliferation. The distance NRK cells traveled to the migratory front was also assessed. GM6001 did not impact this distance, whereas BB-94 caused a significant reduction in the distance by 40% (**Figure 4.17 -C)**.

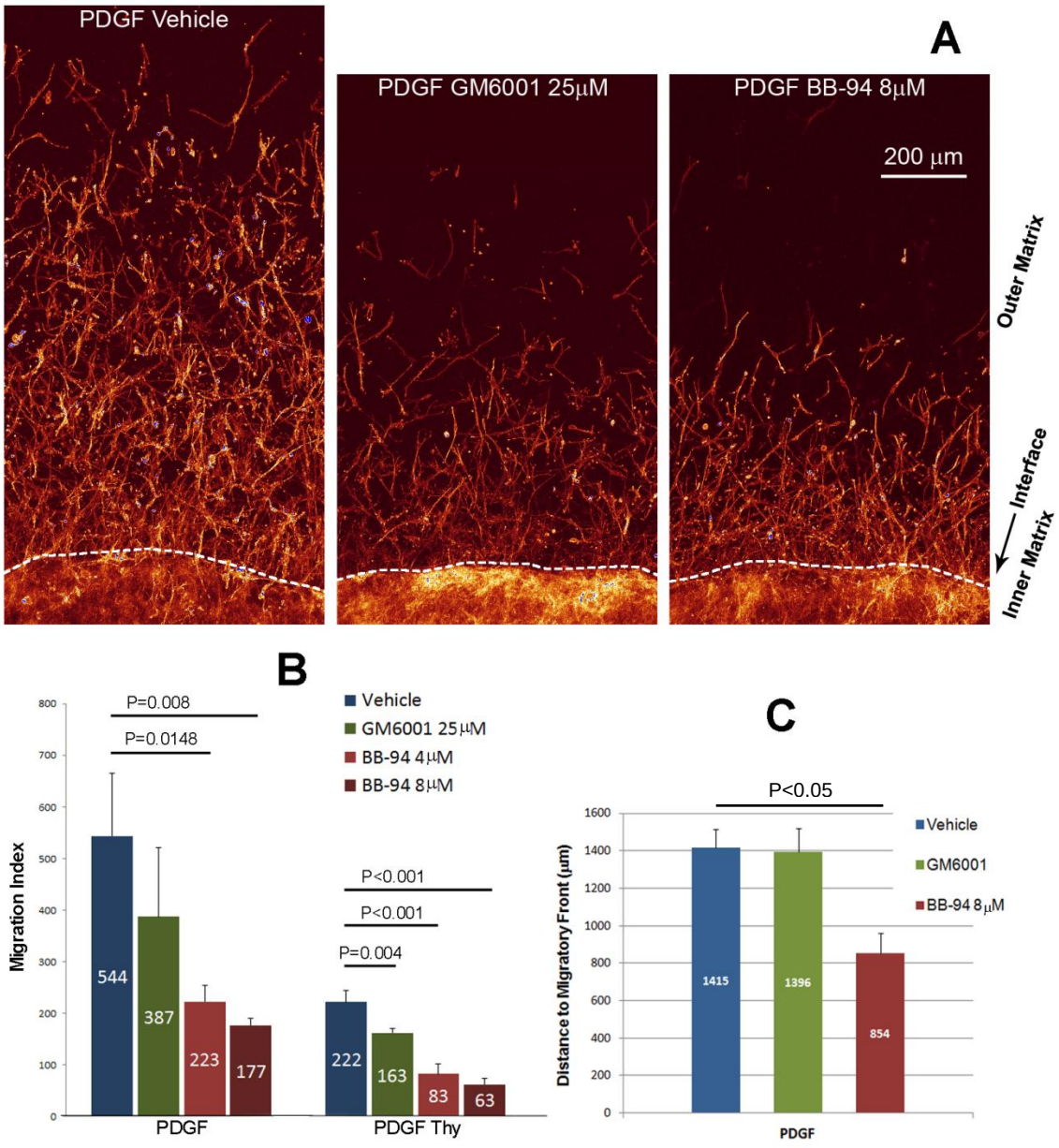

Figure 4.17 : Keratocyte migration through 3-D rat tail collagen matrices. (**A**) 10× confocal maximum intensity projection of f-actin organization in the 3-D nested migration model. Images

were taken after 4 days of incubation. (**B**) Cell migration results. Each migration index (cell number/1.5mm region on the interface) is the average of triplicate experiments. All experimental groups had 0.1% of DMSO vehicle in the culture media. In serum free PDGF culture, migration of primary NRK cells in 3-D collagen matrices was suppressed by MMP inhibition, especially when using the broad spectrum MMP inhibitor BB-94. This dependence on MMPs to migrate was even more significant when cell proliferation was inhibited by using 2mM thymidine (see column series 'PDGF Thy'). (**C**) Distance from matrix interfaces to migratory front of NRK cells in outer matrices. BB-94 had a significant inhibitory effect on the distance that NRK cells traveled into the outer matrices.

Consistent with previous results, migratory keratocytes in the outer matrices were highly elongated and polarized, and had numerous dendritic processes [60]. Time-lapse DIC images showed that migrating cells in PDGF repeatedly extended and retracted their long, thin dendritic extensions while moving into the outer matrix (**Movie 4.6**). Tractional forces were generated at the tips of these branching processes as indicated by inward movement of collagen fibrils close to the tips. Dendritic processes generally formed in front of the cell body, progressively elongated, and retracted as the cell body slid past them. A similar pattern of dendritic cell migration was observed in the presence of GM6001 (**Movie 4.7**) and BB-94 (**Movie 4.8**); however, both translocation from the inner to the outer matrix, and subsequent migration speed appeared to be retarded in BB-94. Continuous areas and/or tracks of matrix degradation were not observed. Consistent with DIC imaging results, f-actin labeling showed dendritic morphologies under all three conditions studied, and no stress fibers were observed (**Figure 4.18**).

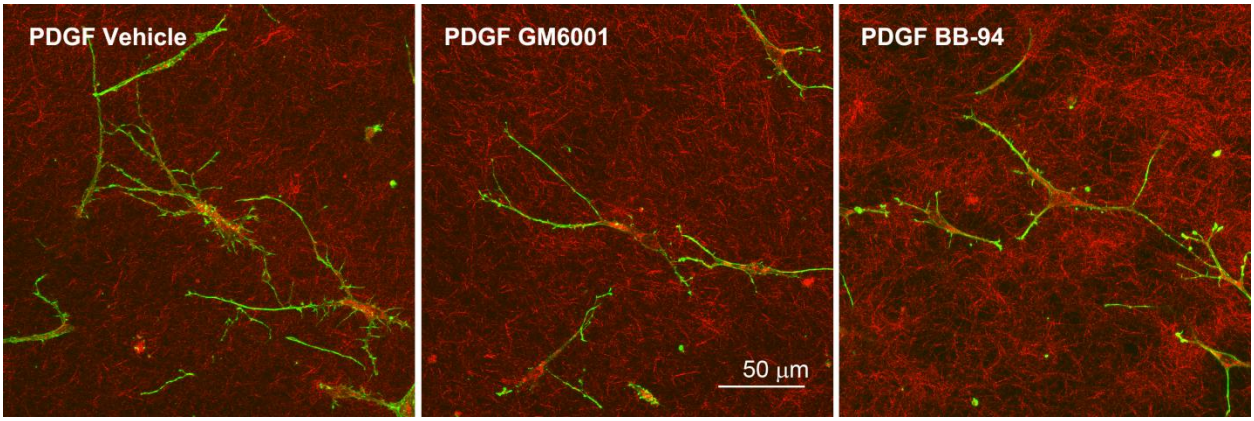

Figure 4.18: Maximum intensity projection overlay of 63× confocal fluorescence and reflection images of migratory NRK cells in the nested matrix model after 4 days of culture. *Green*= f-actin organization in migratory NRK cells. *Red* = rat tail collagen fibrils acquired by confocal reflection imaging.

Previous studies have demonstrated that cancer cell migration through rat tail collagen matrices is dependent on MMPs. However, for some types of cancer cells, migration through bovine collagen matrices MMP-independent [96, 98, 114], presumably because of differences in the collagen porosity and cross-linking. In addition to migration experiments in rat tail collagen matrices, we also performed a subset of experiments in which bovine collagen was used for the outer matrices. We found that despite the structural differences between rat tail collagen matrices and bovine collagen matrices, the inhibitory effects of the MMP inhibitors on keratocyte invasion were very similar (**Figure 4.19**).

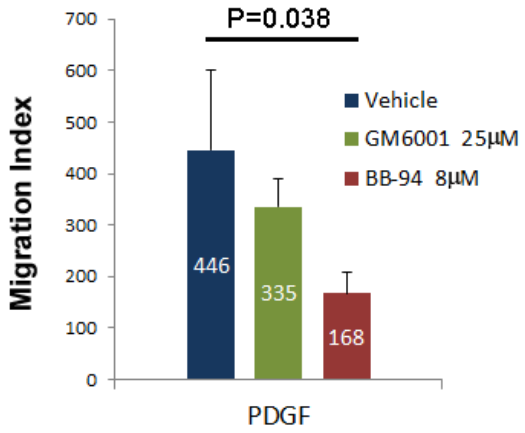

Figure 4.19 : NRK cell migration in 3-D bovine Type I collagen matrices. Each migration index (cell number/1.5mm region on the interface) is the average of triplicate experiments.

4.2.4 Global Matrix Contraction is Suppressed by MMP Inhibition

A global matrix contraction assay was performed to determine whether endogenous MMPs mediate the contractile activities of PDGF-cultured keratocytes in 3-D matrices. Keratocytes cultured in serum-free media and 10% FBS were also included in the assay, as a negative low-contractility control and a positive high-contractility control, respectively [66]. Cells in S- basal media produced only 3.86% and 6.82% matrix contraction after 1 and 4 days, respectively. Culture in 10% FBS transformed NRK cells to a highly contractile fibroblastic phenotype which resulted in the largest contraction percentage among all the experimental groups in this assay (35.8% at 1 day, and 68.5% at 4 days).

Consistent with previous studies [66], PDGF induced much less matrix contraction than serum. NRK cells cultured in PDGF induced 13.28% matrix contraction over 24 hours, and this

was significantly inhibited by BB-94 (P = 0.035, **Figure 4.20**). Four days of culture in PDGF yielded an average contraction percentage of 24%, which was reduced to 13% by BB-94 (P = 0.001). These results suggest that steric blockage of endogenous MMPs by BB-94 can impair the ability of corneal keratocytes to contract extracellular collagen matrices. Interestingly, GM6001 had little effect on global matrix contraction.

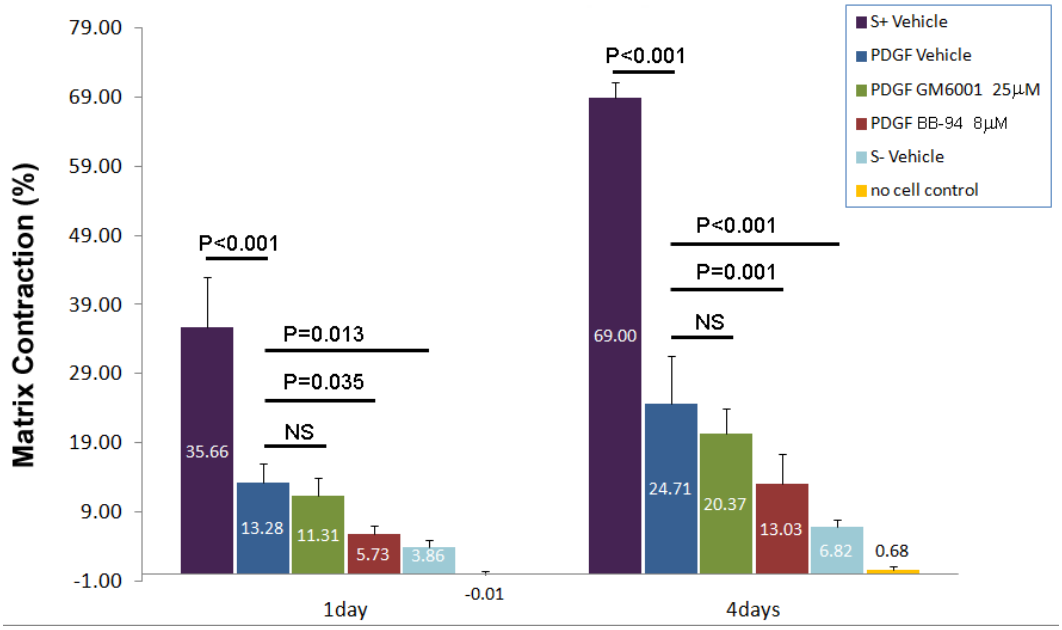

Figure 4.20: Percentage of matrix contraction by NRK cells after 1 and 4 days. Matrix contraction percentage for each culture condition was the average of measurements from 3 experiments.

4.2.5 Cell Spreading and Dynamic Mechanical Activity is Altered by MMP Inhibition

We also investigated whether the pattern of PDGF-induced cell spreading in 3-D collagen matrices was impacted by MMP inhibition. Both with and without MMP inhibition, keratocytes formed dendritic processes and did not develop stress fibers (**Figure 4.21**). Counts of the total number of dendritic processes for each cell after 4 days of culture did not show significant

differences (24.4 ± 9.2, 27.1 ± 8.3 and 27.3 ± 10.2 for vehicle, GM6001 and BB-94, respectively, p=0.515, one-way ANOVA). However, the morphologies of NRK cells among the 3 conditions were significantly different from one another (**Figure 4.21**). Specifically, keratocytes in PDGF vehicle condition were more elongated and dendritic than the other two conditions (higher Feret, and lower A/P and Solidity). Keratocytes cultured with GM6001 were smaller and less polarized than the other two conditions (lower Perimeter and higher Circularity). Keratocytes cultured in BB-94 had larger cell bodies and were more stellar (largest Area and Solidity). These differences can be better appreciated in movies showing 3-D reconstructions over a range of projection angles (**Movie 4.9-4.11**).

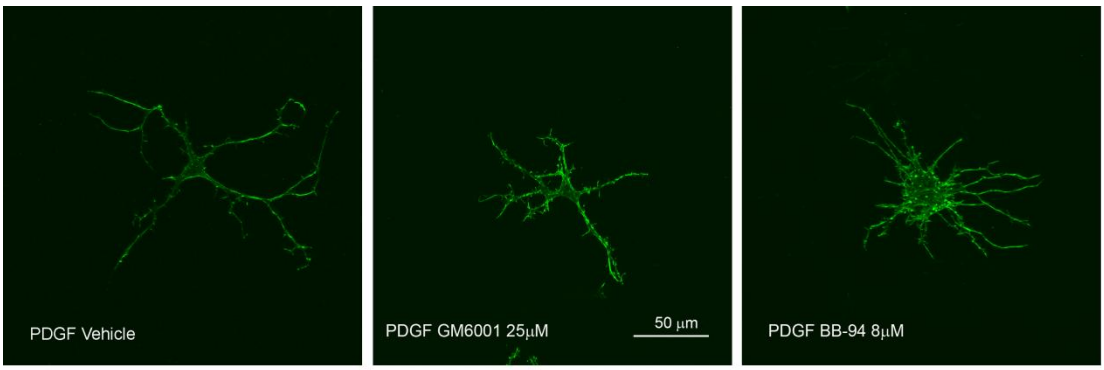

Condition	Area	Perim.	A/P Ratio	Feret	Circ.	Solidity
Vehicle	22477.50	5765.70	3.8153	698.45	0.0089	0.1214
SD	8869.29	1705.87	0.9806	195.16	0.0027	0.0408
GM6001	21654.38	4417.97	4.9599	589.61	0.0153	0.1542
SD	6085.96	1292.45	0.8264	139.09	0.0053	0.0340
BB-94	32278.52	6544.94	5.0582	596.65	0.0110	0.1929
SD	11508.13	2038.00	1.2278	103.44	0.0053	0.0519

(value in red = P<0.05, pariwise multiple comparisons through one-way ANOVA)

Figure 4.21 : Images: F-actin organization of keratocytes cultured in 3-D collagen matrices. Images are the maximum intensity projections of 63× confocal Z-stacks. Cells in PDGF with vehicle generally formed elongated, branching dendritic processes, and had a small cell body. Cells in PDGF w/ BB-94 developed shorter, thinner processes, and had a larger cell body (see **Movies 4.9-4.11**). **Table**: Morphological evaluation from 24 cells, randomly sampled from each condition. NRK cells in PDGF vehicle condition were better spread and more dendritic than the other two conditions. NRK cells in culture with GM6001 were shorter and more circular than the other two conditions. NRK cells under the inhibition of MMPs by BB-94 were less elongated, denser and more stellar than the cells cultured in the vehicle condition. **A/P Ratio** = Area/Perimeter. Generally lower for more dendritic morphologies. **Feret** = Feret's diameter is the longest distance between any two points along the cell boundary, and is used as a measure of cell elongation. **Circ.** = Circularity. A value of 1.0 indicates a perfect circle. As the value approaches 0.0, it indicates an increasingly elongated shape; **Solidity** = [Area of cell] / [Area of the convex hull for cell]. The convex hull can be thought of as a rubber band wrapped tightly around the points that define the selection. Higher values indicate a more compact morphology.

DIC time lapse imaging of live NRK cells provided additional insights into their dynamic mechanical behavior in collagen matrices. Extension and retraction of cell processes was greatest in the PDGF vehicle condition according to the cumulative dynamics analysis. This activity of cell processes declined with both GM6001 and BB-94, and the decrease was statistically significant with GM6001 (Cumulative dynamics over 24 hrs : 347 $\pm$ 93.81, 251.2 $\pm$ 43.44, 292.4 $\pm$ 65.47, for PDGF vehicle, PDGF GM6001, and PDGF BB94 respectively, P = 0.016 between vehicle and GM600). Cells in PDGF vehicle had more processes that extended into the outer rings than cells in PDGF BB94 and PDGF GM6001. Thus we normalized the cumulative activity by the average total number of process segments. Interestingly, there was no significant difference in the protrusive dynamics for a given length of cell process (number of process segments), with or without MMP inhibitors (Normalized dynamics : 9.79 $\pm$ 1.20, 10.02 $\pm$ 1.73, 10.17 $\pm$ 1.95, for PDGF vehicle, PDGF GM6001, and PDGF BB94 respectively, P = 0.653). Thus the difference in cumulative cell dynamics is likely due to the reduced length of cell processes following MMP inhibition, which undergo smaller extensions and retractions.

4.2.6 Discussion.

Following lacerating injury or incisional surgery, contractile force generation by fibroblasts/myofibroblasts is needed to facilitate wound closure and prevent loss of the mechanical integrity of the cornea. However, following refractive surgical procedures such as PRK or LASIK, it is preferable to minimize cellular force generation and fibrosis during stromal repopulation, since these processes can alter corneal shape and transparency [22, 78]. Such non-

disruptive stromal repopulation is also needed following UV cross-linking of the cornea, which is increasingly used as a treatment for keratoconus, since this procedure kills corneal keratocytes in the area of treatment. We recently demonstrated that corneal keratocytes can effectively migrate through 3-D collagen matrices using both a high-contractility *mesenchymal* mechanism stimulated by serum, and a low-contractility *dendritiform* mechanism stimulated by PDGF. Low-contractility migration in PDGF was consistently observed in both pepsinized and non-pepsinized matrices, and was not impacted by altering the mechanical constraints of the constructs. A similar mechanism of cell migration was induced when serum-cultured corneal fibroblasts were cultured with Y-27632, which blocks cell contractility and fibroblast and myofibroblast transformation of keratocytes in both 2-D and 3-D culture [12, 66]. From a clinical standpoint, low-tension *dendritiform* keratocyte migration may facilitate keratocyte repopulation of the stroma following surgery or injury, without alterations in the structural properties of the stromal ECM or increased cellular light scattering that can reduce corneal clarity. In this study we investigate the dependence of PDGF-induced keratocyte spreading, migration and ECM remodeling on MMP activation and collagen degradation, using a unique combination of 3-D culture models.

4.2.6.1 Growth factor regulation of MMP expression and proteolytic activity

Fibrotic wound healing is generally accompanied by increased expression of matrix metalloproteinases (MMPs) by corneal fibroblasts [26, 27, 35]. In the uninjured cornea, proMMP-2 is present in normal corneal epithelium and stroma of rabbits, rats and humans, but is

associated with tissue inhibitor of MMP type two (TIMP-2), which blocks its protease activity [8]. MMP-9, collagenases and stromelysins are not normally detected in the cornea [35]. Following injury, however, expression of MMP-2, MMP-9 and other MMP species by activated corneal fibroblasts is elevated [18]. In cell culture, primary corneal keratocytes in serum-containing media (corneal fibroblasts) express similar MMP species as those observed during corneal wound healing, such as MMP-2, MMP-9, collagenases and stromelysins [25, 34]. In vitro studies also have shown that MMP expression by corneal fibroblasts is regulated, in part, by growth factors and cytokines found in the tear film, epithelium and stroma during wound healing, such as interleukine-1 (IL-1) and transforming growth factor-β (TGF-β). IL-1 (α and β), which are secreted by corneal epithelial cells, can significantly increase MMP production and collagen degradation by corneal epithelial and stromal cells [40, 63, 70, 71, 76]. TGF-β stimulates MMP-2 and MMP-9 secretion by corneal epithelial cells, but has no significant effect on MMP-2 and MMP-9 expression by corneal fibroblasts or myofibroblasts. It also has an inhibitory effect on collagenase and stromelysin secretion [34, 109]. PDGF has not been shown to have a significant effect on MMP expression by either corneal epithelial cells or fibroblasts, with the exception of a slight increase of MMP-2 [68, 86].

While MMP-2 and MMP-9 have been well characterized in corneal studies, other MMP species are also expressed in normal and wounded corneas, including membrane-anchored type 1 MMP (MT1-MMP or MMP-14) [11, 14, 84, 101, 116]. MT1-MMP expression is elevated in wounded corneal epithelium and stroma, and may have a significant regulatory role in different

stages of corneal stroma matrix repair/regeneration. In vitro, MT1-MMP expression by serum-exposed human corneal keratocytes can be elevated by addition of Con A in the culture system, and expression is correlated with the level of proMMP-2 activation [14]. These findings suggest that MT1-MMP may play a role in regulating the activation of other downstream MMPs [43] and the turnover and remodeling of ECM.

Our matrix dissolution assay produced results that are generally consistent with those cited above. However, unlike previous studies, we used primary cultures of rabbit corneal keratocytes, without pre-exposure to serum or other factors which can permanently alter growth factor signaling responses [52]. Dissolution of the fibril collagen matrix was dramatically elevated in the presence of IL-1α and plasminogen, and the degradation pattern extended beyond the area of cell plating. However, in the absence of plasminogen, IL-1α culture stimulated much lower levels of collagen degradation, which did not extend beyond the cell area. These data suggest that IL-1α stimulates latent collagenolytic MMP expression [108], and that these latent soluble MMPs are subject to plasmin-mediated activation [40]. Plasmin-mediated activation and diffusion of these water-soluble MMPs resulted in collagen degradation in distal areas of the well. In contrast to IL-1α, keratocytes in 10%FBS, PDGF, TGF β1 and S- basal media produced more localized collagen degradation both with and without plasminogen in the media, suggesting recruitment of MT1-MMP in these culture conditions [42, 97]. This notion was further validated by MT1-MMP immunochemical staining and the DQ-collagen assay. Taken together, the data

suggest that PDGF-induced pericellular collagen degradation was due to membrane-associated MMP.

The broad spectrum MMP inhibitors GM6001 and BB-94 both demonstrated inhibitory effects on keratocyte-induced collagen degradation in our study. While GM6001 only partially blocked matrix degradation, results of the matrix dissolution assay and our DQ-collagen fluorimetric assay indicated that pericellular collagen degradation was completely suppressed by BB-94. This is consistent with previous studies, in which BB-94 has been reported to effectively block both secreted and membrane-associated MMPs (such as MT1-MMP), while GM6001 is more specific to secreted types [74, 96, 97, 104]

4.2.6.2 The dependency of PDGF induced migration on MMPs

PDGF stimulates migration of corneal keratocytes within Type I collagen matrices, without causing a loss of their dendritic morphology or inducing formation of intracellular stress fibers. In this study, the ability of NRK cells to invade and migrate into the rat tail Type I collagen matrices was more significantly suppressed by BB-94 than GM6001, suggesting the PDGF-stimulated NRK cell migration in rat tail collagen has a dependency on membrane type-MMPs. This is consistent with previous studies using skin or lung fibroblasts [93, 97] and cancer cells [117], in which BB-94 or similar synthetic MMP inhibitors inhibited most of cell invasion/migration activities in 3D matrices (usually 80~90%). In three-dimensional collagen matrices, proteolytically potent HT-1080 fibrosarcoma and MDA-MB-231 carcinoma cells

exhibited a constitutive mesenchymal-type movement including the coclustering of β1 integrins and MT1–MMP at fiber binding sites and the generation of tube-like proteolytic degradation tracks [114]. Such areas of matrix degradation were not detected in our high magnification imaging studies using corneal keratocytes. Thus in S- PDGF culture, lower levels of highly localized pericellular collagen cleavage may enable NRK cells to overcome the obstructive barrier of reconstituted collagen matrices and efficiently migrate through the matrix, without producing large-scale collagen degradation or matrix remodeling.

Previous studies have shown that in bovine collagen matrices (which have reduced stiffness and increased porosity), HT-1080 exhibited protease-independent migration at near undiminished migration rates [114]. Sustained protease-independent migration required transformation to an amoeba-like morphology, cytoskeletal organization and migration mode; i.e. a diffuse cortical distribution of the actin cytoskeleton, formation of constriction rings and propulsive squeezing through preexisting matrix gaps. We also performed a subset of experiments in which bovine collagen was used for the outer matrices (2.5mg/ml, the same concentration as the rat tail collagen). However, we found that despite the structural differences between rat tail collagen matrices and bovine collagen matrices, the inhibitory effects of the MMP inhibitors on keratocyte migration were very similar, and transformation to an amoeboid migration mode was not observed in either case. Thus corneal fibroblasts do not appear to have the same migratory and morphologic plasticity as some cancer cells.

In the case of MMP-dependent migration, MT1-MMP is generally the main player. Many common types of fibroblasts and tumor cells utilize MT1-MMP to overcome the steric barrier of the ECM [96, 97]. Blocking, knockdown or mutation of MT1-MMP can disable the migration of several cell types in rat tail collagen matrices [96, 118]. MT1-MMP is often clustered in the invasive front of migrating cells, and can colocalize with integrins such as αvβ3 on the breast carcinoma cell membrane [20], and CD44, a cell-surface glycoprotein [79, 118]. These interactions can result in enhanced cell migration. Another mechanism underlying the migration promoting effect of MT1-MMP is the pericellular proteolysis activity conducted by MT1-MMP directly and indirectly via activation of proMMP-2 on the cell membrane. Both MT1- MMP and MMP-2 are reactive to collagen substrates in cell periphery. ProMMP-2 conjugates with TIMP-2, and then binds to MT1-MMP on the cell membrane. MT1-MMP processes the adjacent proMMP-2 into active MMP-2, which degrades collagen in the cell periphery, promoting cell migration and other relevant events. After active MMP-2 is eventually released from cell membrane, its collagenolytic effect is blocked by TIMPs in the extracellular matrix. This well-recognized model of MT1-MMP·TIMP-2·MMP-2 trimolecular interaction [20, 69] allows the localized matrix degradation needed for cell to navigate through 3-D matrices, while limiting harmful MMP activities in other areas of the tissue. This limited degradation would be particularly important during corneal stromal wound healing.

4.2.6.3 MMP regulation of PDGF-induced cell spreading and matrix reorganization

Consistent with previous studies, PDGF induced much less global matrix contraction than serum [66]. PDGF-induced matrix reorganization was even further reduced by BB-94, suggesting that MMPs play a role in this process. Evaluation of keratocyte morphology and dynamic activity added insights to the matrix contraction results. When NRK cells are cultured within un-nested 3-D collagen matrices, cells extend and retract processes but are generally in a non-migratory state. Tractional forces are generated during extension and retraction, and this results in matrix reorganization and global matrix contraction [89]. We found that MMP inhibition induced significant changes in PDGF-induced cell spreading. Specifically, keratocytes in PDGF vehicle condition were more elongated than cells in either GM6001 or BB-94. Branching of cell processes, which was often observed in the vehicle condition, was also reduced following culture with BB-94. Cumulative cell activity (the frequency and amount of extension and retraction of cell processes) also declined with both GM6001 and BB-94, and reached statistical significance with GM6001. This may explain, in part, the decrease in global matrix contraction. Normalization of the cumulative activity revealed no significant difference in the protrusive dynamics for a given length of process, with or without MMP inhibitors. Thus while cells remain active under MMP inhibition, the formation of long dendritic processes in 3-D collagen matrices is impaired. This may be due to the spatial constraints imposed by the surrounding ECM, and the need for localized degradation to create an unobstructed path for cell extension. Alternatively, MMP regulation of adhesion receptors and their downstream signaling pathways may also play a role [6].

Overall, the data suggests that even under conditions in which low levels of cell contractility and extracellular matrix proteolysis are maintained, MMPs still play an important role in mediating cell spreading and migration within 3-D collagen matrices. This appears to be mediated primarily by membrane-tethered MMPs, such as MT1-MMP

CHAPTER FIVE
Conclusions and Recommendations

5.1 THE ROLE OF RHO GTPASES IN REGULATING THE MECHANICAL BEHAVIORS OF ACTIVATED CORNEAL FIBROBLASTS IN SERUM-CONTAINING MEDIA

A new tensile cell force monitoring system was first developed and tested. The new system is able to measure force changes made by cells seeded in the 3-D rat tail collagen matrix in real time. This system features: 1) high-sensitivity, low background noise, signal stability, and minimal baseline drift; 2) minimal friction along the force transmission axis; and, 3) a biologically compatible environment suitable for cell culture. This combination of features was not found in previous t-CFM systems reported by other research laboratories in the field. The new force transduction axis integrated a state-of-art transducer and re-designed attachment bars, which make the force measurement more accurate, responsive and efficient. The use of this system can be further extended to many other biomechanical experiments where tissue and/or cell tensional force generation and response is to be investigated. Various stimuli or factors that can potentially affect the force generation by cells in 3D ECM could be evaluated using this system, such as: pharmacologic reagents, different cell types, matrix architectures, material stiffness, or variations in mechanical constraints. The cell-populated 3D matrix fabricated in the culture chamber and the culture supernatant can be harvested and further analyzed for cell organization, cell differentiation, matrix remodeling, or other properties of interest after force monitoring is complete.

I next tested the role of Rho kinase in mediating contractile force generation by corneal fibroblasts. The mean maximum tractional force generated by 9 million HTK cells in 10% FBS culture over 24 hours was 265 ± 85 Dynes (n=3). The mean rate of cell force generation is 1.82 Dyne/ hour/ 1 million cells. The mean force decrease resulting from Rho kinase inhibition by 10 μM Y-27632 was 162 ± 14 Dynes (= 61.13% reduction of the maximum force). These t-CFM results demonstrated that Rho kinase plays a key role in mediating contractile force generation of HTK cells suspended in 3-D collagen matrices in serum culture. Y-27632 inhibition of Rho kinase induced a great loss on the contractile cell force in a short time, but the force was not completely dissipated (there was approximately 39% residual force). This is most likely due to transfer of tension from the cells to the matrix during matrix remodeling.

Migration of activated corneal fibroblasts plays an important role in matrix patterning during embryonic development and wound repopulation following injury or refractive surgery. Thus we next modified a previously described nested collagen matrix model to facilitate time-lapse imaging, and applied it to investigate the role of Rho kinase in regulating fibroblast migration mechanics. Human corneal fibroblasts were cultured in nested matrices with media containing either 1% fetal bovine serum (FBS), or 1% FBS plus the Rho kinase inhibitor Y-27632. Time-lapse DIC imaging of cell and extracellular matrix (ECM) movements was performed for up to 72 hours, and static confocal imaging was used to assess 3-D cell morphology and matrix reorganization. In 1% FBS, significant tractional forces were generated during migration, as indicated by inward displacement and reorganization of collagen in front of

cells. When Rho kinase was inhibited, cells became more elongated, and extended thinner dendritic processes into the outer matrix. While these dendritic cells were still able to generate tractional forces at their leading edge, cell translocation was more substantially reduced, suggesting that the contractile forces needed to overcome cell/matrix adhesions in the rear of the cell and pull the cell body forward during migration were Rho kinase-dependent.

Previous studies have established that the Rho-family of GTPases such as Rho, Rac and Cdc42 play a central role in regulating the cytoskeleton changes associated with cell mechanical activity. Our studies demonstrated that: 1) the generation of corneal stromal fibroblast forces is largely mediated by Rho/Rho-kinase activation, 2) activated corneal fibroblast migration in 3-D collagen matrices is regulated, in part, by the Rho-Rho kinase-actomyosin motor mechanism. Activated Rho stimulates the formation of stress fibers, the development of large focal adhesions, and cellular contraction. Thus, Rho GTPases may serve as good target for various reagents (such as Y-27632 inhibitor) to perturb the downstream effects of activated Rho/ROCK signaling on corneal fibroblast transformation and stress fiber assembly, and the corresponding mechanical behaviors. From a clinical standpoint, this strategy could potentially help to prevent the damage to the unique corneal stroma matrix organization, and loss of corneal transparency, corneal geometry and visual acuity, which often result from corneal fibroblast mechanical activities (e.g exertion of strong contractile forces, abnormal reorganization of ECM) during wound healing. Thus Y-27632 may be a promising therapeutic method for inhibiting the

quiescent keratocyte to fibroblast transformation in vivo (possible bench to beside translation of a new therapy).

5.2 THE ROLE OF MATRIX METALLOPROTEINASES IN CORNEAL KERATOCYTE MIGRATION AND MATRIX CONTRACTION INSIDE 3-D COLLAGEN MATRICES

Previous studies have shown that PDGF can stimulate corneal keratocyte spreading and migration within 3-D collagen matrices, without inducing transformation to a contractile, fibroblastic phenotype. The goal of this study was to investigate the role of matrix metalloproteinases (MMPs) in regulating PDGF-induced changes in keratocyte motility and mechanical differentiation. Rabbit corneal keratocytes were isolated and cultured in serum-free media (S-) to maintain their quiescent phenotype. A nested collagen matrix construct was used to assess 3-D cell migration, and a standard collagen matrix model was used to assess cell morphology and cell-mediated matrix contraction. In both cases constructs were cultured in S- media supplemented with PDGF, with or without the broad spectrum MMP inhibitors GM6001 or BB-94. After 4 days, f-actin, nuclei and collagen fibrils were imaged using confocal microscopy. To assess sub-cellular mechanical activity (extension and retraction of cell processes), time-lapse DIC imaging was also performed. MT1-MMP expression and MMP-mediated collagen degradation by were also examined. Results demonstrated that neither GM6001 nor BB-94 affected corneal keratocyte viability or proliferation in 3-D culture. PDGF stimulated elongation and migration of corneal keratocytes within type I collagen matrices,

without causing a loss of their dendritic morphology or inducing formation of intracellular stress fibers. Treatment with GM6001 and BB-94 inhibited PDGF-induced keratocyte spreading and migration. Relatively low levels of keratocyte-induced matrix contraction were also maintained in PDGF, and the amount of PDGF-induced collagen degradation was similar to that observed in S- controls. The collagen degradation pattern was consistent with membrane-associated MMP activity, and keratocytes showed positive staining for MT1-MMP. Both matrix contraction and collagen degradation were reduced by MMP inhibition. For most outcome measures, the inhibitory effect of BB-94 was significantly greater than that of GM6001. Overall, the data demonstrate for the first time that even under conditions in which low levels of contractility and extracellular matrix proteolysis are maintained, MMPs still play an important role in mediating cell spreading and migration within 3-D collagen matrices. This appears to be mediated primarily by membrane-tethered MMPs, such as MT1-MMP.

Although MMP functions have been studied for decades for tumor cell metastasis, angiogenesis, dermal cell biology, and other biological fields, to our knowledge, few studies have investigated the differences in the MMP-mediated collagenolysis by primary corneal stromal cells in response to various growth factors and cytokines, particularly PDGF, and none have dissected the roles of MMP-mediated pericellular degradation in primary corneal keratocyte migration in 3D collagen matrices.

Following corneal wounding, activated corneal fibroblasts proliferate, migrate into wounded region, generate mechanical force to contract corneal wound, remodel the provisional matrix, and synthesize new matrix. These physiological events are accompanied by up-regulated MMP expression/production by corneal fibroblasts [35] and often involve the activities of MMPs [26]. In some cases, the opacity gradually diminishes over time, due to MMP-dependent remodeling [27]. These evidences suggest that MMPs may play important roles in maintaining a balance in ECM synthesis and degradation in both normal cornea and wounded cornea. The research findings of this dissertation provide new insights into the regulation of MMP-mediated collagenolysis by corneal keratocytes in response to relevant growth factors and cytokines, and the essential role of cellular MMPs in corneal remodeling and keratocyte migration in wounded corneal tissue. The knowledge gained and techniques developed can potentially contribute to the development of new therapeutic approach for regenerative corneal healing in the future.

Future work for continuing this MMP study could include: 1) further investigating the cellular and molecular roles of membrane-type MMPs in proteolytic activities, promoting PDGF-stimulated corneal keratocyte migration and other mechanical behaviors during corneal repair; 2) performing cell migration experiments in un-compressed 3D collagen matrices and 2D surfaces, and comparing with nested migration behavior; 3) investigating the correlation between MT1-MMP and integrin recruitment in cell processes.

One new experimental approach that could be employed would be to knock-down MT1-MMP expression in cultured corneal keratocytes to more directly assess the fundamental mechanism of MT1-MMP in pericellular collagenolysis by corneal keratocytes, and in promoting corneal keratocyte invasion/migration, protrusive activity, and other biomechanical aspects in 3D collagen matrices. The new t-CFM system developed for **Aim 1** can also be used to quantitatively examine the role of MMPs in regulating force generation by corneal keratocytes.

BIBLIOGRAPHY

1. Abou Neel, E.A., et al., *Use of multiple unconfined compression for control of collagen gel scaffold density and mechanical properties.* Soft Matter, 2006. **2**(11): p. 986-992.
2. Amano, M., et al., *Phosphorylation and activation of myosin by Rho-associated kinase (Rho-kinase).* J Biol Chem, 1996. **271**(34): p. 20246-9.
3. Bard, J.B. and E.D. Hay, *The behavior of fibroblasts from the developing avian cornea. Morphology and movement in situ and in vitro.* The Journal of Cell Biology, 1975. **67**(2): p. 400-418.
4. Beningo, K.A., M. Dembo, and Y.-l. Wang, *Responses of fibroblasts to anchorage of dorsal extracellular matrix receptors.* Proceedings of the National Academy of Sciences, 2004. **101**(52): p. 18024-18029.
5. Birkedal-Hansen, H., et al., *Matrix Metalloproteinases*, in *Curr Protoc Cell Biol*. 2001, John Wiley & Sons, Inc.
6. Bouroulia, D. and W.G. Stetler-Stevenson, *Matrix metalloproteinases (MMPs) and tissue inhibitors of metalloproteinases (TIMPS): positive and negative regulators in tumor cell adhesion.* Seminar Cancer Biol, 2010. **20**: p. 161-168.
7. Brejchova, K., et al., *Matrix metalloproteinases in recurrent corneal melting associated with primary Sjörgen's syndrome.* Molecular Vision, 2009. **15**.
8. Brown, D., et al., *Characterization of the major matrix degrading metalloproteinase of human corneal stroma. Evidence for an enzyme/inhibitor complex.* Experimental Eye Research, 1991. **52**(1): p. 5-16.
9. Brown, R.A., et al., *Ultrarapid Engineering of Biomimetic Materials and Tissues: Fabrication of Nano- and Microstructures by Plastic Compression.* Advanced Functional Materials, 2005. **15**(11): p. 1762-1770.
10. Carrington, L.M., et al., *Differential Regulation of Key Stages in Early Corneal Wound Healing by TGF-β Isoforms and Their Inhibitors.* Investigative Ophthalmology & Visual Science, 2006. **47**(5): p. 1886-1894.
11. Chang, J.-H., K. Han, and D. Azar, *Wound healing fibroblasts modulate corneal angiogenic privilege: Interplay of basic fibroblast growth factor and matrix metalloproteinases in corneal angiogenesis.* Japanese Journal of Ophthalmology, 2010. **54**(3): p. 199-205.
12. Chen, J., J. Wong-Chong, and N. SundarRaj, *FGF-2 and TGF-β1-induced downregulation of lumican and keratocan in activated corneal keratocytes by JNK signaling pathway.* Invest Ophthalmol Vis Sci, 2011. **52**: p. 8957-8964.
13. Cintron, C., et al., *Heterogeneity of collagens in rabbit cornea: type III collagen.* Investigative Ophthalmology & Visual Science, 1988. **29**(5): p. 767-75.
14. Collier, S.A., M.C. Madigan, and P.L. Penfold, *Expression of membrane-type 1 matrix metalloproteinase (MT1-MMP) and MMP-2 in normal and keratoconus corneas.* Current Eye Research, 2000. **21**(2): p. 662-668.

15. Collier, S.A., *Is the corneal degradation in keratoconus caused by matrix-metalloproteinases?* Clinical & Experimental Ophthalmology, 2001. **29**(6): p. 340-344.
16. Cukierman, E., et al., *Taking Cell-Matrix Adhesions to the Third Dimension.* Science, 2001. **294**(5547): p. 1708-1712.
17. Cukierman, E., R. Pankov, and K.M. Yamada, *Cell interactions with three-dimensional matrices.* Current Opinion in Cell Biology, 2002. **14**(5): p. 633-640.
18. Daniels, J.T., et al., *Temporal and spatial expression of matrix metalloproteinases during wound healing of human corneal tissue.* Experimental Eye Research, 2003. **77**(6): p. 653-664.
19. Davison, P.F. and E.J. Galbavy, *Connective tissue remodeling in corneal and scleral wounds.* Investigative Ophthalmology & Visual Science, 1986. **27**(10): p. 1478-84.
20. Deryugina, E.I., et al., *MT1-MMP Initiates Activation of pro-MMP-2 and Integrin αvβ3 Promotes Maturation of MMP-2 in Breast Carcinoma Cells.* Exp Cell Biol, 2001. **263**(2): p. 209-223.
21. Doane, K.J. and D.E. Birk, *Fibroblasts retain their tissue phenotype when grown in three-dimensional collagen gels.* Experimental Cell Research, 1991. **195**(2): p. 432-442.
22. Dupps, W.J. and S.E. Wilson, *Biomechanics and wound healing in the cornea.* Exp Eye Res, 2006. **83**: p. 709-720.
23. Eastwood, M., D.A. McGrouther, and R.A. Brown, *A culture force monitor for measurement of contraction forces generated in human dermal fibroblast cultures: evidence for cell-matrix mechanical signalling.* Biochimica et Biophysica Acta (BBA) - General Subjects, 1994. **1201**(2): p. 186-192.
24. Eastwood, M., et al., *Effect of precise mechanical loading on fibroblast populated collagen lattices: Morphological changes.* Cell Motility and the Cytoskeleton, 1998. **40**(1): p. 13-21.
25. Fini, M.E., et al., *Unique regulation of the matrix metalloproteinase, gelatinase B.* Investigative Ophthalmology & Visual Science, 1995. **36**(3): p. 622-33.
26. Fini, M.E., *Keratocyte and fibroblast phenotypes in the repairing cornea.* Progress in Retinal and Eye Research, 1999. **18**(4): p. 529-551.
27. Fini, M.E. and B.M. Stramer, *How the Cornea Heals: Cornea-specific Repair Mechanisms Affecting Surgical Outcomes.* Cornea, 2005. **24**(8): p. S2-S11.
28. Fischer, R.S., et al., *Local cortical tension by myosin II guides 3D endothelial cell branching.* Current Biology, 2009. **19**(3): p. 260-5.
29. Fournie, P.R., et al., *Correlations of Long-term Matrix Metalloproteinase Localization in Human Corneas After Successful Laser-Assisted In Situ Keratomileusis With Minor Complications at the Flap Margin.* Arch Ophthalmol, 2008. **126**(2): p. 162-170.
30. Fournie, P.R., et al., *Correlation Between Epithelial Ingrowth and Basement Membrane Remodeling in Human Corneas After Laser-Assisted In Situ Keratomileusis.* Arch Ophthalmol, 2010. **128**(4): p. 426-436.
31. Friedl, P., et al., *Migration of Coordinated Cell Clusters in Mesenchymal and Epithelial Cancer Explants in Vitro.* Cancer Research, 1995. **55**(20): p. 4557-4560.

32. Friedl, P. and E.B. Bröcker, *The biology of cell locomotion within three-dimensional extracellular matrix.* Cellular and Molecular Life Sciences, 2000. **57**(1): p. 41-64.
33. Friedl, P. and K. Wolf, *Plasticity of cell migration: a multiscale tuning model.* The Journal of Cell Biology, 2010. **188**(1): p. 11-19.
34. Girard, M.T., M. Matsubara, and M.E. Fini, *Transforming growth factor-beta and interleukin-1 modulate metalloproteinase expression by corneal stromal cells.* Investigative Ophthalmology & Visual Science, 1991. **32**(9): p. 2441-54.
35. Girard, M.T., et al., *Stromal fibroblasts synthesize collagenase and stromelysin during long-term tissue remodeling.* Journal of Cell Science, 1993. **104**(4): p. 1001-1011.
36. Grinnell, F., *Fibroblast–collagen-matrix contraction: growth-factor signalling and mechanical loading.* Trends in Cell Biology, 2000. **10**(9): p. 362-365.
37. Grinnell, F., et al., *Dendritic Fibroblasts in Three-dimensional Collagen Matrices.* Molecular Biology of the Cell, 2003. **14**(2): p. 384-395.
38. Grinnell, F., et al., *Nested collagen matrices: A new model to study migration of human fibroblast populations in three dimensions.* Exp Cell Res, 2006. **312**: p. 86-94.
39. Grinnell, F. and W.M. Petroll, *Cell motility and mechanics in three-dimensional collagen matrices.* Annu Rev Cell Dev Biol, 2010. **26**: p. 335-61.
40. Hao, J.-L., et al., *Galardin Inhibits Collagen Degradation by Rabbit Keratocytes by Inhibiting the Activation of Pro-Matrix Metalloproteinases.* Experimental Eye Research, 1999. **68**(5): p. 565-572.
41. Helena, M.C., et al., *Keratocyte apoptosis after corneal surgery.* Investigative Ophthalmology & Visual Science, 1998. **39**(2): p. 276-83.
42. Holmbeck, K., et al., *MT1-MMP-Deficient Mice Develop Dwarfism, Osteopenia, Arthritis, and Connective Tissue Disease due to Inadequate Collagen Turnover.* Cell, 1999. **99**(1): p. 81-92.
43. Holopainen, J.M., et al., *Activation of Matrix Metalloproteinase-8 by Membrane Type 1-MMP and Their Expression in Human Tears after Photorefractive Keratectomy.* Invest Ophthalmol Vis Sci, 2003. **44**(6): p. 2550-2556.
44. Hong, J.-W., et al., *Proinflammatory Chemokine Induction in Keratocytes and Inflammatory Cell Infiltration into the Cornea.* Investigative Ophthalmology & Visual Science, 2001. **42**(12): p. 2795-2803.
45. Horino, K., et al., *Tumor cell invasion of model 3-dimensional matrices: demonstration of migratory pathways, collagen disruption, and intercellular cooperation.* FASEB J, 2001. **15**(6): p. 932-939.
46. Imanishi, J., et al., *Growth factors: importance in wound healing and maintenance of transparency of the cornea.* Progress in Retinal and Eye Research, 2000. **19**(1): p. 113-129.
47. Jalbert, I., et al., *In vivo confocal microscopy of the human cornea.* British Journal of Ophthalmology, 2003. **87**(2): p. 225-236.
48. Jester, J.V., et al., *Corneal keratocytes: in situ and in vitro organization of cytoskeletal contractile proteins.* Investigative Ophthalmology & Visual Science, 1994. **35**(2): p. 730-43.

49. Jester, J.V., W.M. Petroll, and H.D. Cavanagh, *Corneal stromal wound healing in refractive surgery: the role of myofibroblasts.* Progress in Retinal and Eye Research, 1999. **18**(3): p. 311-356.
50. Jester, J.V. and J. Ho-Chang, *Modulation of cultured corneal keratocyte phenotype by growth factors/cytokines control in vitro contractility and extracellular matrix contraction.* Experimental Eye Research, 2003. **77**(5): p. 581-592.
51. Jester, J.V., et al., *Myofibroblast Differentiation of Normal Human Keratocytes and hTERT, Extended-Life Human Corneal Fibroblasts.* Investigative Ophthalmology & Visual Science, 2003. **44**(5): p. 1850-1858.
52. Jester, J.V. and J.-H. Chang, *Modulation of cultured corneal keratocyte phenotype by growth factors/cytokines control in vitro contractility and extracellular matrix contraction.* Exp Eye Res, 2003. **77**: p. 581-592.
53. Jiang, H., et al., *Distinguishing fibroblast promigratory and procontractile growth factor environments in 3-D collagen matrices.* The FASEB Journal, 2008. **22**(7): p. 2151-2160.
54. Karamichos, D., R.A. Brown, and V. Mudera, *Collagen stiffness regulates cellular contraction and matrix remodeling gene expression.* Journal of Biomedical Materials Research Part A, 2007. **83A**(3): p. 887-894.
55. Karamichos, D., N. Lakshman, and W.M. Petroll, *An experimental model for assessing fibroblast migration in 3-D collagen matrices.* Cell Motility and the Cytoskeleton, 2009. **66**(1): p. 1-9.
56. Kenney, M.C., et al., *Localization of TIMP-1, TIMP-2, TIMP-3, gelatinase A and gelatinase B in pathological human corneas.* Current Eye Research, 1998. **17**(3): p. 238-246.
57. Kim, A., N. Lakshman, and W.M. Petroll, *Quantitative assessment of local collagen matrix remodeling in 3-D Culture: The role of Rho kinase.* Experimental Cell Research, 2006. **312**(18): p. 3683-3692.
58. Kim, A. and W. Matthew Petroll, *Microtubule regulation of corneal fibroblast morphology and mechanical activity in 3-D culture.* Experimental Eye Research, 2007. **85**(4): p. 546-556.
59. Kim, A., et al., *Growth Factor Regulation of Corneal Keratocyte Differentiation and Migration in Compressed Collagen Matrices.* Investigative Ophthalmology & Visual Science, 2010. **51**(2): p. 864-875.
60. Kim, A., et al., *Corneal stromal cells use both high- and low-contractility migration mechanisms in 3-D collagen matrices.* Experimental Cell Research, 2012. **318**(6): p. 741-752.
61. Kim, W.J., R.R. Mohan, and S.E. Wilson, *Effect of PDGF, IL-1alpha, and BMP2/4 on corneal fibroblast chemotaxis: expression of the platelet-derived growth factor system in the cornea.* Investigative Ophthalmology & Visual Science, 1999. **40**(7): p. 1364-72.
62. Kolodney, M.S. and E.L. Elson, *Correlation of myosin light chain phosphorylation with isometric contraction of fibroblasts.* Journal of Biological Chemistry, 1993. **268**(32): p. 23850-23855.

63. Kondo, Y., et al., *Inhibition by a Selective IκB Kinase-2 Inhibitor of Interleukin-1–Induced Collagen Degradation by Corneal Fibroblasts in Three-Dimensional Culture.* Investigative Ophthalmology & Visual Science, 2008. **49**(11): p. 4850-4857.
64. Lakshman, N., et al., *Rho plays a central role in regulating local cell-matrix mechanical interactions in 3D culture.* Cell Motility and the Cytoskeleton, 2007. **64**(6): p. 434-445.
65. Lakshman, N., A. Kim, and W.M. Petroll, *Characterization of corneal keratocyte morphology and mechanical activity within 3-D collagen matrices.* Exp Eye Res, 2010. **90**(2): p. 350-359.
66. Lakshman, N. and W.M. Petroll, *Growth Factor Regulation of Corneal Keratocyte Mechanical Phenotypes in 3-D Collagen Matrices.* Investigative Ophthalmology & Visual Science, 2012. **53**(3): p. 1077-1086.
67. Lee, P.F., A.T. Yeh, and K.J. Bayless, *Nonlinear optical microscopy reveals invading endothelial cells anisotropically alter three-dimensional collagen matrices.* Exp Cell Res, 2009. **315**(3): p. 396-410.
68. Li, D.-Q., et al., *Regulation of MMP-9 Production by Human Corneal Epithelial Cells.* Experimental Eye Research, 2001. **73**(4): p. 449-459.
69. Lu, K.V., et al., *Upregulation of tissue inhibitor of metalloproteinases (TIMP)-2 promotes matrix metalloproteinase (MMP)-2 activation and cell invasion in a human glioblastoma cell line.* Lab Invest, 2003. **84**(1): p. 8-20.
70. Lu, Y., et al., *Inhibition by Triptolide of IL-1–Induced Collagen Degradation by Corneal Fibroblasts.* Investigative Ophthalmology & Visual Science, 2003. **44**(12): p. 5082-5088.
71. Lu, Y., et al., *Dexamethasone Inhibition of IL-1–Induced Collagen Degradation by Corneal Fibroblasts in Three-Dimensional Culture.* Investigative Ophthalmology & Visual Science, 2004. **45**(9): p. 2998-3004.
72. Mackiewicz, Z., et al., *Collagenolytic Proteinases in Keratoconus.* Cornea, 2006. **25**(5): p. 603-610 10.1097/01.ico.0000208820.32614.00.
73. Maltseva, O., et al., *Fibroblast Growth Factor Reversal of the Corneal Myofibroblast Phenotype.* Investigative Ophthalmology & Visual Science, 2001. **42**(11): p. 2490-2495.
74. Martin-Martin, B., et al., *The effect of MMP inhibitor GM6001 on early fibroblast-mediated collagen matrix contraction is correlated to a decrease in cell protrusive activity.* Eur J Cell Biol, 2011. **90**(1): p. 26-36.
75. Meek, K.M. and C. Boote, *The organization of collagen in the corneal stroma.* Experimental Eye Research, 2004. **78**(3): p. 503-512.
76. Mishima, H., et al., *Collagenolytic Activity of Keratocytes Cultured in a Collagen Matrix.* Japanese Journal of Ophthalmology, 1998. **42**(2): p. 79-84.
77. Moller-Pedersen, T., et al., *Corneal haze development after PRK is regulated by volume of stromal tissue removal.* Cornea, 1998. **17**(6): p. 627-39.
78. Moller-Pedersen, T., et al., *Stromal wound healing explains refractive instability and haze development after photorefractive keratectomy: a 1-year confocal microscopic study.* Ophthalmology, 2000. **107**(7): p. 1235-1245.
79. Mori, H., et al., *CD44 directs membrane-type 1 matrix metalloproteinase to lamellipodia by associating with its hemopexin-like domain.* EMBO J, 2002. **21**(15): p. 3949-3959.

80. Nakamura, K., et al., *Intact corneal epithelium is essential for the prevention of stromal haze after laser assisted in situ keratomileusis.* British Journal of Ophthalmology, 2001. **85**(2): p. 209-213.
81. Neel, E.A.A., et al., *Use of multiple unconfined compression for control of collagen gel scaffold density and mechanical properties.* Soft Matter, 2006. **2**: p. 986-992.
82. Netzel-Arnett, S., et al., *Collagen Dissolution by Keratinocytes Requires Cell Surface Plasminogen Activation and Matrix Metalloproteinase Activity.* J Biol Chem, 2002. **277**(47): p. 45154-45161.
83. Niggli, V., *Rho-kinase in human neutrophils: a role in signalling for myosin light chain phosphorylation and cell migration.* FEBS Letters, 1999. **445**(1): p. 69-72.
84. Onguchi, T., et al., *Membrane Type-1 Matrix Metalloproteinase Potentiates Basic Fibroblast Growth Factor-Induced Corneal Neovascularization.* The American Journal of Pathology, 2009. **174**(4): p. 1564-1571.
85. Parizi, M., E.W. Howard, and J.J. Tomasek, *Regulation of LPA-Promoted Myofibroblast Contraction: Role of Rho, Myosin Light Chain Kinase, and Myosin Light Chain Phosphatase.* Exp Cell Res, 2000. **254**(2): p. 210-220.
86. Parkin, B., V. Smith, and D. Easty, *The control of matrix metalloproteinase-2 expression in normal and keratoconic corneal keratocyte cultures.* European Journal of Ophthalmology, 2000. **10**(4): p. 276-85.
87. Petroll, W.M. and L. Ma, *Direct, dynamic assessment of cell-matrix interactions inside fibrillar collagen lattices.* Cell Motility and the Cytoskeleton, 2003. **55**(4): p. 254-264.
88. Petroll, W.M., L. Ma, and J.V. Jester, *Direct correlation of collagen matrix deformation with focal adhesion dynamics in living corneal fibroblasts.* Journal of Cell Science, 2003. **116**(8): p. 1481-1491.
89. Petroll, W.M., et al., *Analysis of the Pattern of Subcellular Force Generation by Corneal Fibroblasts After Rho Activation.* Eye & Contact Lens, 2008. **34**(1): p. 65-70 10.1097/ICL.0b013e3181580d5b.
90. Petroll, W.M., et al., *Dynamic assessment of fibroblast mechanical activity during Rac-induced cell spreading in 3-D culture.* Journal of Cellular Physiology, 2008. **217**(1): p. 162-171.
91. Provenzano, P.P., et al., *Contact guidance mediated three-dimensional cell migration is regulated by Rho/ROCK-dependent matrix reorganization.* Biophys J, 2008. **95**(11): p. 5374-84.
92. Rhee, S., et al., *Microtubule function in fibroblast spreading is modulated according to the tension state of cell–matrix interactions.* Proceedings of the National Academy of Sciences, 2007. **104**(13): p. 5425-5430.
93. Rowe, R.G., et al., *Pulmonary fibroblasts mobilize the membrane-tethered matrix metalloproteinase, MT1-MMP, to destructively remodel and invade interstitial type I collagen barriers.* Am J Physiol Lung Cell Mol Physiol, 2011. **301**(5): p. L683-L692.
94. Roy, P., et al., *Exertion of tractional force requires the coordinated up-regulation of cell contractility and adhesion.* Cell Motil Cytoskeleton, 1999. **43**(1): p. 23-34.

95. Roy, P., et al., *Effect of Cell Migration on the Maintenance of Tension on a Collagen Matrix.* Annals of Biomedical Engineering, 1999. **27**(6): p. 721-730.
96. Sabeh, F., et al., *Tumor cell traffic through the extracellular matrix is controlled by the membrane-anchored collagenase MT1-MMP.* The Journal of Cell Biology, 2004. **167**(4): p. 769-781.
97. Sabeh, F., et al., *Secreted Versus Membrane-anchored Collagenases.* J Biol Chem, 2009. **284**(34): p. 23001-23011.
98. Sabeh, F., R. Shimizu-Hirota, and S.J. Weiss, *Protease-dependent versus -independent cancer cell invasion programs: three-dimensional amoeboid movement revisited.* J Cell Biol, 2009. **185**(1): p. 11-19.
99. Sameni, M., et al., *Functional Imaging of Proteolysis: Stromal and Inflammatory Cells Increase Tumor Proteolysis* Mol Imaging, 2003. **2**(03): p. 159.
100. Seasholtz, T.M., et al., *Rho and Rho Kinase Mediate Thrombin-Stimulated Vascular Smooth Muscle Cell DNA Synthesis and Migration.* Circulation Research, 1999. **84**(10): p. 1186-1193.
101. Smine, A. and J.J. Plantner, *Membrane type-1 matrix metalloproteinase in human ocular tissues.* Current Eye Research, 1997. **16**(9): p. 925-929.
102. Tomasek, J.J., E.D. Hay, and K. Fujiwara, *Collagen modulates cell shape and cytoskeleton of embryonic corneal and fibroma fibroblasts: Distribution of actin, α-actinin, and myosin.* Developmental Biology, 1982. **92**(1): p. 107-122.
103. Tomasek, J.J., et al., *Myofibroblasts and mechano-regulation of connective tissue remodelling.* Nat Rev Mol Cell Biol, 2002. **3**(5): p. 349-363.
104. Townley, W.A., et al., *Matrix Metalloproteinase Inhibition Reduces Contraction by Dupuytren Fibroblasts.* J Hand Surg, 2008. **33**(9): p. 1608-1616.
105. Tsai, K.K.C., et al., *Cellular Mechanisms for Low-Dose Ionizing Radiation–Induced Perturbation of the Breast Tissue Microenvironment.* Cancer Res 2005. **65**(15): p. 6734-6744.
106. Vishwanath, M., et al., *Modulation of corneal fibroblast contractility within fibrillar collagen matrices.* Invest Ophthalmol Vis Sci, 2003. **44**(11): p. 4724-35.
107. Wang, Y.L. *Exploring the basic principles of cell shape control*. in *Frontiers in Cell Migration: From Mechanism to Disease*. 2008. Natcher Conference Center, National Institutes of Health, Bethesda, MD.
108. West-Mays, J.A., et al., *Competence for collagenase gene expression by tissue fibroblasts requires activation of an interleukin 1 alpha autocrine loop.* Proc Natl Acad Sci 1995. **92**(15): p. 6768-6772.
109. West-Mays, J.A., et al., *Differential inhibition of collagenase and interleukin-1alpha gene expression in cultured corneal fibroblasts by TGF-beta, dexamethasone, and retinoic acid.* Investigative Ophthalmology & Visual Science, 1999. **40**(5): p. 887-96.
110. West-Mays, J.A. and D.J. Dwivedi, *The keratocyte: Corneal stromal cell with variable repair phenotypes.* The International Journal of Biochemistry & Cell Biology, 2006. **38**(10): p. 1625-1631.

111. Wilkins-Port, C.E., et al., *TGF-β1 + EGF-Initiated Invasive Potential in Transformed Human Keratinocytes Is Coupled to a Plasmin/MMP-10/MMP-1–Dependent Collagen Remodeling Axis: Role for PAI-1*. Cancer Research, 2009. **69**(9): p. 4081-4091.
112. Wilson, S.E., et al., *Epithelial Injury Induces Keratocyte Apoptosis: Hypothesized Role for the Interleukin-1 System in the Modulation of Corneal Tissue Organization and Wound Healing.* Experimental Eye Research, 1996. **62**(4): p. 325-338.
113. Wilson, S.E., et al., *RANK, RANKL, OPG, and M-CSF Expression in Stromal Cells during Corneal Wound Healing.* Investigative Ophthalmology & Visual Science, 2004. **45**(7): p. 2201-2211.
114. Wolf, K., et al., *Compensation mechanism in tumor cell migration: mesenchymal–amoeboid transition after blocking of pericellular proteolysis.* J Cell Biol, 2003. **160**(2): p. 267-277.
115. Ye, H.Q. and D.T. Azar, *Expression of gelatinases A and B, and TIMPs 1 and 2 during corneal wound healing.* Investigative Ophthalmology & Visual Science, 1998. **39**(6): p. 913-21.
116. Ye, H.Q., et al., *Differential Expression of MT1-MMP (MMP-14) and Collagenase III (MMP-13) Genes in Normal and Wounded Rat Corneas.* Investigative Ophthalmology & Visual Science, 2000. **41**(10): p. 2894-2899.
117. Zaman, M.H., et al., *Migration of tumor cells in 3D matrices is governed by matrix stiffness along with cell-matrix adhesion and proteolysis.* P Natl Acad Sci, 2006. **103**(29): p. 10889-10894.
118. Zarrabi, K., et al., *Inhibition of Matrix Metalloproteinase 14 (MMP-14)-mediated Cancer Cell Migration.* Journal of Biological Chemistry, 2011. **286**(38): p. 33167-33177.
119. Zhou, C. and W. Petroll, *Rho Kinase Regulation of Fibroblast Migratory Mechanics in Fibrillar Collagen Matrices.* Cell Mol Bioeng, 2010. **3**(1): p. 76-83.
120. Zieske, J.D., S.R. Guimarães, and A.E.K. Hutcheon, *Kinetics of Keratocyte Proliferation in Response to Epithelial Debridement.* Experimental Eye Research, 2001. **72**(1): p. 33-39.